Design of a Flexible Containment System for Deep Ocean Oil Spills

by

Natasha Maas

Submitted to the Department of Civil and Environmental Engineering
in partial fulfillment of the requirements for the degree of

Master of Science in Civil and Environmental Engineering

at the

MASSACHUSETTS INSTITUTE OF TECHNOLOGY

June 2013

Author .....
Department of Civil and Environmental Engineering
May 10, 2013

Certified by .....
Dr. E. Eric Adams
Senior Lecturer and Senior Research Engineer of Civil and Environmental Engineering
Thesis Supervisor

Accepted by .....
Prof. Heidi M. Nepf
Chair, Departmental Committee for Graduate Students

Design of a Flexible Containment System for Deep Ocean Oil Spills

by

Natasha Maas

Submitted to the Department of Civil and Environmental Engineering
on May 10, 2013, in partial fulfillment of the
requirements for the degree of
Master of Science in Civil and Environmental Engineering

Abstract

BP needed almost 3 months to cap the Deepwater Horizon spill; improved response techniques are needed for the future. This work presents the design and deployment plan for a new type of containment system that captures the vast majority of hydrocarbons exiting the wellhead. The structure is lightweight, flexible and modular, using a passively induced chimney affect as its working principle. It is modular to create one design that fits any number and size of wells. Modularity comes from 100m sections of thin Kevlar fabric, forming a cylinder that starts several meters above the seabed and ends several meters below the sea surface. The system is stored onshore mostly assembled until needed.

The 3m-diameter shroud induces a flow that dilutes the gas to avoid hydrate formation. Yet the velocity is sufficiently small for gas to dissolve, reducing surface gas concentrations below workers' safety thresholds. The chimney effect causes a pressure differential over the material; reinforcement ribs are required to keep the system from collapsing inward. At the shroud top, the jet enters a containment pen, which is loosely attached to the shroud allowing it to ride the waves in heave, but constraining roll, pitch and yaw. The pen diameter allows oil to separate from the water; a skimmer weir in the pen collects almost pure oil and pumps it to a tanker. An air can at the shroud top provides pre-tension that restrains lateral deflections due to a uniform current, and helps reduce the collapse due to the pressure differential. The deflection and collapse are calculated for a uniform current using catenary equations. The results are used to verify the applicability of OrcaFlex, software commonly used by the offshore industry, which is then used to confirm the systems ability to satisfy design requirements under realistic conditions (a sea spectrum and non-uniform current).

The 'one design fits all' objective is tested by initially designing the system for a moderate size reference well, and then scaling it up (with minor modifications) to fit the Macondo well. The results confirm that one design of the system can contain spills of moderate size in addition to those similar to the Deepwater Horizon.

Thesis Supervisor: Dr. E. Eric Adams
Title: Senior Lecturer and Senior Research Engineer of Civil and Environmental Engineering

Acknowledgments

I would like to thank my adviser, Eric Adams, firstly for offering me this project upon my arrival to MIT and for his endless support since. His enthusiasm and guidance have made the last two years a great learning opportunity and an incredible personal development experience. I would also like to thank ENI S.p.A for making it possible for Eric and me to work on this project. Special thanks to Roberto Ferrario who was a wonderful resource on ENI's side and was a great support throughout the project. Similarly, I would like to thank Marco Calza for spending hours helping me setup the OrcaFlex model during my visit to Milan, as well as Nicola De Blasio, Mario Marchionna and Mario Chiaramonte for their support for this project. The collaboration with all of you at ENI was wonderful and I have learned a lot from you.

At MIT I would further like to thank professor Ole Madsen for being a great teacher and help for my research. From the Ocean Engineering department I would like to thank professor Thomaz Wierzbicki and his student Kirki Korfiani, professor Paul Sclavonous as well as professor Micheal Triantafyllou and his student Haining Zheng for making time to help me on topics that were new to me, even though I was not their student or colleague. Without all of your help my project could not have been as multidisciplinary as it has turned out to be.

I would also like to thank the other students in my lab group; Marianna, Ruo-Qian and Godine. You welcomed me into the group in my first semester here and were a great support then and throughout the time that followed. You guided me in how to do research at MIT, as I was a rookie, fresh out of undergraduate in Delft and gave advice on specific research questions where needed. The experience also would not have been the same without all the great friends that came into Parsons in my year. Being part of this tight group of friends has made my life at MIT a great adventure. Parsons as whole has been an amazing place, and I feel very lucky that I got the chance to spend time here.

Finally, I would like to thank my family and friends for their unconditional support throughout the good and the bad times. My parents, for supporting me unconditionally, but even more so for encouraging me to aim high and never give up; without you I would not be where I am today. Along the same lines, I would like to thank my sister, Alexandra, for inspiring me in more ways than she can imagine. To all three of you; I am indefinitely grateful for supporting me in my decision to leave home to pursue my dreams. Lastly, but definitely not the least, I would like to thank my friends. The ones here for making the past two years incredible, but most definitely also those at home; Kim and Jennifer, thank you for being there for me over the past two years. I thank you all for supporting me and at times putting up with me during the hard times that any project goes through.

The past two years have been an amazing journey, thank all of you who have been a part of it.

Contents

List of Figures

List of Tables

Chapter 1

Introduction

1.1 Background

The difficulty of capping the Macondo well blowout and the consequential environmental effects have emphasized the need to find better response programs for the future. In order to reduce the environmental effect of the spill, the industry-wide preferred approach is to cap the well and stop the blowout. Since this is not always possible, other strategies have to be devised to cope with living subsea blowouts. There are two high level approaches available: dispersing the hydrocarbons using chemical dispersants or containing the hydrocarbons and then guiding them up to the surface. Attempts to contain the Macondo spill (and others) included a combination of the two, partially due to a failure of the containment systems. Since then a number of research institutions have investigated the behavior of free hydrocarbon plumes (*Socolofsky et al.*, 2011) and the influence of dispersants (*Brandrik et al.*, 2013), (*Johansen et al.*, 2013). In parallel to that a preference to contain the hydrocarbons rather than diluting them, has since led to the development of an extensive range of containment systems. These systems can be categorized into sealed (no interaction of hydrocarbons and ambient seawater, including capping stack-like systems that rest on a BOP or cofferdam-like systems that rest on seabed) or non-sealed (off the seabed) systems that then can either be flexible or not (Appendix A). The advantage of the sealed system is the conformity with the drilling standards and their ability to disconnect the top facility. However, important disadvantages include high weight, lack of oil water separation, need for accurate positioning and minimal dilution of gas concentrations.

The design presented here is a different (and new) kind of containment system, based on a passively induced chimney effect as working principle. Lessons learned from the problems with BPs cofferdam and the previously mentioned advantages for a containment system are included into the design concept, on which the next paragraph will elaborate.

1.2 Concept

The proposed design is a lightweight, flexible structure with the ability to capture at least 90% of the spilled hydrocarbons during an expected lifetime of approximately six months. The buoyancy of the oil and gas creates a chimney effect, which is the working principle of this

system. The design ensures that the hydrocarbons are contained as they rise to the surface, see Figure 1-1. Since the chimney effect causes a pressure difference between interior and exterior of the shroud, this leads to a contraction of the shroud walls. Reinforcement ribs spaced approximately every ten meters constrain this narrowing of the internal cross-section.

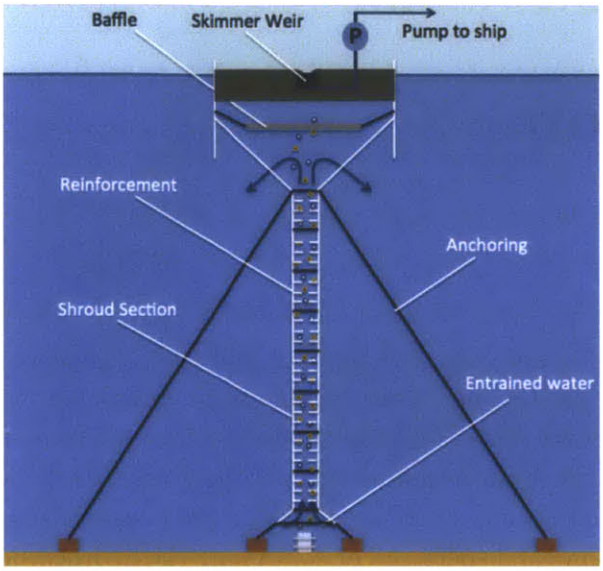

Figure 1-1: Shroud concept

The shroud is stored onshore, ready to serve any number of offshore wells. In order for the system to fit the conditions at different wells, the design has a modular character built up of 100m identical sections. The deepest section is short and flared; the latter attribute guarantees the capture of the hydrocarbons from both a distributed as well as a point source.

In order to generate the chimney effect the shroud extends from about 20 meters above the seafloor to approximately 10 meters below sea level. A big advantage of designing the system this way is that the shroud has a minimal impact on any work going on at the wellhead. Moreover, the majority of the deployment steps are performed from the water surface at a location offset from the wellhead, therefore reducing safety risks.

During installation a crane lowers the shroud sections through the moon pool of a multi-purpose vessel, starting with the flared bottom and consecutively adding on sections as the rest is lowered. Therefore each of the sections has a positive wet weight (in order to sink), but an air can mounted to the top section gives the total design a negative wet weight and keeps the shroud under tension. ROV's guide the shroud as it is lowered and finally they connect the bottom mooring lines that are already connected to ballast blocks, to the flared section.

At the surface a deep, circular pen collects the hydrocarbons. It is designed to hold a satisfactory volume, withstand wave motions, and promote the separation of the oil droplets from the water exiting the shroud. A secondary pen could be used as a backup to contain whatever small quantities of oil that escape the primary pen due to, e.g., extreme weather.

1.3 Design Cases

One of the fundamental design principles is the modularity of the system so that it can operate on a large range of wells. One system can therefore serve a large geographical region, e.g. the Gulf of Mexico. To achieve this multipurpose system, the design process includes two distinct sites; together they will generate a design that can function in a combination of extreme conditions. The first is a well of interest to the sponsor (that is not yet in use), hereafter referred to as the 'reference well'. The conditions at this well are relatively mild (*Exploration and Division*, 2011). The other is the Macondo well in the Gulf of Mexico (see Figure 1-2), where the conditions are much more demanding (*Camilli et al.*, 2011) and the well has a flow rate that represents the larger wells operating today. Chapter 2 presents further data.

Figure 1-2: Location of the Macondo well in the Gulf of Mexico

Table 1.1: Environmental conditions for the reference and Macondo well

Parameter	Reference well	Macondo well
Water Depth	830m	1500m
Typical Current	0.1 m/s	0.1 m/s
Bottom Temperature	13°C	4°C
Significant Wave Height	0.1 - 2.5m	1.0 - 2.7m
Peak Wave Period	2 - 8.5s	6 - 7.5s
Oil Flow Rate	0.015 m^3/s	0.10 m^3/s
Gas Flow Rate (at well)	0.0028 Am^3/s	0.09 Am^3/s

From this point the analysis proceeds to look into the behavior of a free blowout plume to get insight into consequences of introducing the shroud system. After that Chapter 4 gives the full description of the shroud compartments, with their chosen dimensions. The next section goes on to describe analytical analysis on the fluid mechanics in and around the shroud, as well as primary structural analysis. Chapter 6 then describes the use of the software tool OrcaFlex to model the shroud response to different, more complex environmental conditions. That is the last stage of the design and analysis phase for the reference well. Before moving on to describe the installation and validation (future work), Chapter 8 will discuss the small variations to the design parameters for the system to operate for the Macondo well conditions as well.

Chapter 2

Data Design Cases

The design process for the shroud requires a range of data about the environmental as well as flow conditions associated with the respective wells. This section presents all the data needed for the further analysis per topic for both the reference and the Macondo well.

2.1 Environmental Data

2.1.1 Reference Well

This data set refers to the ambient conditions such as water temperature and salinity, water density (*Trieste*) and the currents (*Poulain et al.*, 1996).

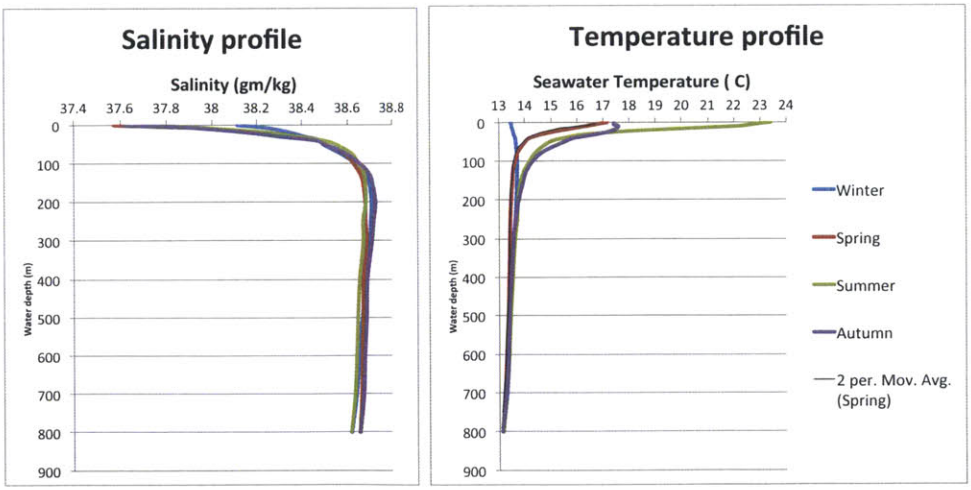

(a) (b)

Figure 2-1: Salinity (a) and temperature (b) profiles measured at the reference well (*Trieste*).

The degree of ambient stratification and the strength of the currents are factors that influence the behavior of the hydrocarbon plume and/or the shroud. Figures 2-1 and 2-2 indicate a moderate density change over depth, without any strong stratification.

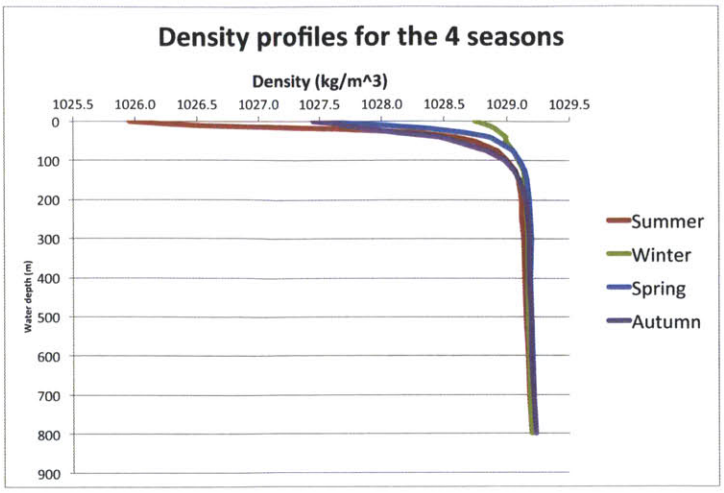

Figure 2-2: Water density profile at the reference well.

As shown in Figure 2-3 both the magnitude and the direction of the currents change over depth and throughout the year. The absolute magnitudes are generally less than 0.1 m/s and they rarely exceed 0.2m/s at any given time of the year. Hence 0.1 m/s is used as a typical current and 0.2 m/s is used as a design current for calculating drag forces. It can also be noted that the direction of the current over depth changes strongly over the year. Consequently, during some seasons the current is close to uniform over depth (causing a high net drag force), while in other seasons the current direction changes up to 180 degrees over depth (giving rise to a smaller net drag force on the shroud).

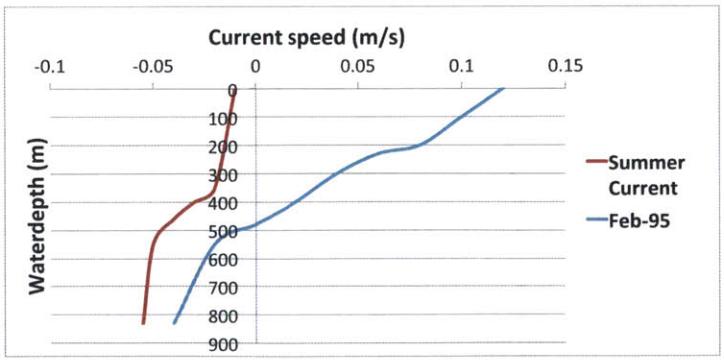

Figure 2-3: Current profiles at the reference well site for the different seasons. Two sources were used.

2.1.2 Macondo Well

For the Macondo well the temperature and density profiles (Figure 2-4) originate directly from the NOAA Buoy Data Center (*NOAA*, 2012) and *Socolofsky et al.* (2011) respectively. The current profile (Figure 2-5) is obtained from a report on the currents in the Gulf of Mexico for the US Department of Interior.

Since the shroud only reaches to within several meters of the sea surface, the design is tested on a 0.2m/s current. This value is considered a good depth- and time-average (yearly average).

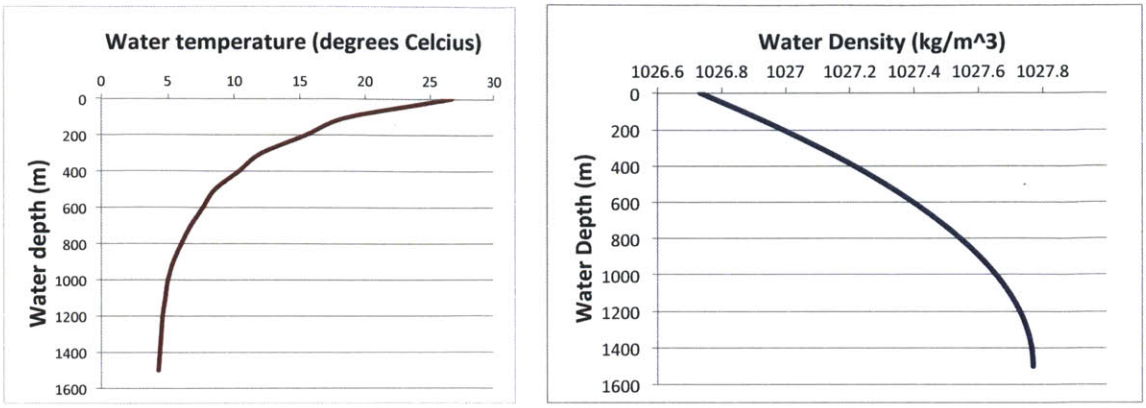

(a) (b)

Figure 2-4: (a) Temperature and (b) density profiles for the Macondo well (*Socolofsky et al.*, 2011)

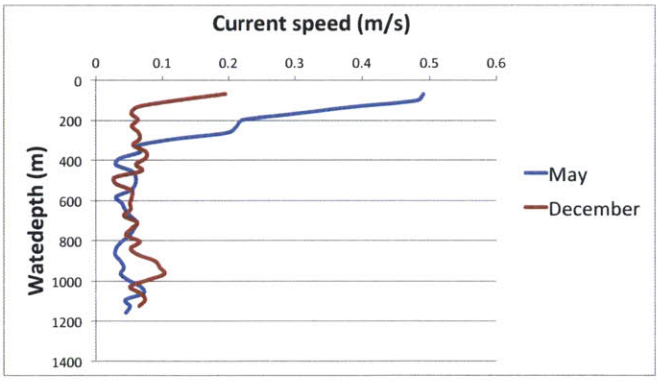

Figure 2-5: Current profiles for the the Macondo well for two months showing two extreme conditions *Sturges et al.* (2004)

2.1.3 Surface Tension

Oil droplet behavior requires data on the surface tension between the hydrocarbons and the water :

- Surface tension Oil - Water: 0.025 kg/s^2 (*Federal Interagency Solutions Group and Team*, 2010)

- Surface tension Gas - Water: 0.055 kg/s^2 (*Sacks and Meyn*, 1995)

2.2 Flow Data

2.2.1 Outlet Diameter

We are interested in the diameter of the outlet because its dimensions influence the size of the bubbles/droplets that will create the hydrocarbon plume. In the case of the reference well, three outlet diameters for the blowout jet are to be considered according to ENI S.p.A.:

- 5" $\approx$ 0.13m
- 9" $\approx$ 0.23m
- 18" $\approx$ 0.46m

For the calculations here we focus on the smallest outlet with an opening of 0.13m, due to its similarity to the 0.12m opening used for the Deep Spill experiment (*Johansen*, 2001), which operates as a reference to check calculations. Furthermore the smaller opening size causes the bubbles to be more in the atomized range, which means that they will have a smaller slip velocity. A low slip velocity causes the free plume to be more influenced by a cross current to become trapped by ambient stratification at a level of neutral buoyancy.

For the Macondo well observations suggest that the effective diameter of the broken riser through which the oil spilled in the initial weeks, was approximately 42cm (*Camilli et al.*, 2011). After the riser was cut the effective diameter was about 49cm. We will use the 42cm diameter in combination with estimated flow rate found by *Camilli et al.* (2011) to calculate the bubble and droplet diameters in Chapter 4.

2.2.2 Hydrocarbon Flow Data

Table 2.1 presents data for the oil wells, providing further detail on the oil/gas flow and their characteristics for the reference (*Exploration and Division*, 2011) and Macondo well (*Camilli et al.*, 2011). Two types of units are used for the flow rate; Am^3/s is used for the flow rate measured at the well head (under local pressure and temperature) and Sm^3/s as units for the flow rate under Standard conditions (atmospheric pressure and temperature of 293K). The difference is needed due to the large density change that gasses undergo between deep ocean conditions (large pressure and low temperature) to atmospheric conditions.

The dissimilarities between the gas flow rates at the well head and the surface at each site are due to volume expansion and gas that is dissolved in the oil at the well head but comes out of solution during its ascent. Given the oil/gas composition in Table 2.1 the contribution of the components other than methane, ethane or propane are neglected in the analysis for the shroud design.

Table 2.1: Hydrocarbon flow data

Parameter	Reference well	Macondo well
Oil		
- Flow rate	0.015 Am^3/s	0.10 m^3/s
- Density	761.7 kg/m^3	858 kg/m^3
Gas		
At the well head		
- Flow rate	0.0028 Am^3/s	0.09 Am^3/s
- Density	95 kg/m^3	120 kg/m^3s
At the surface		
- Flow rate	1.435 Sm^3/s	31 Sm^3/s
	(0.014 m^3/s at the bottom)	(0.162 m^3/s at the bottom)
- Density	0.82 kg/m^3	0.73 kg/m^3s
Composition (mol %)		
- Methane	87.4	82.5
- Ethane	7.1	8.3
- Propane	2.1	5.3
- Others	3.4	3.9
Total	100%	100%

Chapter 3

Free Blowout Plume

The analysis of the free plume can be compared to the use of a control study; before moving on to the shroud design it is important to understand what the behavior of the hydrocarbons is without any interference. Will the environmental conditions cause the plume to stratify or will it rise as a coherent plume? Other points of interest are the location at which the hydrocarbons surface and what percentage that is of the total released volume. The first step is to determine the bubble and droplet diameter, after which we can analyze the global plume behavior, since the rise velocity of individual bubbles and droplets depends on their size. From the individual behavior of the bubbles and droplets we can consequently determine the gas (and oil) concentrations at the surface. These concentrations are important, because they need to satisfy industry requirements with respect to workers safety. This analysis is only done for the reference well.

3.1 Bubble and Droplet Size

There are at least three reasons why it is necessary to know the individual bubble/droplet sizes:

- Size influences the effect that stratification and cross current have on the free plume
- Workers' safety is related to surface gas concentrations, which depend on gas dissolution rates, which in turn depend on bubble diameter.
- Oil droplet size helps determine whether the oil and water will separate after exiting the shroud, which then influences the required pen size.

3.1.1 General Theory

The starting point to calculate the size of the droplets and bubbles is the outlet diameter of the wellhead. The equivalent diameter of this nozzle, together with the flow rate of the jet velocity, govern the initial stable size of the bubbles and droplets. A higher jet velocity is associated with smaller droplets/bubbles (atomization), while larger outlet diameters produce large droplets/bubbles. The initial diameter is then reduced to a smaller, stable diameter based on a balance between turbulent kinetic energy tending to break up the bubbles and

droplets and surface tension tending to stabilize them. For low values of surface tension, as would occur when chemical dispersants are used, viscosity can also help stabilize droplets and bubbles (Johansen et al., 2013). Once the bubbles/droplets reach the bottom of the shroud they have already obtained a diameter equal to or smaller than the critical diameter. As they ascend further, dissolution and volume expansion are competing effects influencing the diameter of the droplets/bubbles. The net of the two effects combined determines the change in diameter of the droplets/bubbles as they travel up through the shroud. The turbulent flow in the shroud will not affect them, since the diameters are already equal to or smaller than the critical value.

Johansen et al. (2013), as part of SINTEF, developed a model that finds a volume median droplet size D_{50}, so half of the volume is in the form of droplets/bubbles with a smaller diameter. On the basis of this characteristic diameter various models exist to find the diameter distribution; here we use the Rosin-Rammler model. Under stationary conditions the characteristic bubble/droplet size (D_{50} here) is defined by

$$D_{50} = c\left(\frac{\sigma}{\rho_w}\right)^{3/5} \varepsilon^{-2/5} \tag{3.1}$$

where σ and ρ_w are the surface tension and water density, ε is the fluid turbulent dissipation rate and c is a constant. In a turbulent jet, like in our case, the bubbles and droplets experience a time varying turbulent energy, whose magnitude scales as

$$\varepsilon \sim \frac{U_j^3}{D_j} \tag{3.2}$$

Name	Unit	Description
ρ_w	kg/m^3	Density of the water $\approx 1028 kg/m^3$
σ	kg/s^2	Surface tension
ε	m^4/s^2	Fluid turbulent dissipation rate
U_j	m/s	Jet velocity
D_j	m	Jet diameter

Combining Equations 3.1 and 3.2 leads to Equation 3.3 for D_{50}.

$$D_{50} = A\ D_j\ We^{-3/5} \tag{3.3}$$

where We is the Weber number, which is defined as in Equation 3.4 and A is an empirical constant.

$$We_j = \frac{\rho_w\ U_j^2\ D_j}{\sigma} \tag{3.4}$$

For small surface tension, viscosity becomes important and We is replaced by We^*:

$$We^* = \frac{We}{1 + B\ Vi\ (D_{50}/D_j)^{1/3}} \tag{3.5}$$

where Vi represents the viscosity ($\mu U/\sigma$, where μ is the dynamic viscosity). Viscosity becomes important when chemical dispersants are used to reduce the surface tension, but in our case the surface tension is relatively large, therefore overpowering the importance of viscosity, which means that we do not need to use the modified Weber number to find D_{50}.

The above theory is based on a two phase jet in which a single dispersant phase (oil) is discharged into a second continuous fluid; however in the case of an oil spill the jet is often a mix of oil and gas. The heterogeneity of the fluid affects the break-up dynamics in two ways. Firstly, due to the much smaller density of the gas relatively to the oil, it forces the oil to flow through a smaller cross-sectional area of the orifice. Secondly, due to the high buoyancy of the gas, the discharge of the heterogeneous fluid is going to behave more like a plume. Following *Johansen et al.* (2013), the first effect can be accounted for here by defining a nominal velocity as in Equation 3.6 and an effective orifice diameter D' (Equation 3.7), for the oil or gas through the orifice, where θ is the void fraction occupied by the gas. The nominal velocity is associated with a jet of only oil droplets or gas bubbles that has the same kinematic momentum as the jet with both oil and gas.The nominal velocity can then be used to find the nominal value of the Weber number, in order to define the D_{50} associated with the heterogeneous jet.

$$U_n = \frac{U_j}{\sqrt{1-\theta}} \tag{3.6}$$

$$D' = D\sqrt{(1-n)} \tag{3.7}$$

The second effect is accounted for by further modifying the jet exit velocity so that it has the same velocity as a buoyant jet at a characteristic distance from the orifice which is known as the momentum length. Again, following *Johansen et al.* (2013), this velocity is given by

$$U_C = U_n\ (1 + Fr^{-1}) \tag{3.8}$$

where Fr is the densimetric Froud number, which is defined as follows

$$Fr = \frac{U_n}{\sqrt{D\ g[\rho_w - \rho(1-n)]/\rho_w}} \tag{3.9}$$

By combining Equations 3.6, 3.8, 3.9 and 3.4 we can determine D_{50} by using U_C in Equation 3.3.

As mentioned before, coefficients A and B are empirical coefficients. In absence of the viscosity dependence like in our case, Equation 3.3 only has A as an empirical coefficient. The predicted value of D_{50}, therefore, becomes directly dependent on the value of A. *Brandrik et al.* (2013) found A = 24.8 (and B = 0.08) for an experiment using only oil. In parallel,

Johansen et al. (2013) found A = 15 (and B = 0.8) for experiments also involving only with oil. In experiments where the oil viscosity plays a role, the chosen value for A can be balanced out by a certain choice for B. Since this is not possible in our case, we needed to calibrate the model in a different way. A deep spill experiment off the coast of Norway in 2000 had very similar conditions to those of the reference well as can be seen in Table 3.1 (*Johansen*, 2001); therefore observational data from that experiment can be used to calibrate a right value of A for our model. This value for A can then be used to predict the D_{50} for both the reference and Macondo well.

Table 3.1: Comparison of the reference well data to data from the Deep Spill experiment

	Reference well	Deep Spill
Water depth (m)	830	840
Currents (m/s)	0.1	0.1
Jet diameter (m)	0.13m	0.12m
Oil flow rate (m^3/s)	0.015	0.017
Gas flow rate (m^3/s)	0.0028	0.007

The observed bubble and droplet distributions for the Deep Spill experiment are shown in Figure 3-1, from which we can compare the values for D_{50} with our calculated values.

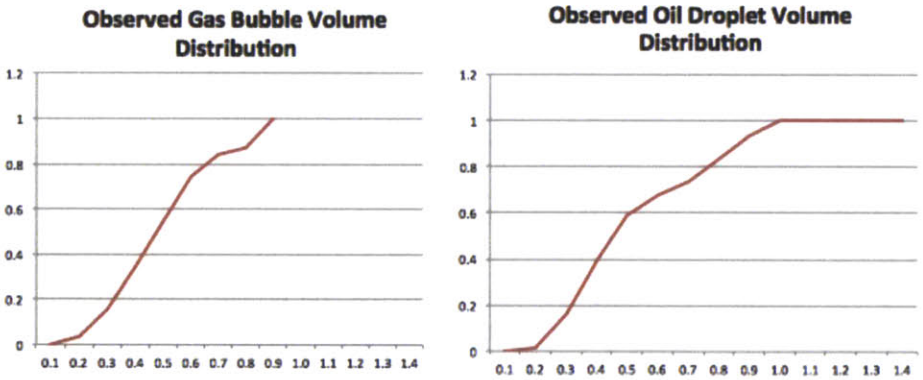

Figure 3-1: (a) Gas bubble and (b) oil droplet distributions (in cm) observed at the Deep Spill experiment

The observed D_{50}'s are:

- Bubble D_{50}: 0.0047m
- Droplet D_{50}: 0.0044m

Using the model described before, neglecting the viscosity term and using the water density to calculate the Weber number, we find that the 'correct' value for A in our model is 18.7. Using this value we predict the same values for the D_{50}'s as were observed.

Based on the D_{50}'s we can find the cumulative volume distribution using the Rosin-Rammler model [Equation 3.10], which is defined by the following equation, where n is a

fitting parameter. The value of n has a non-negligible affect on the found distribution, but *Bailey et al.* (1983) found that values of $n \geq 3$ produce good results.

$$V(D) = 1 - exp[-0.693(D/D_{50})^n] \tag{3.10}$$

For this research the value of n is validated by fitting it to observed bubble and droplet diameter data for an oil spill with comparable conditions (SINTEF's Deep Spill Experiment (*Johansen*, 2001))

The following two paragraphs discuss the results from the models to find the bubble and droplet distributions for the reference and Macondo well respectively.

3.1.2 Reference Well

As mentioned in Chapter 2.2.1, for the reference well we work with a 13cm jet diameter. For this diameter, the given oil and gas characteristics and the value for the coefficient A (in Equation 3.3), the characteristic bubble and droplet diameters can be determined. The results are presented in Table 3.2.

Table 3.2: 50% bubbles/droplets for the reference well

Input		Output	
Jet diameter	0.13m	Gas D_{50}	0.0043m
Jet velocity	1.34m/s	Oil D_{50}	0.0064m
Coefficient A	15		
Surface tension	0.025kg/s (Oil)		
	0.055kg/s (Gas)		

Since we were able to calibrate the SINTEF model (using coefficient A) to fit the observed data, we will use the SINTEF model to predict the bubble and droplet sizes exiting the well (Figure 3-2).

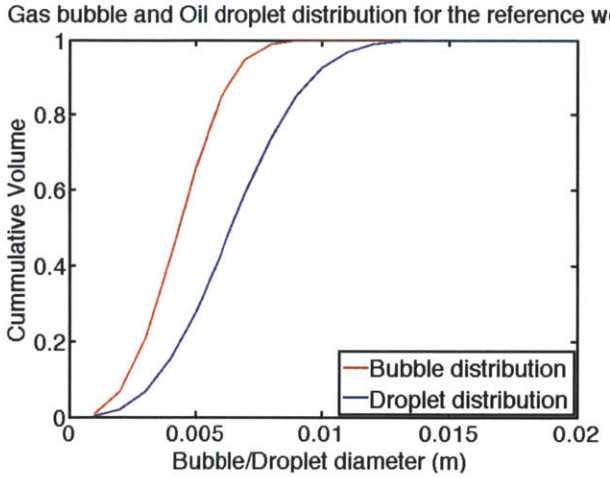

Figure 3-2: Predicted (a) gas bubble and (b) oil droplet distributions (in cm) for the reference well

3.1.3 Macondo Well

The general model described earlier can also be used to describe a bubble/droplet distribution for the Macondo well. The input parameters are the following:

- Rossin-Ramler fitting parameter $n = 3$
- Gas fraction $(n) = 0.43$
- Jet diameter $= 0.42$m (observed equivalent diameter for the broken riser)
- Jet Velocity $= 1.5$m/s

As mentioned before, the fitting (spreading) parameter can be chosen to be any value equal to or larger than 3. Unfortunately there is no data to which we can fit the distribution for this case, so for continuity n is kept at 3. The SINTEF model, with A $= 18.7$, gives the following values for the critical diameters:

- Gas bubbles; $D_{50} = 0.0088$m
- Oil droplets; $D_{50} = 0.0072$m

Using the Rossin-Rammler equation (3.10) we can use the D_{50}'s to determine the volume distributions. These bubble and droplet distributions are presented in Figure 3-3.

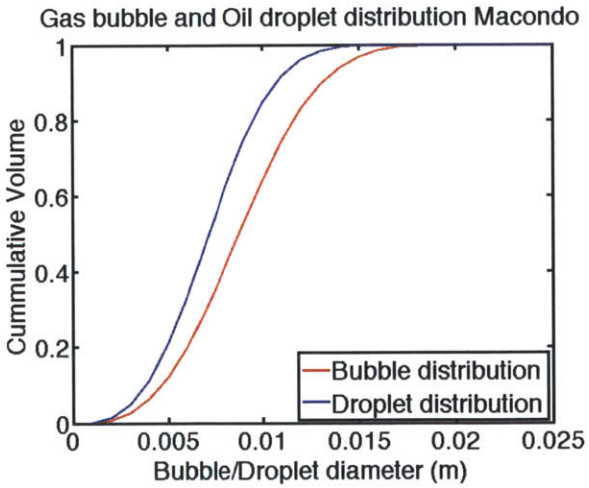

Figure 3-3: Modeled bubble/droplet distribution for the Macondo well

The SINTEF model has two important uncertainties to be aware of: firstly, should the Weber number be calculated using the density of water or the density of the dispersed phase (oil), and secondly, what are the values for coefficients A (and B). The first issue is still a point of discussion in the field of droplet dynamics. The effect of oil versus water density is small (and can be accounted for in the coefficient A), but the effect of gas versus water density is huge. For this reason we used the water density. We have tried to address the

second uncertainty by calibrating it to observed data from the Deep Spill Experiment. Regardless of these uncertainties, the SINTEF model is the best that is currently available to predict bubble/droplet diameters in a multi-phase jet, which is why we decided to work with it.

3.2 Free Plume Behavior for the Reference Well

There are two idealized multiphase plume behaviors: stratified dominated or current dominated. The difference between these global behaviors indicates how the hydrocarbons rise to the surface. Which of the two behaviors will dominate depends on the relative magnitude of the peel height (h_p) and the separation height (h_s); both depend on the buoyancy flux and the rise velocity of the bubbles/droplets. See Figure 3-4 for the definitions of both heights (*Socolofsky et al.*, 2011).

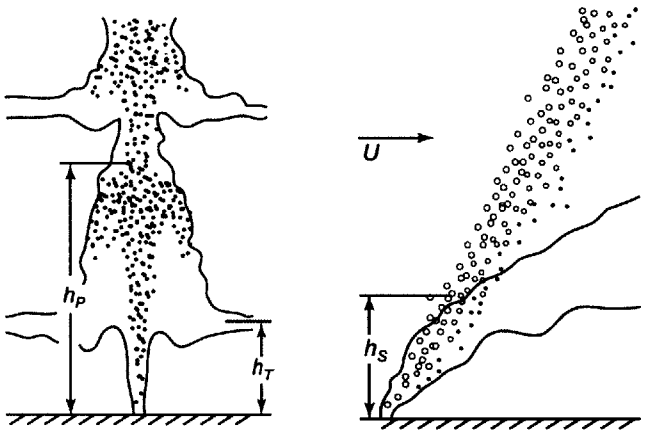

Figure 3-4: Free plume behavior; (a) stratification dominated ($h_p < h_s$) and (b) current dominated ($h_p > h_s$)

Parameter	Equation
Buoyancy flux	$B_0 = Q_0(\rho_a - \rho_0)/\rho_r$
Buoyancy frequency	$N = \sqrt{-g/\rho_r(\partial\rho_a/\partial z)}$
Separation height	$h_s = 5.1B_0/(Uu_s^{2.4})^{0.88}$
Peel height	$h_p/(B_0/N^3)^{1.4} = 5.2exp[-(u_s/(B_0/N)^{\frac{1}{4}} - 1.8)^2/10.1]$

For the buoyancy frequency we use a linear approximation of the density profile for $\partial\rho_a/\partial z$. In order to find inclusive results, the buoyancy frequency was calculated for the summer and winter conditions, which have the steepest slope of water density over depth. Furthermore, for the calculations of the separation and peel height the slip velocities used are those for the largest and smallest diameter bubble/droplet, which range from 0.10 - 0.21m/s (*Zheng and Yapa*, 2000).

For the reference well the peel height is bigger than the separation height under all circumstances (Table 3.3), which implies a strongly current dominated behavior. Consequently, most of the hydrocarbons in a free plume will surface downstream of the blowout (Figure 3-5).The horizontal distance from the well to the surface location of the hydrocarbons depends on the slip velocity (which depends on the droplet/bubble size) relative to the current speed. For the bubble and droplet sizes described in Section 3.1.2 with rise velocities between 0.1 and 0.21 m/s, and a current speed of 0.1 m/s, it is found that the hydrocarbons from the reference well would surface between 1200m and 3600m downstream from the wellhead.

Table 3.3: Reference well free plume separation and trap height

Parameter	Reference well
Buoyancy flux (m^4/s^3)	0.062
Buoyancy frequency (1/s)	Winter: 0.000833
	Summer: 0.001
Separation height (m)	Biggest bubble/droplet: 65
	Smallest bubble/droplet: 254
Peel height (m)	Winter: 554
	Summer: 452

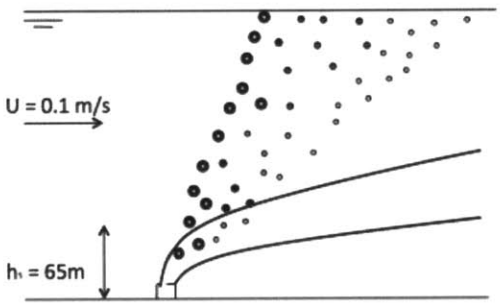

Figure 3-5: Predicted current dominated blowout plume under the reference well conditions

3.3 Gas Dissolution

During their ascent to the surface the bubbles and droplets will partially dissolve due to mass transfer into the ambient water. It is important to understand the change in gas volume during the rise of the bubbles to the surface, because gas concentrations at the surface need to be below flammable thresholds. Of oil droplets generally there is negligible mass transfer, the dissolution calculations therefore focus on the gas bubbles.

Two competing mechanisms influence the change in total volume of the gas bubbles over depth; gas dissolution will decrease the bubble volume as it ascends towards the surface, while volume expansion results from a reduction in hydrostatic pressure. The combined effect is

described as the change of diameter for individual bubbles of a given starting diameter. *Hirai et al.* (1996) found that this behavior is expressed by the equation:

$$\frac{\mathrm{d}D}{\mathrm{d}z} = \frac{2kS}{u_z \rho} - \frac{\mathrm{d}\rho}{\mathrm{d}z}\frac{D}{3\rho} \tag{3.11}$$

Name	Unit	Description
k	m/s	Mass transfer coefficient
S	kg/m^3	Solubility of the gas in (sea) water
ρ	kg/m^3	Density of the gas at ambient pressure/temp
D	m	Bubble diameter
u_z	m/s	Rise velocity of the bubbles (which will be a combination of the slip velocity and the velocity of the water-hydrocarbon mixture through the shroud)

The first term in the equation represents the mass transfer, which depends on the diffusivity and solubility of the gas in the ambient water (since the gas concentration in the ambient water is considered negligible). The mass transfer depends on the diffusivity in the following way (*Johansen*, 2004):

$$k = \frac{Sh\ \kappa}{D} \tag{3.12}$$

In which the Sherwood number is defined as follows:

$$Sh = \frac{2}{\sqrt{\pi}}\sqrt{1 - \frac{2.89}{\sqrt{Re}}}\sqrt{Pe} \tag{3.13}$$

in which κ (m^2/s) is the molecular diffusivity of the solute in the water, Sh is the Sherwood number, $Pe = wD/\kappa$ is the Peclet number (where w is the slip velocity), and Re is the Reynolds number.

The second term in Equation 3.11 accounts for the volume expansion of the bubble due to the reducing hydrostatic pressure during the ascent. The reduction in pressure causes a change in densities of the gasses over the water depth. The way the density changes over depth is defined by the Peng-Robinson equation of state (*McCain*, 1990):

$$\left[p + \frac{a_T}{V_m(V_m + b) + b(V_m - b)}\right](V_m - b) = RT \tag{3.14}$$

Name	Unit	Description
p	N/m^2	Pressure
V_m	m^3/mol	Molar volume
R	J/K/mol	Universal gas constant
T	K	Absolute temperature
a_T	-	Coefficient
b	-	Coefficient

Most of the parameters in Equation 3.11 - Equation 3.14 are component specific; therefore the calculations are done for bubbles of pure methane, ethane or propane separately. The total gas volume (0.0028 m^3/s) is distributed over the individual components. The bubble diameters then govern the number of bubbles for each of the gasses. Figure 3-6 shows the change of the bubble diameters over depth for the free plume.

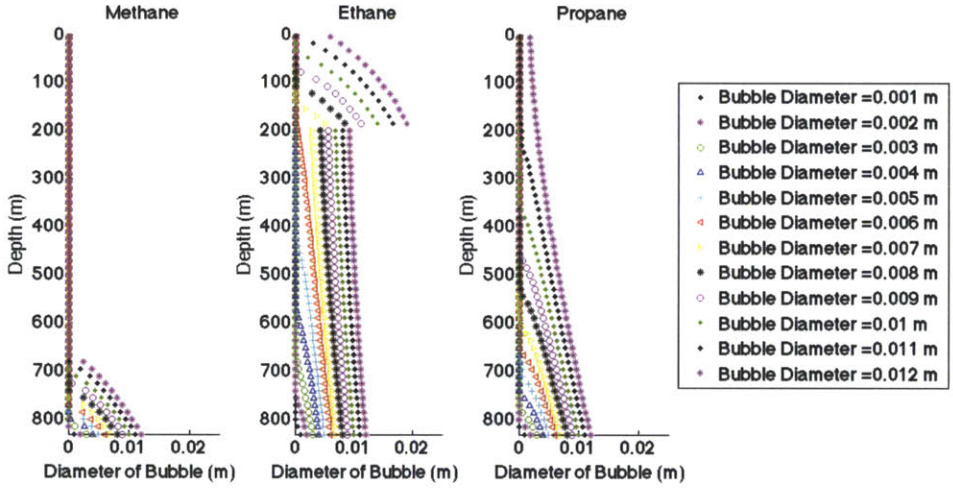

Figure 3-6: Reference well free plume predicted bubble diameter change over depth

The jumps in the curves for the ethane bubbles/droplets in Figure 3-6 indicate the depth at which the ethane transitions from liquid to gas. This phase change is accompanied by a large jump in the density. The results presented in Figure 3-6 show that all the methane bubbles, the smaller two-thirds of the ethane and all the propane bubbles can dissolve entirely.

Based on this data the gas concentrations can be determined as a function of the water depth (Figure 3-7).

The hydrocarbons exit the jet to form a free plume, which entrains a large volume of water as it rises. At the separation height the hydrocarbons leave the plume and rise as individual droplets to the surface. The conditions at the reference well result in a small separation height (relative to the water depth), which made it possible to calculate the concentrations based on the behavior of individual bubbles.

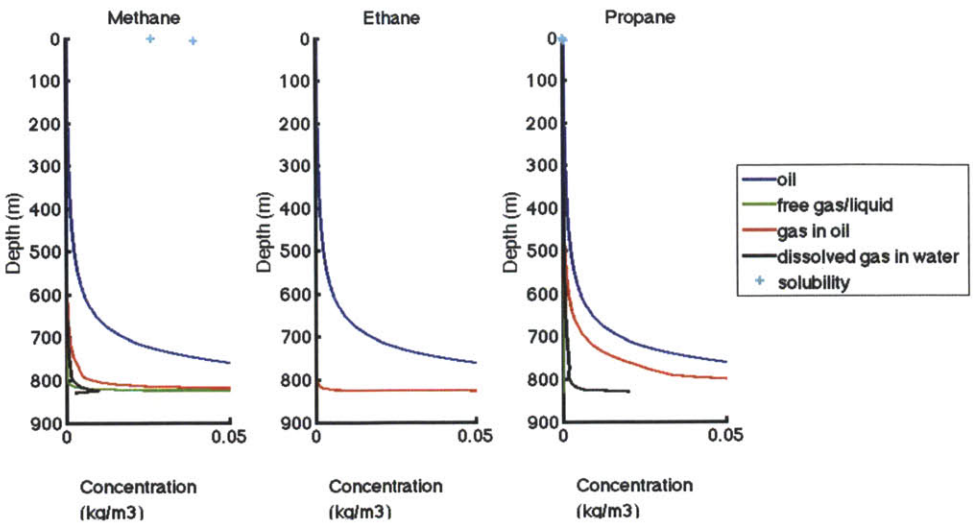

Figure 3-7: Reference well free plume predicted concentration change over depth

Similar calculation will be done in Sections 5.3 and 8.5 for the change of the bubble diameters and gas concentration during the ascent through the shroud, for the reference and Macondo well respectively.

Chapter 4

Shroud System Design

In this section details on the components of the general design are described. This will include a description of the chosen material and its characteristics, reinforcement ribs, the buoyancy compartments, collection system and the mooring configuration. The concept as it is described here can be applied to wells due to the modularity of the system and the two diverse cases for which it was tested in the simulations. Therefore this chapter only includes dimensions that are applicable to the generally applicable design, but does not go into specifics for individual wells. Chapter 5 and Chapter 8 will go into details for the reference and Macondo well respectively.

4.1 General Concept Considerations

Some aspects of the system can be determined based on initial practical considerations. These include:

- The shroud diameter should be relatively small to minimize drag and mooring/deployment complications; industry standards of pipe-like structures have diameters smaller than approximately 1m. On the other hand, the diameter needs to be large enough to dilute hydrates and gasses, as well as generate a rise velocity that is small enough to give the gas bubbles time to (partially) dissolve. A compromise was reached at a shroud diameter of 3 meters.

- The material should have a high strength-to-weight ratio and a density close to that of seawater, to reduce its (wet) weight during deployment and operation. A material that satisfies these requirements, especially in being very strong yet flexible, is Kevlar fabric with a tensile strength of approximately 1300MPa (there is some uncertainty with regard to this value, since it depends on the manner and directionality of the waving of the fibers, as well as manufacturer), and density (1440 kg/m^3) acceptably close to that of the seawater. To reduce the weight of the system, we want to reduce the thickness of the fabric as much as possible; however we use a minimum of 2mm in order to reduce risk of the fabric tearing during deployment. Furthermore, a slightly thicker material will help reduce the tensile stress caused by the pre-tension.

- Each of the 100m sections should have a positive wetted weight (meaning they would want to sink) in order to make deployment easier.

- The shroud needs to have enough positive buoyancy to create a pre-tension. The pre-tension will limit the reduction of the shroud's cross-sectional area (due to a pressure differential) to an acceptable level. A buoyancy compartment attached to the top of the shroud can provide the required pre-tension.

- The connection between the sections has a minimal number of components of low complexity (to simplify deployment), so as not to restrict freedom of motion, and then allow the shroud to follow the water motions.

- Station keeping should be simple, using mooring lines connecting only at the top and bottom of the system. Further stationkeeping is aided by the buoyancy compartment at the top of the shroud (i.e. the pre-tension).

The following sections will further elaborate on the design of the shroud sections as well as specific components of the shroud design.

4.2 Shroud Sections

The shroud is a modular structure built up of 100m sections made of 2mm thick Kevlar fabric. In order to protect the 2mm thick Kevlar during storage and deployment each section is folded up (like an accordion) and hung in a steel frame ($\sim$ 1m high, 4m diameter). A similar concept is already used for mesocosms designed at the University in Kiel, Germany (Figure 4-1) from *Riebesell et al.* (2013). Each folded 100m section will fit entirely in the steel frame, so that during deployment it only needs to be unfolded. In order to have the Kevlar unfold slowly to avoid snapping of the material, a combination of rope and pulleys can be used.

Figure 4-1: University of Kiel mesocosm design (*Riebesell et al.*, 2013)

4.2.1 Connection Between Sections

The sections have to be connected such that together they work as a uniform system. The connection needs to be watertight to keep extra water from being sucked into the shroud, while keeping flexibility to adjust to the surrounding environmental conditions. This connection is achieved using the shackles attached to the reinforcement ribs. Each rib will be formed from three 120 degree parts and the shackles will be attached to the flanges that connect the 120 degree parts. The last rib of each section is located about 20cm from the bottom of the section, so that the shackles on the top of the next section can be attached to the shackles on the lower rib of the upper section. The first 20cm of the lower section are therefore located inside the upper section (Figure 4-2), which is the first step in obtaining a seal between the sections. Due to the differential pressure a seal is required between the sections to avoid excess water from being drawn in. However, the differential pressure will now also suck the skirt of the upper section again the lower shroud section, thereby passively preventing intrusions of ambient seawater. Since this type of seal has not been used under these conditions before, addition of another seal type using a metal ring, e.g., could be considered, as shown below.

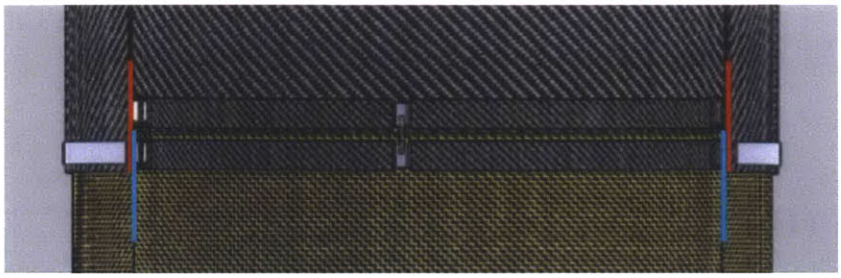

Figure 4-2: Connection of two consecutive shroud sections using shackles that are attached to the flanges connecting the 120 degree circular I-beam ribs.

4.2.2 Reinforcement Rib Design

The last important component of the shroud sections is the reinforcement ribs themselves, which were already mentioned briefly in discussing the connection between sections. The ribs are needed due to the differential pressure between the interior and exterior of the shroud, that otherwise would significantly reduce the cross-sectional area of the system. The ribs are made of steel and have an I-cross section (Figure 4-3), with dimensions shown in Table 4.1. The advantage of this type of cross section is its high mass moment of inertia relative to other shapes. A first requirement of the ribs is based on a lower bound mass moment of inertia needed to withstand buckling due to the differential pressure. Secondly, the ribs function to achieve almost neutral buoyancy of each section. This is achieved by attaching syntactic foam to the steel cross section. The I-shape makes it possible to fit the syntactic foam in its flanks, making it easy to keep all parts together using rings that wrap around the I-beam and the foam.

The I-beam is bent into a circular form to fit the shroud interior. Each rib is built connecting three 120-degree parts that fit into a Kevlar sleeve that is attached to the interior of

the shroud. The 120-degree parts are bolted together to a flange (Figure 4-3), which can be covered by the syntactic foam in the operational phase.

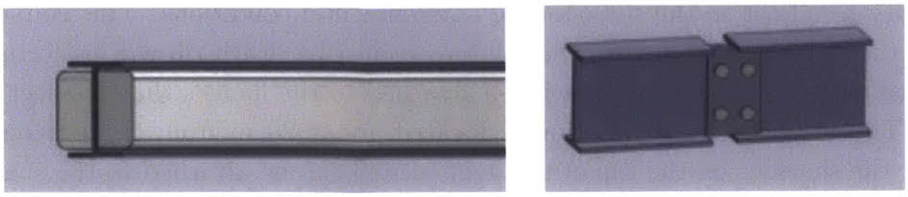

(a) (b)

Figure 4-3: (a) I cross-section beam with foam and (b) connection of the 120° rib sections.

Table 4.1: Reinforcement rib design dimensions

Parameter	Design Value
Height of body	0.1m
Thickness of flank	0.005m
Width of flank	0.06m

4.3 Flared (Bottom) section

The bottom section will be flared in order to capture as much of the hydrocarbons as possible as they exit the well head, either from a point source or a distributed source. The chosen design is fundamentally just a Kevlar sheet (Figure 4-4), though this might require additional design components (e.g. a frame) for it to obtain the desired shape, as is discussed below.

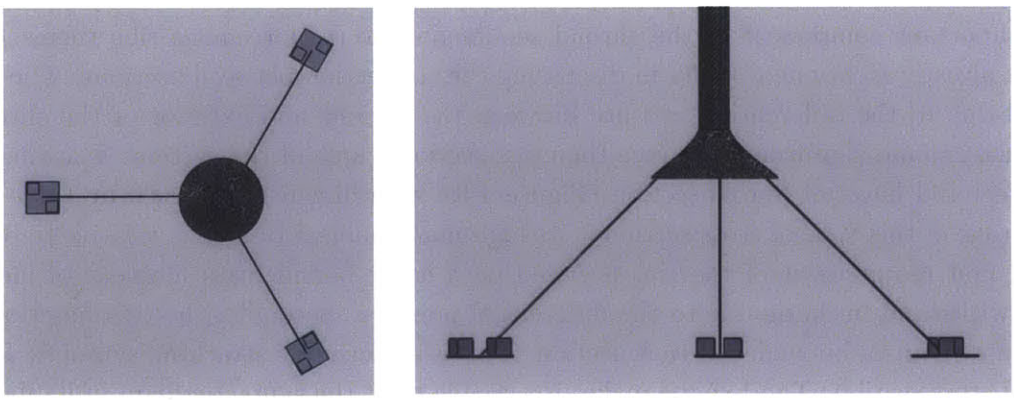

(a) (b)

Figure 4-4: Flared section design; (a) top view and (b) side view.

The preferred shape has a height of 5 meters with sides oriented at a 45-degree angle, giving the shroud a final diameter of 13 meters at its bottom.

There are a number of considerations that need to be taken into account when designing this section:

1. As mentioned in Section 1.2 the system will be deployed through the moon pool of a multipurpose vessel. Since the flared section will have a bottom diameter of 13 meters (which is much bigger than typical moon pool dimensions), the section needs to be designed to accommodate this change in dimensions.

2. The final configuration of this bottom section is very non-aerodynamical, which makes its ability to descend to the seafloor a second design consideration.

3. An efficient and practical manner of connecting the mooring lines to the bottom of the flared section needs to be developed.

4. Thought needs to be put into the connection of this section to the first regular section that is above it.

Consideration 1 requires the frame to be foldable and therefore have a mechanism that could open it to obtain the funnel shape. The solution comes in the form of a design of the section that only consists of a fabric funnel that is connected to the bottom mooring, where winches shorten the mooring lines to open up the flared section. The advantage is that there is no longer a need for a complex frame and active components. By adding some ballast to the bottom of the flared section, it can be lowered from the moon pool in a controlled manner that will also keep the entire shroud straight as it makes its descent.

Consideration 3 means that ROV's would need to connect the mooring lines to rings/flanges on the bottom of the flared section. This is something that ROV's are capable of doing, but it gets more complicated with increasing water depth. Already having the mooring lines connected to the ballast blocks before lowering the sections from the vessel might be a good alternative design to avoid this problem. However, then long mooring lines would already be connected to the shroud during deployment, and these would need to be shortened during the descent of the system, which might be complex.

For the connection of the flared section to the shroud section above it (Consideration 4), the design that is used to connect other consecutive sections is applicable here too. The top of the flared section can have the same type of reinforcement rib with 'flanges' with shackles that connect to the bottom ring of the first regular shroud section.

4.4 Buoyancy Compartment

The buoyancy compartment mentioned in Section 4.1 is designed as a steel air can that fits around the first 10 - 20 meters of the top shroud section. Its design, connection to the rest of the shroud system, and connection to the shroud top, are described in the paragraphs below.

4.4.1 Design

The air can is made of steel rather than a rigid plastic, as is sometimes the case. Even though steel is heavier, it will guarantee the cans integrity during transportation and deployment. Different sized air cans will be available, to accommodate the range in required buoyancy levels. The inner diameter of the air can is fixed for all well sizes, since it will fit nicely around the shroud (Figure 4-5), which has a fixed 3 meter diameter for all well conditions. The outer diameter of the air can will vary, with a number of different options being available. Further accommodation to well specific conditions can be accounted for by adjusting how much of the can's volume is filled with air versus water. During deployment the air can is initially filled with water, which is slowly replaced by air depending on the weight that it needs to compensate for. If necessary a second can can be attached to the first to create a larger air volume.

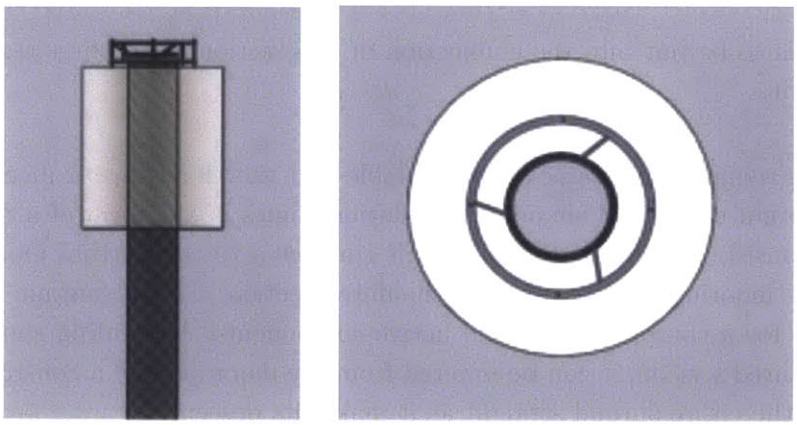

(a) (b)

Figure 4-5: Air can design; (a) side view and (b) top view.

4.4.2 Connection to the Shroud

The steel can(s) are connected to the steel frame of the top section of the shroud. Flanges on the buoyancy can are connected to flanges on the steel frame by shackles. Since the air can is placed around the shroud, it is already attached to this shroud section onshore and transported as one compartment to the blowout location. Depending on the location and size of the blowout, a second air can could be added. During the deployment the air can will fill with water. Once the shroud system is fully connected and the mooring lines are hooked onto the shroud system, a hose can be connected to the air can to replace the water by air and create the required buoyancy/pre-tension.

4.5 Mooring Lines and Foundation Blocks

The total mooring configuration consists of three mooring lines that constrain the shroud top and three bottom mooring lines. Each line is connected to a ballast module (plate with two ballast blocks; Figure 4-6), as is described in Section 4.5.2.

4.5.1 Mooring Lines

The mooring lines connected to the top of the shroud are a combination of nylon wire and chain, 48% and 52% of the mooring line total length respectively. They guarantee a deflection of the shroud top of maximum 10 meters, depending on the water depth and strength of the cross-currents. The mooring lines are already pre-assembled onshore. During deployment a buoy will be attached to the upper end of the mooring line until it is connected to the shroud top (see Chapter 7). The connection of these mooring to the top of the shroud takes place at the frame of the section. Since this is also the connecting point for the air cans and the pen, this frame will need to be stronger than the other frames, that only have the protecting/deployment function. The lower end of the chain is already connected to the mooring block that it belongs to during deployment.

The short mooring lines, holding down the bottom section, are 50m long chains, which are shortened to a final length of approximately 28m using winches. In their final configuration they make sure the bottom of the shroud is "anchored" (see Chapter 6).

4.5.2 Mooring Blocks

Each mooring point requires at least three ballast steel blocks totaling $\sim$ 120 tons. Due to the maximum lifting capacity of the crane on the vessel used for deployment ($\sim$ 60 tons), smaller blocks need to be used at each mooring point that together sum up to 120 tons. The chosen design to do this includes

- Mooring plate: $\sim$ 30tons, 5m x 5m x 0.15m of steel.
- Two mooring blocks (cubes): each $\sim$ 45tons, 1.8m x 1.8m x 1.8m.

The mooring plate has a connection point where the mooring line can be attached. The dimensions mentioned above are for the system for the reference well; bigger systems like for Macondo would require each mooring point to have additional steel. The design would be similar, but would include three mooring cubes per mooring plate.

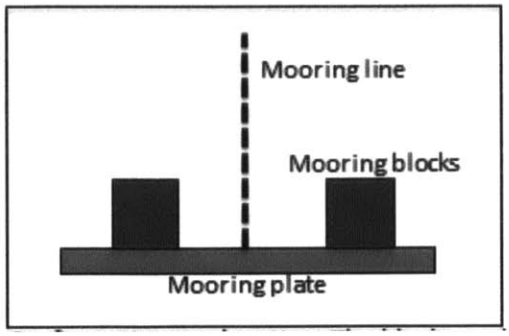

Figure 4-6: Mooring blocks design

4.6 Pen

Once the oil reaches the surface it needs to be contained in a separate, enclosed system, here referred to as a pen, from which it can be extracted. A simple system consists of a circular buoyancy ring which is reinforced, and filled with syntactic foam to provide buoyancy, plus a skirt hanging beneath the ring to contain the oil. Because oil from some wells can be quite light (762 kg/m^3 for the reference well), the pen must extend a significant distance above the water surface as well as below if substantial storage is to be obtained. Hence a vertical "fence" is included, extending above the surface, and squeezed between two buoyancy rings. The oil density can vary quite a bit between wells, which means that the percentage of the thickness of the oil layer that floats above the water level in the pen, varies too. In order for the pen to be able to contain oil with different densities, we have designed the skit and the fence to be made of one (long) part. The buoyancy rings can then be attached to this wall (onto the longitudinal reinforcement) at different heights, thereby changing the relative length of the skirt versus the fence depending on the oil density. A cross-sectional sketch of the system (not to scale) is shown in Figure 4-7.

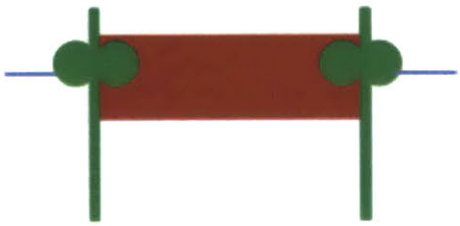

Figure 4-7: Containment boom/pen design with skirt plus fence.

The design combines the following characteristics.

- The containment volume needs to guarantee enough storage space in the pen to contain the oil in case the tanker gets backed up. In the case of the reference well the pen will fill by 1300 m^3 per day. Assuming that the pen can safely hold oil if filled to 25% of its capacity, we need to choose a diameter and length to fit the filling rate such that the pen can store oil for approximately 24 hours.
- The pen diameter should be large enough to allow the water to separate from the oil after they exit the shroud.
- The design has to be able to interact adequately with the waves, i.e. by "riding the waves".
- The freeboard of the pen should be sufficient to avoid significant wave overtopping during the majority of the time.

The pen is built up of several components (Figure 4-8), each helping the system ride the waves properly, contain sufficient oil, be lightweight and aid the separation of the oil from the water. Design variables of each of the components are described below, for diameter of the pen is chosen to be 20m.

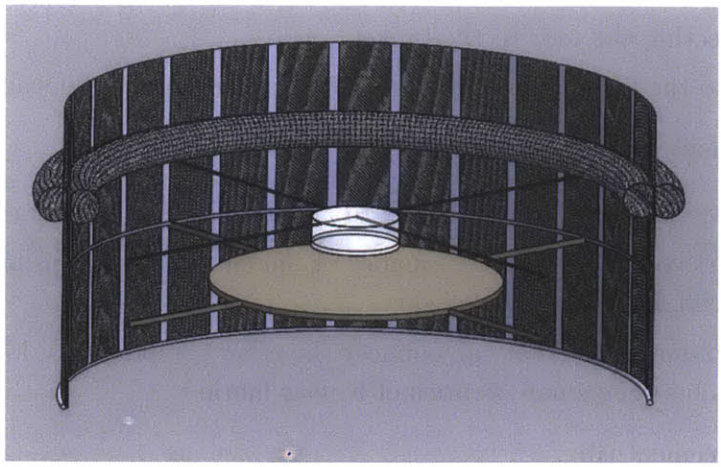

Figure 4-8: Pen system

1. Buoyancy rings surrounding the pen
    - 0.002m thick Kevlar
    - Air filled
    - 0.5m radius
2. Skirt
    - 0.002m thick Kevlar
    - 7.5m long
    - Bottom of the skirt contains ballast (e.g. sand in a sleeve)
3. Fence
    - 0.002m thick Kevlar
    - 2.5m high
4. Horizontal Baffle
    - Intended to slow down the jet exiting the shroud, giving the oil and water more time to separate
    - Needs to be low enough on the skirt that even during roll of the pen it is always under water (3m above the bottom of the skirt)
    - Rigid plastic
    - 5m radius
    - Spokes connect it to the longitudinal reinforcement on the skirt of the pen
5. Collection system
    - Skimmer weir, 1m radius, 1m deep

- Hose connecting the weir to the tanker
- Attached to the longitudinal reinforcement, just below the buoyancy rings

6. Longitudinal reinforcement

   - On the fence, needed every 0.5m-1m to help it resist the wave forces
   - On the skirt could use half the number of reinforcement bars as on the fence (it is not as crucial for it to stay straight)
   - Small aluminum bars (that can connect the other components), located at connection points between small sections of Kevlar fabric

7. Circular reinforcement rib

   - Air pressured rib that will help the skirt keep its circular shape
   - 4m from the bottom of the skirt
   - 0.1m radius

4.6.1 Connection of Pen to the Shroud Top

The connection between the pen and the shroud needs to be flexible enough for the pen to move separately from the shroud in its interaction with the waves while allowing the shroud to move freely in response to waves and currents. To achieve this the pen is connected to the shroud using four wires that connect to four of the longitudinal reinforcements on the pen skirt and to the frame of the top section of the shroud at the other end (Figure 4-9).

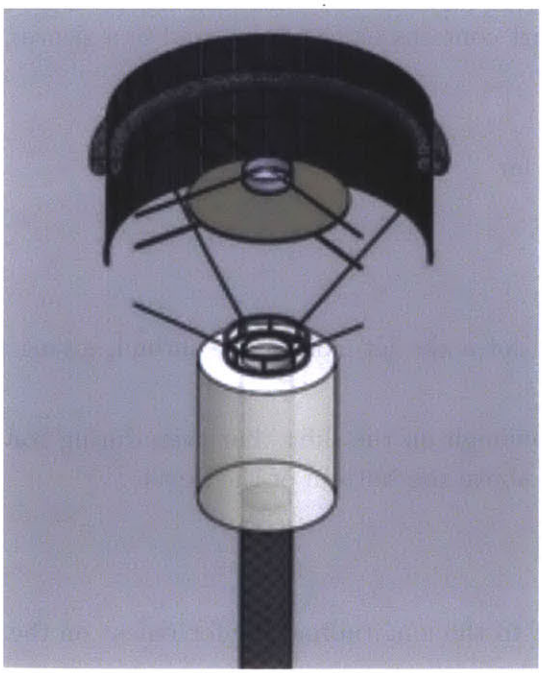

Figure 4-9: Connection of the pen to the top of the shroud, using four links connected to the frame of the top section of the shroud, 2.5m above the top of the shroud.

The wires will have the following characteristics

- 500 kN/m stiffness
- Each wire is 12m long
- 0.15m diameter nylon wire

Positioning the links at a distance offset from the shroud itself will create sufficient restoring torque to keep the pen from rotating around its own axis (yaw) beyond 100 degrees. The frame on the top section of the shroud can be used to facilitate the design, making the distance between the points of connection 5 meters. Results from OrcaFlex simulations indicate that this design satisfies the requirement on yaw of the pen.

4.7 Oil Collection System

The oil that is captured in the pen should ideally be harvested after pumping it to a vessel; however this is only economically viable if the oil is practically free of water. Given the large depth of the pen, and the volume of oil within the pen, the residence time of the oil in the pen should be long enough for the two fluids to separate. In that case the simplest design for an integrated oil collection system in the pen is a skimmer weir. It is located at the center of the pen and is attached to the pen by four spokes that are connected to the frame in the pen (see Figure 4-8 and Figure 4-9). This device passively collects the oil floating in the pen, which is then pumped to a tanker. The assumption is that this system is able to collect (skim) oil with low water content due to the thickness of the oil layer in the pen, from which a thin layer of oil continuously flows over the weir. For safety reasons, the oil is required to have a low water content in order to be safely stored on board of the tanker. The tanker can store the oil and eventually bring it back to shore for refining. The tanker would be positioned far enough from then pen such that the employees are protected from the (methane) gas surfacing in the pen.

Furthermore, if (lab) testing were to show that the requirement on the maximum water content can not consistently be met, consideration should be given to adding a hydrophobic mesh in the pen (between the baffle and the skimmer weir) as an additional way to separate the oil from the water (*Deng et al.*, 2013). The mesh would only let oil through, therefore making sure that the weir receives pure oil that is then pumped out to the tanker.

4.8 Logistics

One of the strengths of the shroud system is that it can be deployed within several days, because most components of the system are already pre-assembled and stored onshore. Both the 100m shroud sections and the frame of the pen can already be completely assembled onshore. The baffle and skimmer weir, however, will still need to be attached to the pen frame. In case of a blowout event the components would be lifted onto a multi-purpose vessel with a moon

pool to be taken offshore.

One factor that influences the deployment time is the availability of a vessel with the capabilities to install the system, where lift capacity and size of the moon pool are important requirements. The total system is designed to be light enough that it can be lifted by a medium-sized crane, therefore minimizing the waiting time for an appropriate vessel. The availability of a tanker vessel to pump out the oil from the pen also influences the deployment time, since the pen can only store oil for up to approximately 24 hours. However, it is assumed that by the time the rest of the system is installed, a tanker will have arrived at the blowout scene. This is likely the case since one will probably be available at the nearest port since it is close to at least one oil field.

Further details on the installation of the system are described in Chapter 7.

Chapter 5

Reference Well

Moving on from the general description of the shroud system in the previous chapter, here we will focus on the specifics for the reference well system. The analysis is setup by choosing a design and associated parameters, for which we then analyze the flow and hydrocarbon concentrations and perform a structural analysis. Lastly, we check the behavior of a chosen pen design that would fit with the required hydrocarbon storage.

5.1 System Architecture

Most of the system design is independent of the well location and the local conditions. However, there are a couple of differences between the sites that need to be considered to enable the system to withstand more severe conditions. Some of these details are relevant for the analysis done on the flow and structure so are stated here for completion.

- Shroud Length: 800m
- Mooring Lines: There are three mooring lines at the top, their configuration is shown in Figure 5-1.

  Total Length: 1880m

  Wire: 900m

  Chain: 980m

- Air Can Volume: 520 m^3
  This volume should be able to create enough pre-tension to constrain the shroud from large lateral movements.
- Pen Design

  Diameter: 20m

  Skirt Length: 7.5m

  Fence Height: 2.5m

- Pen Links

  Length: 12m

  Stiffness: 500 kN/m

  Offset from shroud diameter: 2.5m

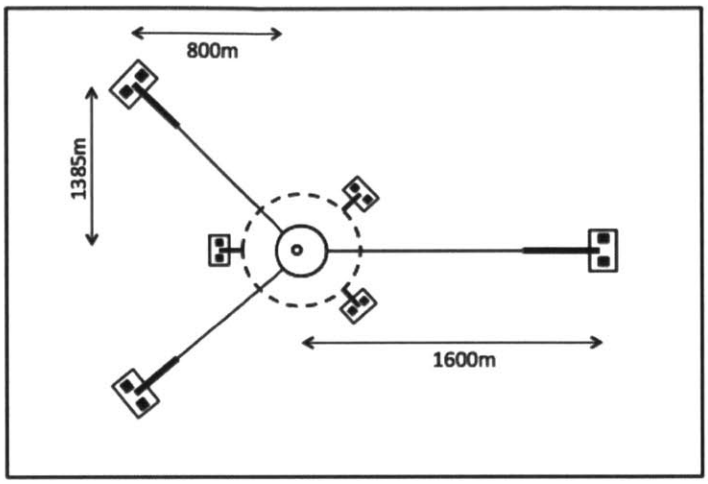

Figure 5-1: Mooring configuration for the reference well. The distances at which the individual mooring lines will be anchored at the seabed are indicated in the figure. The mooring lines anchoring the bottom of the shroud are approximately 10m from the shroud.

The dimensions of the pen are primarily driven by the desire to be able to store up to a day's worth of oil without needing it to be pumped continuously to a tanker. This way the immediate availability of a tanker would not affect the operations of the system. Besides, the large diameter of the pen will contribute to diluting the gas that surfaces, therefore helping to protect the crew on surrounding vessels.

With all parameters specified now, the next paragraphs will focus on different types of analysis to check whether the chosen design minimizes/obliterate hydrate formation, satisfies requirements of workers safety (related to gas concentrations), whether the deflections of the shroud system and stress in the material are within acceptable values, and finally whether the pen will be able to respond well to waves, in order to store oil for several hours.

5.2 Flow Assurance

The buoyancy of the oil and gas causes a chimney effect in the shroud, which is the working principle for this containment system. The equation for the induced flow rate is given in *Chow and Adams* (2010) to be:

$$Q = (\mathrm{B}\ \mathrm{A}^2\ \mathrm{H}\ \varphi)^{1/3} \tag{5.1}$$

$$B = \left(\frac{\rho_w - \rho_{oil}}{\rho_w}\right) g\ Q_{oil} + \left(\frac{\rho_w - \rho_{gas}}{\rho_w}\right) g\ Q_{gas} \tag{5.2}$$

$$\varphi = \frac{2}{(1 + \mathrm{K} + \mathrm{f}\frac{\mathrm{H}}{\mathrm{D}})} \tag{5.3}$$

Name	Unit	Description
B	m^4/s^3	Kinematic Buoyancy flux due to hydrocarbons
A	m^2	Cross-sectional area of the shroud
H	m	Length of the shroud
φ	-	Head loss parameter
ρ_w	kg/m^3	Density of the ambient water
K	-	Entrance loss coefficient for the shroud ($K \approx 0$ for a rounded entrance and $K = 1$ for a re-entrant inlet). Here we use K = 0.8 due to the design of the flared section.
f	-	Darcy-Weisbach friction factor
D	m	Diameter of the shroud

A value for f can be determined from a Moody diagram based on the Reynolds number Re ($\sim 1.8 * 10^6$) and a relative roughness ($k = \epsilon/\mathrm{D} = 0.048$), which reflects the periodic change in shroud cross-section between ribs, due to internal suction. For the parameter range used here, f can be approximated as 0.07.

The chimney effect described above creates a pressure differential across the Kevlar, which is found by writing a Bernoulli equation for a streamline form outside to inside the shroud, resulting in:

$$\frac{\Delta \mathrm{p}}{\rho} = \frac{\mathrm{u}^2}{2}(1 + \mathrm{K}) = \frac{\varphi^{2/3}\ \mathrm{B}_0^{2/3}\ \mathrm{H}^{2/3}}{\mathrm{A}^{2/3}} \tag{5.4}$$

Name	Unit	Description
Δp	N/m^2	Pressure difference on the shroud
ρ	kg/m^3	Density of the ambient seawater
Q	m^3/s	Flow through the shroud
A	m^2	Cross-sectional area of the shroud
Φ	-	Friction coefficient
K	-	Entrance loss coefficient (≈ 0.9)

Table 5.1 gives an example of output of the depth-averaged flow parameters for given design variables. The maximum pressure differential is found at the bottom of the shroud, which is the value of interest and therefore the one presented in Table 5.1. Furthermore, it is interesting to note that some of the benchmarked designs mention that they would use a pump at the top of their system to create a flow. If one would want to create a flow rate as close to $6m^3/s$

using that type of design, it would require a incredible amount of energy, making it a very costly operation. For larger wells, like the Macondo well, the flow rate we can induce using the chimney effect are even higher. As Section 8.4 points out, for Macondo we can induce a flow rate of about $15m^3/s$, which is comparable to Boston's Waste Water Plant Deer Island. From this analogy we know that in order to create a flow rate that big, would create an unrealistic amount of energy. This means that designs that use a pump to bring the hydrocarbons to the surface, will probably not be able to create a flow comparable to that in our system, meaning that they miss out on the benefits from the large flow rate (dilution of the gas and oil concentrations, reduction/mitigation of hydrate formation, etc.).

Table 5.1: Depth-averaged flow parameters for the reference well based on design variables

Design variables			
Length shroud	800m		
Diameter	3m		
Input		Output	
Oil flow rate	$0.015m^3/s$	Flow rate	$6.1m^3/s$
Oil density	$762kg/m^3$	Velocity in shroud	0.9m/s
Gas flow rate	$0.003m^3/s$	Pressure difference	676Pa
Gas density	$94.6kg/m^3$	φ	<0.09

For simplification, the calculations above assume a negligible influence of both the ambient water stratification and change of the free gas volume along the shroud on the chimney effect. However, in reality there is some ambient stratification (see Figure 2-2), which would reduce the flow rate. In the case of the reference well, the stratification is highest during the summer, causing a reduction of the flow of 7%.

At the same time, the reduction of free gas in the shroud (due to dissolution) will further reduce the induced flow rate. Back of the envelope calculations estimate that this reduction could be as much as 20% for the reference well shroud. Even though the influence of stratification and dissolution are not negligible, we are going to continue working with the flow rate calculated without these two effects; since a higher flow rate generally gives conservative results (smaller flow allows for better oil-water separation at the pen, a smaller pressure differential over the material which causes less collapse of the walls, and does not affect gas concentrations at the surface much because most of the gas comes out of solution again (Figure 5-3)). The only non-concervative result is related to hydrate formation; a higher flow rate reduces dissolved gas concentrations and therefore overestimates the safety margin with which the design avoids hydrate formation. Section 5.4 will get back to this to check whether a reduced flow rate could cause hydrates to form.

In the same way, based on the flow data and environmental conditions for Macondo (Section 2.1.2) we find that stratification would reduce the flow rate by 2%, but gas dissolution would reduce the induced flow rate by at least 20%. Together the two effects have a large effect

on the flow rate, however, we will use the high flow rate throughout the rest of the analyses. This is because using a high flow rate is conservative, except for the case of hydrate formation.

The checks on hydrate formation are stated in Sections 5.4 and 8.6, the results imply that a flow reduction as high as 50% would still not cause hydrate formation. Therefore, we will continue to work with the higher flow rate that does not take stratification and gas dissolution into account, since it is conservative with respect to all other design checks.

5.3 Gas Concentrations

Due to concern with workers safety at the sea surface, there are a number of regulatory thresholds governing maximum acceptable gas concentration. Gas concentrations are reduced to values below the flammability thresholds (*TEA report* (2011)), by choosing a shroud diameter that results in velocities and flow rates in the shroud that allow for enough gas to dissolve into the water. The flammability thresholds are given in % mol; a maximum number of mol of hydrocarbon relative to the mol air in a given volume:

- Upper flammable limit: 12.04 % mol
- Lower flammable limit: 2.90 % mol
- 0.5 of Lower flammable limit: 1.45 % mol

The calculations for the gas concentrations at the water surface are the same for the case with the shroud as for the free plume presented previously. Based on the bubble sizes and rise velocity the total volume of gas (free and dissolved) can be determined over depth. Equation 3.11 can still be used with the following two adjustments:

- Here the velocity includes both the slip velocity and the velocity induced by the chimney effect (which is related to the chosen shroud diameter).
- Due to a possible hydrate shell on the bubble, the rate of diameter change is reduced by a factor of 3, due to slower mass transfer and obstructed volume expansion (*Rehder et al.*, 2009)

Figure 5-2 shows how the diameter of the individual bubbles changes over depth. Combining that with the volume distribution of the bubbles, the concentration of free and dissolved gas in the water can be derived as they vary over depth. The total volume of dissolved gas at any given point has two origins; dissolution of the bubbles themselves, or gas that was dissolved in the oil at the wellhead but comes out of this solution as the oil ascends. For the latter it is assumed that the gas dissolved in the oil will immediately dissolve into the water, without becoming free gas first. If the dissolved gas concentration reaches the saturation level of that gas in the water (which changes over depth), the gas will come out of solution again to form free gas bubbles. This is why the free gas concentration increases again in the last $\sim$ 200m (Figure 5-3).

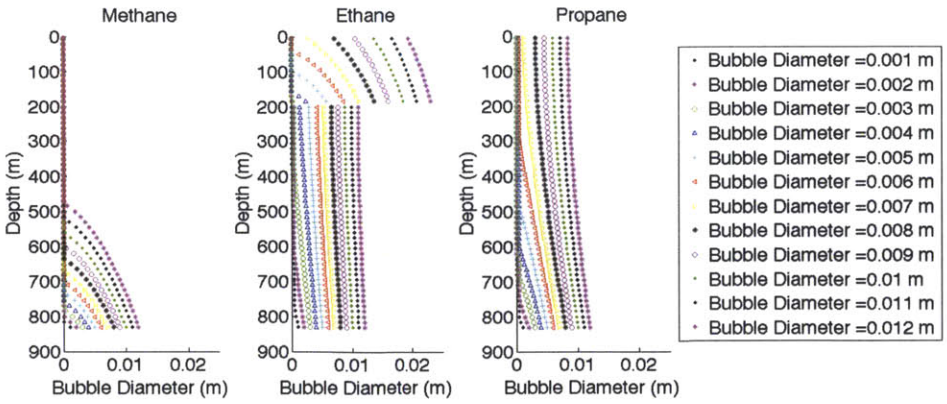

Figure 5-2: Reference well - Bubble/droplet diameter over depth

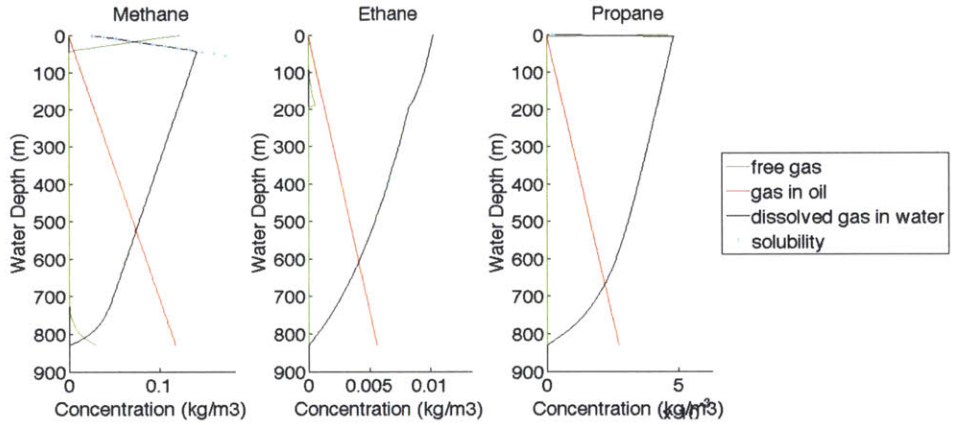

Figure 5-3: Reference well - Gas concentrations, oil concentrations and total gas out of well over depth, in the shroud. The blue stars indicate how much gas could dissolve in the water.

Once the gas reaches the top of the shroud, it gets slightly further diluted due to the larger diameter of the pen compared to the shroud. Above the water surface the gas concentrations need to be lower than the flammability thresholds. The concentrations in the air are based on the rate of free gas arriving at the surface and dilution by a wind speed of 6 m/s (*Glenn*, 1984) over a 20m pen diameter and an elevation of 10m. Table 5.2 gives the computed gas concentrations in the flow through the shroud for the reference well, as a percentage of the flammability thresholds.

Table 5.2: Reference well - Gas concentrations as % of flammable limits

Gas	% of 0.5 lower limit	% of lower limit	% of upper limit
Methane	5.95	2.98	0.72
Ethane	0.00018	0.00009	0.00002
Propane	0.081	0.040	0.010

Since these concentrations are well below the flammable limits, the shroud diameter of 3 meters and the pen diameter of approximately 20 meters satisfy the worker safety condition.

5.4 Hydrate Formation

When natural gas comes into contact with water under some conditions it forms ice-like crystals, that are referred to as hydrates, these have a tendency to agglomerate and form an ice-like slush. The dome BP used in an attempt to contain the spill from the Macondo well got plugged due to the formation and agglomeration of these hydrate crystals. Therefore it is important for us to understand the mechanism of hydrate formation to make sure that the shroud design eliminates any potential for hydrate clogging.

Hydrate formation is influenced by the following combination of conditions:

- High pressure
- Low temperature
- Gas composition
- Dissolved gas concentrations approaching their saturation concentration in water

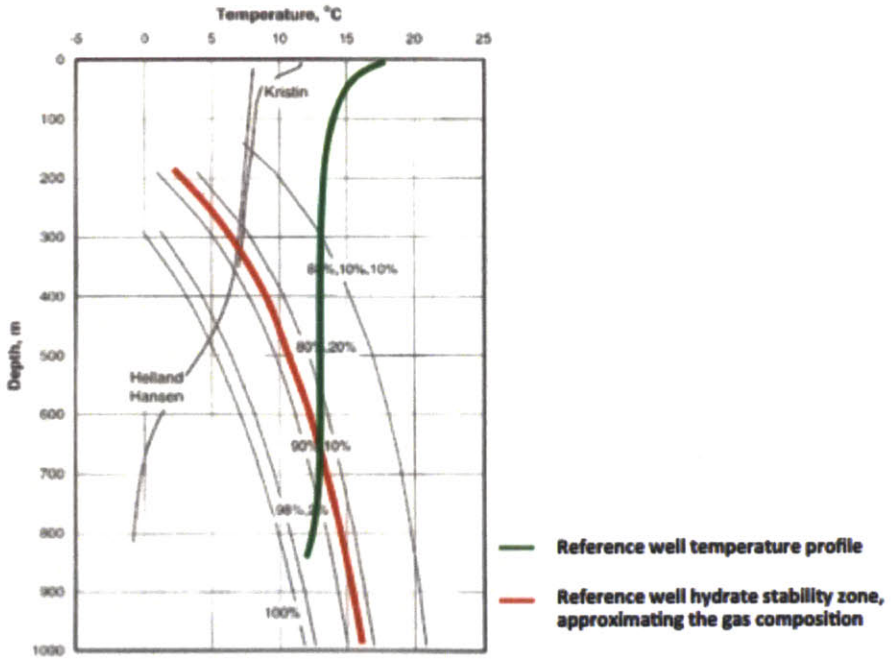

Figure 5-4: Thermodynamic conditions for hydrate formation (after *Johansen et al.* (1999)). The line referred to as 'Helland Hansen' represents the temperature-pressure combination for the Deep Spill experiment.

For the Macondo well we know that the conditions support hydrate formation; however for the reference well the conditions are more marginal. To understand if they will form the check is clearly to determine whether or not the combination of temperature and pressure at the reference well could support stable hydrate formation. Since higher C-chain hydrocarbons are more likely to crystalize (*Sloan and Koh*, 2008), the composition of the gasses influences the

zone in which the hydrates would be thermodynamically stable. Figure 5-4 indicates that for the reference well and its given gas composition, hydrates are thermodynamically stable in water depths below 650m, above the well depth of 830m. In order to prevent hydrate formation, the design of the shroud should guarantee that the dissolved gas concentrations are well below saturation.

For simplicity the calculations related to the hydrate issues are done for individual gasses (Table 5.3). Interpretation of the results should, however, take into account that the gas mixture would form hydrates more easily.

Table 5.3: Gas concentration data for the reference well

	Gas concentration in shroud (kg/m^3)	Saturation concentration (kg/m^3)	% of saturation in shroud
Flow rate = $242Am^3/day \approx 0.0028m^3/s$			
Methane	0.026	1.92	1.36
Ethane	0.004	5.12	0.08
Propane	0.002	5.19	0.04
Flow rate stock tank condition = $1.435m^3/s \approx 0.0144\ m^3/s$			
Methane	0.134	1.92	7.0
Ethane	0.020	5.12	0.40
Propane	0.009	5.19	0.18

The saturation concentrations of the individual gasses are calculated over depth using Henry's Law at 800m water depth, since this is where the hydrates would be most stable. The second column in Table 5.3 states the concentration of the gasses in the flow induced by a shroud with a 3m diameter (6.1 m^3/s), assuming that all gas dissolves. From the last column it can be seen that the gas concentrations are much lower than the saturation concentration. This means that at most the bubbles could obtain a hydrate shell on their surface, but would not form solid crystals.

Furthermore, the low percentages in Table 5.3 indicate that even if stratification and gas dissolution would cause a reduction of the flow rate by 50% (as mentioned in Section 5.2), hydrates still would not form. This justifies the assumption we made in Section 5.2 to work with the higher flow rate (ignoring the stratification and dissolution effect).

Two different gas flow rates are used in Table 5.3 to calculate the gas concentration as a percentage of saturation. The first is the actual gas flow rate at the wellhead. However, using this gas flow rate does not take into consideration that there is a large volume of gas dissolved in the oil. Using this gas flow rate therefore represents a non-conservative scenario, resulting in lower-bound percentages of saturation concentration. In response to that a second calculation is one using the stock tank conditions. The 'surface' flow rate is larger because as the hydrocarbons rise, some of the gas comes out of the oil. For this second calculation

all the available gas is assumed to contribute to the dissolved gas concentrations, which in reality is an unrealistic worst-case scenario, since not all the gas coming out of the well will be dissolved in water. But even with the surface value the concentrations are well below saturation. Furthermore, as can be seen in Figure 5-3 the gas concentrations in the shroud are (far) below the saturation concentrations, especially in the water depths where the hydrate crystals would be thermodynamically stable.

Another way to analyze the potential hydrate problem is to determine what percentage of the flow would be occupied by hydrate crystals, if all the gas were actually to form hydrate. If this percentage is high, the hydrates could conceivably plug the shroud, if there were a place for them to agglomerate. Assuming that hydrates are characterized approximately as $CH_4 \cdot 5.75H_2O$ (for methane and $C_2H_6 \cdot 7.67H_2O$ for ethane and $C_3H_8 \cdot 17H_2O$ for propane), stoichiometry can be used to determine how many mols of hydrates could form from the given gas flow. Given a hydrate density (which is approximately 10% lower than that of water), the hydrate volume, and therefore the percentage of the flow through the shroud, can be obtained as indicated in Table 5.4.

Table 5.4: Hydrate volume as % of the flow

Gas	Hydrate volume (m^3)	% of flow in Shroud
Methane	0.0015	0.024
Ethane	0.00017	0.0027
Propane	0.00013	0.0021
Total	0.0018	0.0288

The results show that even if all the gas were to react with seawater to become solid hydrate crystals, these crystals would only constitute a small fraction of the total flow through the shroud. Sloan and his collaborators have found through flow loop experiments that for water dominated systems the plugging risks are negligible for hydrate concentrations below 20%vol (*Sloan and Koh*, 2008). Given the fact that the hydrates are lighter than seawater, they will want to rise to the surface even without the flow from the shroud. During this ascent the crystals will start to "melt" as they approach the boundary of the thermodynamically stable zone, which is reached well before the surface. This implies that as long as there are no stagnant zones where the crystals could agglomerate, the hydrates would not obstruct the flow. The stagnant zones can be avoided by preventing flow separation. This is achieved by requiring that the angle of the shroud material relative to the vertical be less than about 10° (see Section 5.5.1).

We conclude that, even if solid hydrates were to form, which is extremely unlikely, they would not jeopardize the functionality of the shroud.

5.5 Structural Analysis

Shroud design is also influenced strongly by required strength. These structural requirements are related to the allowable deformation of the shroud due to induced pressure and drag and

the fact that the tensile stress on the shroud has to remain below the tensile stress of the Kevlar, with a safety factor of 1.5.

5.5.1 Global and Local Deformations

- *Mid-depth deflection*: drag from a current with uniform velocity will cause the shroud to bow, with maximum deflection at mid-depth (assuming mooring lines at the top and bottom only that constrain these points from any horizontal movement). We pick an allowable deformation (Δ/H, see Figure 5-5(a)) of 2.5% of the shroud length to ensure that the top of the shroud does not lower too far from the pen.

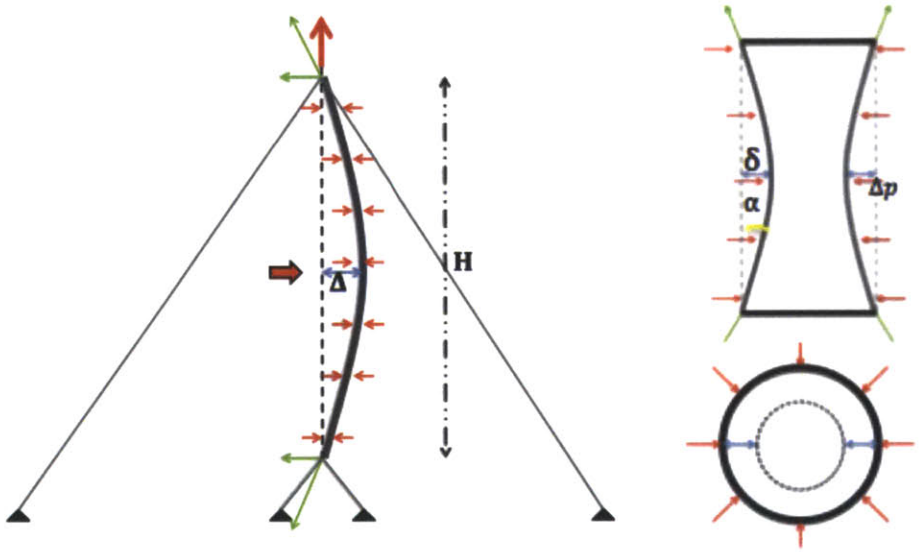

(a) (b)

Figure 5-5: (a) Global scale deflection due to current and the relevant parameters and (b) local deflection due the pressure differential over the material. The top figure in (b) is the side view, the bottom one shows the top view.

- *Remaining cross-sectional area*: the pressure difference between the outside and inside of the shroud will cause the sides of the shroud to be sucked inwards (Figure 5-5(b)). In order to avoid too much obstruction of the flow, we allow a maximum reduction in cross-sectional area of 20% ($\delta/D \sim 0.05$). In addition to reducing friction, this requirement will help avoid the formation of stagnant zones, which could encourage hydrate agglomeration.

- *Tensile stress*: composite fabrics require a high factor of safety. Therefore the calculated tensile stress in the material should not be higher than 67% of the tensile strength.

- *Pre-tension force*: this force needs to be generated by a buoyancy ring(s) at the top of the shroud. For example, for a shroud diameter of 3 meters and a rib spacing of 20 m, the maximum buoyancy is based on 210m^3 of air, which results in a maximum

pre-tension of 2.1 x 10^6 N. As discussed below, the magnitude of the pre-tension on the shroud and the spacing of the reinforcement ribs are design parameters that can be adjusted to satisfy all the requirements.

The forces on the shroud can be categorized into two groups: one on a global scale (the drag force) and the other on a local scale (pressure difference over the material). The chosen diameter has a strong influence on the magnitude of both forces.

The drag force on the shroud is given by:

$$F_D = 0.5\ \rho\ C_D\ D\ H\ u^2 \tag{5.5}$$

Name	Unit	Description
F_D	N	Drag force on the shroud
ρ	kg/m^3	Density of the ambient seawater
C_D	-	Drag coefficient (~ 1.2)
D	m	Diameter of the shroud
H	m	Length of the shroud
u	m/s	Average current velocity over depth

On the local scale, the maximum pressure difference is found at the bottom of the shroud an is described by Equation 5.6 as was described in Section 5.2:

$$\frac{\Delta p}{\rho} = \frac{u^2}{2}\ (1 + K) = \frac{\varphi^{2/3}\ B_0^{2/3}\ H^{2/3}}{A^{2/3}} \tag{5.6}$$

Name	Unit	Description
Δp	N/m^2	Pressure difference on the shroud
ρ	kg/m^3	Density of the ambient seawater
Q	m^3/s	Flow through the shroud
A	m^2	Cross-sectional area of the shroud
Φ	-	Friction coefficient
K	-	Entrance loss coefficient (≈ 0.8)

From the equations it is clear that a smaller diameter would decrease the drag force on the system, but would increase the pressure difference.

While our analysis will ultimately utilize a numerical model (OrcaFlex) to model the response of the shroud to realistic conditions, the analytical solutions can give us an initial understanding of the response of the system (to simplified environmental conditions). Furthermore, using these simple conditions, we can later on validate whether OrcaFlex is producing correct results. The analytical model is based on simplifications of reality using conservative assumptions. We assume that the shroud is moored at the top and the bottom, but that the mooring lines are only under a small tension, which for the stress calculation for the material

can be neglected. We also neglect the immersed weight of the shroud as we assume it is far less than the buoyancy added to the top, (which is true since the weight is less than 10% of the pre-tension) and neglect elastic deformation (assuming the shroud length to remain constant under tension). The ambient current is assumed to be uniform over depth with a speed of 0.2 m/s (whereas in reality it has similar, but opposite values at the top and bottom and is far less than 0.2m/s, so this value is an extreme condition) and the pressure difference between outside and inside of the shroud (Equation 5.6) is also assumed to be uniform over depth. The latter assumptions are conservative, therefore allowing the shroud to be to tested under 'extreme' loading. In OrcaFlex we will be able to model the system's response to more realistic currents (and waves).

In the absence of drag or suction, the shroud would remain vertical under tension due to the buoyancy ring at the top of the shroud. This tension (2.1 x 10^6N for 210T of buoyancy) acts in the vertical direction and, when distributed over the cross-sectional area of the shroud material (shroud perimeter times its thickness, or 0.019m^2 for a 3m diameter shroud with 2mm thickness), gives a tensile stress of about 112MPa, more than an order of magnitude less than the tensile strength of the Kevlar fabric (~1300MPa). In the presence of an ambient current and flow through the shroud, the vertical force due to buoyancy remains the same (with the assumption that the mooring lines do not play a dynamic role), but the horizontal forces due to drag and suction cause both global and local deflections (Δ and δ) which can be described using the catenary equation (Equation 5.7):

$$deflection = -\frac{T}{q_0} cosh(\frac{q_0 x}{T}) + \frac{T}{q_0} \tag{5.7}$$

Where T is the vertical tension force at the end of the the catenary (red vertical arrow in Figure 5-5(a)) and q_0 is the drag force per meter length for the global analysis and the pressure per meter length for the local analysis.

The deflections create an angle between the shroud and the vertical which can be used to compute the axial tension based on the square root of the sum of the squares of vertical and horizontal forces. Again dividing the axial tension by the cross-sectional area of the shroud gives the tensile stress. The horizontal deflections also cause the shroud to collapse vertically. If this contraction is too great, it could affect the ability of the surface pen to collect oil as it exits the shroud.

Table 5.5 summarizes the computed deflections and stresses for varying degrees of surface buoyancy, assuming a shroud diameter of 3m and a rib spacing of 20m. It is clear that as buoyancy increases, the global and local deflections decrease. The global deflection and the vertical collapse are small in all cases, but the local displacement (δ) and hence the remaining area are reasonably sensitive to buoyancy. To keep the remaining area greater than 80% and to avoid the shroud top from dropping more than several meters a surface buoyancy of about 210T is required. The last column shows the stress. Because the shroud is nearly vertical, the stress is only slightly larger than that for a taut shroud without a current or suction.

For example, the total stress with 210T of buoyancy plus drag and suction is 112MPa, only slightly larger than the stress of 111MPa due to buoyancy alone.

Table 5.5: Deflections and stresses for the reference well

Buoyancy (Tons)	Global deflection (Δ, m)	Local deflection (δ, m)	Remaining area %	Vertical displacement (m)	Total stress (MPa)
300	2.0	0.11	86.3	0.07	160
250	2.4	0.13	83.7	0.11	133
200	3.0	0.16	79.9	0.16	106
150	3.9	0.21	73.6	0.29	80
100	5.9	0.32	62.0	0.66	53
50	11.9	0.64	33.0	2.65	27

210T of buoyancy corresponds to approximately 20 rings of air, each of one meter diameter distributed around the circumference of the top shroud section. The required buoyancy scales with the square of the rib spacing, so this requirement could be reduced substantially, while keeping a remaining area equal to 80%, by reducing the rib spacing. The sensitivity of the different design parameters is given in Table 5.6, related to our chosen"base case" (3m diameter, 20m rib spacing and 210T buoyancy).

Table 5.6: Structural sensitivity to design parameters

	Base Case	Diameter = 4m	Rib Spacing = 10m	250tons Pretension
Tensile Stress (MPa)	112	112	112	133
Hydrates (% of flow)	0.029%	0.020%	0.029%	0.029%
Gas Concentrations (% of flammability)	$< 6.4\%$	$< 5.1\%$	$< 6.4\%$	$< 6.4\%$
Mid-depth deflection	2.8m	3.8m	2.8m	2.4m
Remaining area (%)	80%	81%	95%	84%

5.5.2 Reinforcement Rib Integrity

So far two phenomena have been discussed that influence the design of the ribs:

- *Buoyancy*: the design of the ribs should help compensate for the positive wetted weight of the Kevlar; this is why the syntactic foam is added onto the ribs.
- *Structural considerations*: 20m spacing between ribs.

Here we are going to focus on the latter point. The buckling strength needs to be greater than the force on the rib from the net external pressure on the material. The buckling force

(per meter circumference) on each rib is the pressure that is on the material between two consecutive ribs:

$$F = \Delta p * s \tag{5.8}$$

Name	Unit	Description
F	N/m	Force per meter acting on each rib
Δp	N/m^2	Maximum pressure differential on the Kevlar
s	m	Rib spacing

That force can then be compared to the strength of the ribs agains buckling. According to *Timoshenko* (1970) this strength is defined in the following way:

$$q = \frac{EI}{r^3} \tag{5.9}$$

$$I_{zz} = \frac{1}{12}\, t\, h^3 + 2\,(\frac{1}{12} b\, t^3) + b\, t\,(\frac{h}{2} + \frac{t}{2}) \tag{5.10}$$

Name	Unit	Description
q	N/m	Force per meter at which the rib would buckle
E	N/m^2	Young's modulus of the rib material
I	m^4	Mass Moment or Inertia of the cross-section
r	m	Radius of the rib $\sim$ Radius of the shroud
b, t, h	m	Dimensions of the flanges of the I-rib

The design presented in Section 4.2.2 can resist the force from the pressure differential as stated in Equation 5.8 (i.e. $q > F$); meaning that buckling of the ribs is not a concern.

5.6 Pen Behavior

5.6.1 Oil - Water Separation

The separation of the oil from the water is based on their relative velocities. Within the space beneath the oil-water interface, oil droplets will rise vertically toward the pen, relative to the water, at their slip velocity, which depends on the diameter of the droplet. Oil droplets ranging from 1mm - 10mm diameter (as is expected for the reference well) have respective slip velocities range from 0.05m/s - 0.25m/s. Meanwhile water flows out of the shroud at a calculated rate of 6.1 m^3/s. Approximating the water velocity as this flow rate divided by the cross-sectional area of the pen yields a nominal velocity for an 20m diameter pen of 0.019 m/s. This is over 2.5 times smaller than the smallest droplet slip velocity, suggesting that (nearly) all of the oil droplets will be captured. However, the hydrocarbon and water plume exiting the shroud top will not have filled the entire cross-sectional area of the pen by the time it reaches the surface, so realistically the factor between the velocities is smaller than

2.5. In order to aid the separation, the baffle is added which will slow down the jet of water and hydrocarbons exiting the shroud and spread the hydrocarbons across the pen area better, allowing more opportunity for the oil droplets to separate from the water.

5.6.2 Interaction of the Pen with the Waves

The response of the pen to the waves depends on how the natural frequency of the pen compares to the wave frequency. The (angular) wave frequencies can be deduced from the wave periods (T) mentioned in Table 1.1 (i.e., $\omega = 2\pi/\mathrm{T}$), and range from $0.75 - 3.15\ \mathrm{s}^{-1}$. On the other hand the natural frequency of the pen in heave can be found approximately by modeling it as a mass-spring system whose natural frequency is given by:

$$\omega_{\mathrm{n}} = \sqrt{\frac{\rho_{\mathrm{water}} * \mathrm{g} * \mathrm{A_s}}{\mathrm{M_{pen}} + \mathrm{M_{added}}}} \tag{5.11}$$

where ρ_{water} is the density of seawater, $\mathrm{A_s}$ is the areal footprint of the pen at the water surface, g is gravity, $\mathrm{M_{pen}}$ is the mass of the pen and $\mathrm{M_{add}}$ is the added mass. The frequencies can then be compared using a frequency response diagram, as shown in Figure 5-6, which depicts both a damped and an undamped response.

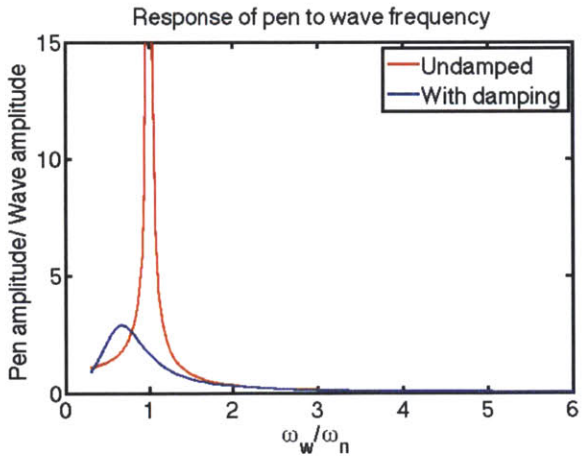

Figure 5-6: Frequency response diagram

Resonance occurs when the natural frequency of the pen is the same as that of the waves, which would jeopardize the proper functioning of the pen. Therefore the pen needs to be designed such that the non-dimensional wave frequency ends up far away from (on either side of) this resonance peak. On the right side of the peak, $\omega_{\mathrm{waves}} \gg \omega_{\mathrm{pen}}$, the pen would tend to be stationary (not responding to the waves). However, the natural frequency would have to be very low, requiring excessive pen depths or densities, which are impractical. Left of the peak, where $\omega_{\mathrm{waves}} \ll \omega_{\mathrm{pen}}$, the pen would ride the waves which is the preferred behavior. This requires a large natural frequency compared to the wave frequencies, which in turn dictates small pen depths or densities. To be conservative we choose a relatively short design wave

period (3 sec) giving a relatively large wave frequency of $\sim 2s^{-1}$. This is conservative because such short waves usually have small amplitudes, which should not cause problems. For initial design purposes, we require the pen's natural frequency to be at least three times the wave frequency (i.e. $\omega_{pen} > 6s^{-1}$). For a system consisting of two rings (each with a diameter of 1m and a net density of 300 kg/m^3, based on combination of air and Kevlar and their respective volumes), a fence/skirt combination (Kevlar with thickness of 2mm, net density of 1400 kg/m^3, height above the water surface of 2.5m, and depth below the surface of 7.5m), and assuming an added mass equal to half of the total pen mass, the natural frequency is 6.4, consistent with $\omega_{pen} > 3\omega_{wave}$. Many other combinations of the design variables are possible as well, but the ones mentioned above are chosen since then allow the pen to ride the wave with realistic/practical dimensions.

Further analysis regarding pen behavior will be performed using the OracaFlex software tool and is described in the next chapter.

Chapter 6

Reference Well - OrcaFlex Simulations and VIV Analysis

OrcaFlex (developed by Orcina Ltd.) is a finite element software package for dynamic analysis of the behavior between offshore structure and waves and currents. OrcaFlex has a large library of structural elements commonly used by the offshore industry, making it a widely used tool in the offshore engineering industry.

This chapter describes the design components used in the simulation to correctly model the behavior of the shroud. Further, a short description of the environmental input is given before proceeding to describe the aspects of the design that are not included into the simulations due to constraints of the software. The second half of the chapter gives the results of the OrcaFlex simulations for the reference well.

6.1 Modeling Setup

6.1.1 Model Components

The components of the model are the following:

- Shroud
- Mooring lines
- Air can(s)
- Pen (and its connection to the shroud)
- Environment

6.1.2 Shroud

The shroud is modeled as a general line component; the line type data is presented in Table 6.1. The modeling approach of a line type as well as the design values associated with it represent the shroud design exactly the way it would be in real life.

Table 6.1: OrcaFlex shroud line type data for the reference well

Data Type	Design Value
Outer Diameter [m]	3
Inner Diameter [m]	2.996
Mass per unit length (in air) [te/m]	0.023
Bending Stiffness (x-direction) [kNm^2]	$1.608 * 10^6$
Bending Stiffness (y-direction) [kNm^2]	$\sim$
Axial Stiffness [kN]	$1.433 * 10^6$
Poisson Ratio [-]	0.34
Torsional Stiffness [kNm^2]	$254 * 10^3$
Drag Coefficient (x) [-]	1.2
Drag Coefficient (y) [-]	$\sim$
Drag Coefficient (z) [-]	0.008

Shroud Connection

During operation the shroud will be moored from the bottom in a manner that will (almost) entirely restrict it from any movement. Therefore the connection at the bottom is modeled as an anchor 18m above the seabed. At the top of the shroud, it will be connected to the mooring lines. In OrcaFlex the mooring lines are modeled as lines, which cannot be directly connected to another line. Therefore a 3D buoy realizes this connection. The 3D buoy has an initial position at 10m below the sea level and negligible mass, volume and stiffness characteristics.

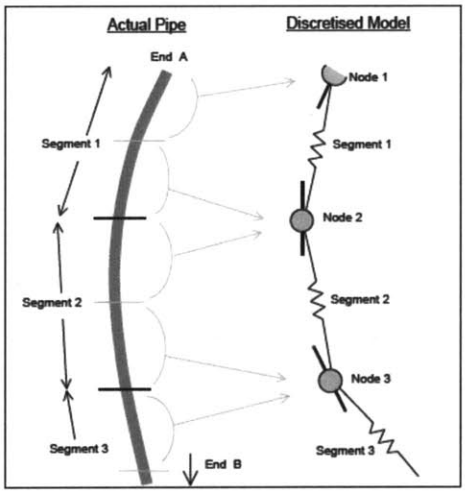

Figure 6-1: Model showing how OrcaFlex simulates a line made up of segments

Structure

The line representing the shroud is divided into three sections, where the first and third sections (each 20m) represent both ends of the shroud, which have a smaller segment length (Figure 6-1). Lines are divided into a series of line segments, which are then modeled by

straight massless model segments with a node at each end. Characteristics of each segment are attributed to the two nodes at either end of it. The choice of segment length therefore governs the accuracy of the model. The smaller the segment length, the more detailed the behavior simulated. The smaller segment length (0.5m instead of 10m elsewhere) is chosen so that OrcaFlex can model the behavior of the shroud around the connections in a more detailed fashion.

Attachments

The air cans are modeled as clumps that are attached to the shroud (see Section 6.1.4). The number of attachments and their position relative to the top of the shroud are given as line data to the shroud. However, further details will be discussed in the section on the air cans.

Contents

Since the shroud is modeled as a hollow, flexible cylinder the content of the hollow cylinder has to be defined. In order for OrcaFlex to account properly for the behavior of the hollow cylinder the contents needs to be set to free flooding, which means that the cylinder is assumed to be filled with ambient water.

6.1.3 Mooring Lines

The mooring lines are a combination of wire and chain. The line types are chosen from the database in the OrcaFlex database (wizard). Table 6.2 presents the characteristics of the chosen line types.

Design

Table 6.2: OrcaFlex mooring chain line type data for the reference well

Data Type		Wire Design Value	Chain Design Value
Diameter [m]		0.04	0.189
Mass per unit length (in air) [te/m]		0.01	0.219
Bending Stiffness [kNm^2]		0	0
Axial Stiffness [kN]		$101 * 10^3$	$1.101 * 10^6$
Poisson Ratio [-]		0.5	0.5
Torsional Stiffness [kNm^2]		80	80
Drag Coefficient [-]		1.2	1
Axial Drag Coefficient [-]		0.008	0.4
Drag/Lift Diameters [m]			
	Normal	-	0.226
	Axial	-	0.019

Connection

Each mooring line is anchored at the bottom end (end B) and attached to the Shroud Top (3D buoy) to connect it to the top of the shroud on the other end. The relative position to the Shroud Top is 0 in all directions. The anchoring position for each of the mooring lines is found in Table 6.2. Furthermore, the connections have no stiffness.

Structure

Slightly less than half of each mooring line is wire; the rest is chain most of which will be resting on the seafloor. Both sections have 10m long segments, no attachments, contents, etc.

6.1.4 Air Can(s)

The air can is modeled as a clump that is attached to the shroud, since in the design the buoyancy will move with the top of the shroud. The mass, volume and height of the clump are assigned according to the design of the system and its requirements. Furthermore, the clump alignment is chosen to be in line with the axis of the line that it is attached to, in this case the shroud. In order to simulate the fact that the air can runs several meters along the shroud, we model the air can as a number of clumps with a smaller volume that are attached to the shroud along its top 10-20m. The total volume of the smaller clumps is equal to the required buoyancy force. The (center of mass of the) first clump is attached 1.5m from the top of the shroud, to account for its height. Each following clump is attached at a distance that leaves a bit of space between the two consecutive clumps, so that they do not interact with each other.

6.1.5 Pen

A 6D-Spar buoy is used to model the pen (Figure 6-2), since it is necessary to model all 6 degrees of freedom, as well as to be able to input the geometry. A lumped 6D buoy would not

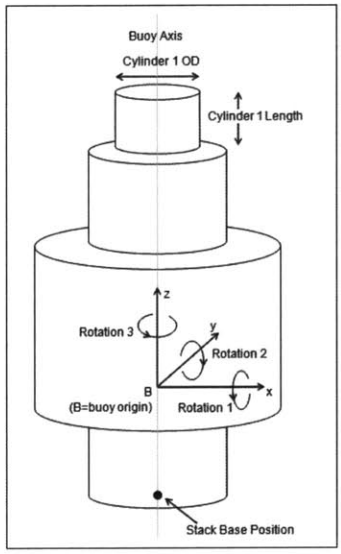

Figure 6-2: OrcaFlex 6D buoy model

allow for the latter; however that type of buoy does give the option to enter the rotational stiffness (related to the yaw of the pen) which would have been useful (as will be discussed in the Results section 6.3.2). In the end it is more important to model the geometry correctly, so a 6D spar buoy is chosen to represent the pen.

Two cylindrical components are used to model the components of the pen. The top cylinder represents the buoyancy rings of the pen and the fence, while the skirt of the pen is embodied by a second, long, very thin cylinder. A disadvantage of the OrcaFlex model is that the cylinders are modeled as rigid cylinders, which could have some effect on the modeled behavior of skirt in relation to reality. In the same wizard, the mass, mass moments of inertia, center of mass and initial position can be identified for the buoy. Furthermore, the buoy is not considered in the static calculations, because, if it is, the solution becomes unstable and OrcaFlex can no longer solve the problem. Therefore, the degrees of freedom of the spar buoy are only included in the dynamic calculations. The last pen characteristics that need to be assigned are the drag coefficients on each of the cylindrical components. The drag areas can be calculated based on the geometry by OrcaFlex, while the drag coefficients are assigned, in this case to have a value of one.

Lastly, when defining the parameters of the buoy itself, no connections should be described. In fact this is similar to what in reality will be the case, since the pen is in fact a free moving object, constrained only by wires connected to the top of the shroud. In OrcaFlex these wires are modeled as springs/dampers, that allow elastic connections to points and specification of the characteristics of the link. Since in theory the spring/dampers can take compression, the characteristics of the links here were set such that they would not go into compression. The links are located at half of the length of the pen skirt; the other end is connected to the 3D buoy representing the shroud top, which is also the location where the mooring lines are connected to the shroud. The links are however attached at an offset of 2.5m from the center of the 3D buoy, so 1m from the shroud edge. This helps constrain the pen from rotating too much around its own axis (yaw).

6.1.6 Environment

This tab of parameters is where the characteristics of the seawater and seabed, as well as the waves and currents are described. A flat seabed is chosen, with a constant water density.

Waves

For most simulations, the waves are modeled as one wave train in a given direction with a specific wave height and wave period. The expectation is that this will simplify the interpretation of the results of the shroud and pen behavior. Several combinations of wave heights and periods are chosen and evaluated to get an understanding of when the response of the systems becomes worse.

Currents

The current is only varied in the vertical direction to test the shroud behavior to realistic conditions. Several data points are inserted into the data table in OrcaFlex, from which a current profile is produced through linear interpolation.

6.1.7 Differences with the Design

There are at least four aspects of the design that cannot be or are not modeled using OrcaFlex (as far as is known); these are the chimney effect, the reinforcement ribs, the 100m sections and the bottom mooring. A way to model the flow through the shroud is to use the 'contents' tab for the line representing the shroud. As described above the simulations use a free flooding content. This means that the water does not flow through the shroud, and therefore there is no pressure differential over the material. OrcaFlex does have the option to introduce a uniform flow through the hollow line; however the results did not seem to match well with expectations. Since it is not known how best to model the pressure difference induced by the hydrocarbon flow, the decision was made to exclude this from the simulations and to rely on the analytical approach described in Chapter 5. Furthermore, OrcaFlex would not be able to show the effect of the differential pressure on the internal cross-sectional area of the shroud. Therefore, attempts to represent the flow correctly were not pursed further.

Even though the reinforcement ribs can not be designed in OrcaFlex, they are still taken into account in the entered weight per meter length of the shroud. That they are not considered in any further way should not affect the results from the mode. This issue combined with the previous point means that the material response to the pressure differential is not taken into account.

Similarly, it is not well understood how to model an articulated line that is split into several sections that are connected by a structural component that has hinge-like characteristics. Therefore, the shroud is modeled as a single long line, instead of 100m sections. This should not have an effect on the results found during the simulations.

Finally, as mentioned before, the bottom of the shroud is assumed to be stationary. In reality it will be moored similarly to the top of the shroud, which means that it could move several meters (like the top of the shroud but to a lesser degree). In order to verify this assumption, several simulations were run with bottom mooring lines, consisting of just chain along their full lengths. These simulations showed indeed that the bottom of the shroud barely moved; therefore the rest of the simulations were run with the bottom of the shroud anchored in the previously stated position.

6.2 Modeling Steps

In order to understand the results that OrcaFlex produces, the modeling is done in incremental steps, leading up to the most realistic scenario with a non-uniform current, and a

monochromatic (characteristic) wave on a shroud with pen. As can be seen in Table 6.3, the first step includes just the uniform current, since these results can be compared to the analytical calculations. Since the results made sense, the next step is to add on the pen. From there, we include other basic steps: the non-uniform current, the monochromatic wave and the monochromatic wave with the uniform current. Each of these can be seen as an elementary step, after which the pen can be added to understand how this affects the behavior of the shroud. Lastly, an attempt was made to create a wave spectrum using the wizard in OrcaFlex. However, as mentioned before, it is not clear whether the results from this spectrum analysis will help determine the response to more realistic conditions.

Table 6.3: OrcaFlex modeling steps

	Uniform Current	Non-Uniform Current	Monochromatic Wave	Wave Spectrum	Pen
1	x				
2	x				x
3		x			
4		x			x
5			x		
6	x		x		
7			x		x
8	x		x		x
9				x	
10	x			x	
11				x	x
12	x			x	x

6.3 Simulations

This section presents the data used for the simulations for the reference well specifically, and walks through the results that we found with OrcaFlex for each of the modeling steps. The results will indicate whether the chosen design works under realistic environmental conditions.

6.3.1 OrcaFlex Data for the Reference Well

The data used for the reference well design is stated in Table 6.4.

Table 6.4: OrcaFlex data for the reference well

Data Type	Design Values	
Shroud Length	800m	
Mooring Line Locations	X	Y
Mooring Line 1	1600m	$0m$
Mooring Line 2	−800m	1385.6m
Mooring Line 3	−800m	−1385.6m
Mooring Lines		
Total Length	1880m	
Wire	900m	
Chain	980m	
Air Can Volume	$520m^3$	
	Split over 4 clumps of $130m^3$. Attachment points of clamps: 1.5m, 4.5m, 6.5m and 9m from the top of the shroud.	
Pen		
Diameter	20m	
Skirt Length	7.5m	
Fence height	2.5m	
Links		
Length [m]	12m	
Stiffness	500kN/m	
Offset from Shroud Top	2.5m	
Environmental Conditions		
Uniform Current	0.2m/s	
Non-Uniform Current	See Figure 2-3	
Monochromatic Wave		
- Significant Wave Height	2.5m	
- Peak Wave Period	6s	

6.3.2 OrcaFlex Results for the Reference Well

Uniform Current

For the pre-tension of 210tons, the analytical results give a mid-depth deflection of 2.8m and a tensile stress of 112MPa, while OrcaFlex gave 3.6m and 111MPa (Table 6.5 and Figure 6-3). The differences between these results can be attributed to the fact that the top and bottom supports are not completely aligned, as assumed in the catenary calculations, and the fact that the buoyancy force is distributed. Simulations run for a shroud with two simply supported ends find values for the stress and displacement that are within a small margin from the analytical values. These simulations therefore imply that the results are in agreement with one another. The analytical results indicate that this pre-tension will make sure that the pressure difference over the material will cause the area in the shroud to reduce by a maximum of only 20%. This means that there will not be any stagnant zones in the shroud where hydrates could form and accumulate.

Table 6.5: Reference well - OrcaFlex results for a uniform current

Variable	OrcaFlex Results
Maximum Deflection	3.58m
Location of Shroud Top	1.45m
Net Tension on the Shroud	2188kN
Tensile Stress	111.5MPa
Tension in the mooring lines	
Mooring Line 1	1563kN
Mooring Line 2	1532kN
Mooring Line 3	1532kN

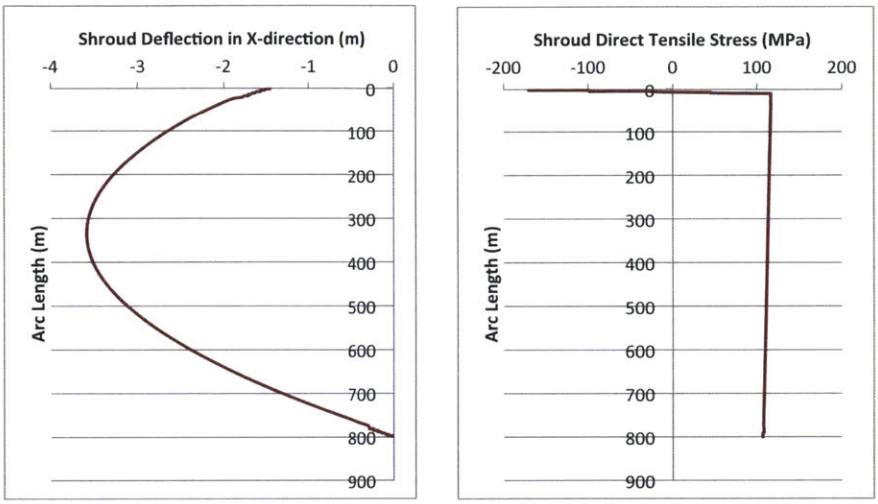

(a) (b)

Figure 6-3: Reference well - Shroud displacement (a) and tensile stress (kPa) (b) due to a uniform current.

Uniform Current with Pen

As can be seen from the results in Table 6.6, Figure 6-4 and Figure 6-5, in comparison to the results in the previous paragraph, addition of the pen does not influence the behavior of the shroud very much. Due to the effect of drag on the pen, the displacement of the shroud in the x-direction (direction of the current) is slightly increased. Since the static analysis is done without the pen, the simulations show how the whole system shifts in the negative x-direction (the current flows from positive to negative x-values) during the dynamic simulation, after which it mostly returns back slightly before finding a new equilibrium position. Another interesting observation is that the pen starts to rotate around its own axis (yaw) due to the current, Figure 6-6(b). However, due to the links, the pen does not rotate beyond 40 degrees, which is when the links become taut.

Table 6.6: Reference well - OrcaFlex results for a uniform current and pen

Variable	OrcaFlex Results
Maximum Deflection	3.64m
Location of Shroud Top	1.56m
Net Tension on the Shroud	2190kN
Tensile Stress	111.6MPa
Tension in the mooring lines	
Mooring Line 1	1565kN
Mooring Line 2	1531kN
Mooring Line 3	1531kN

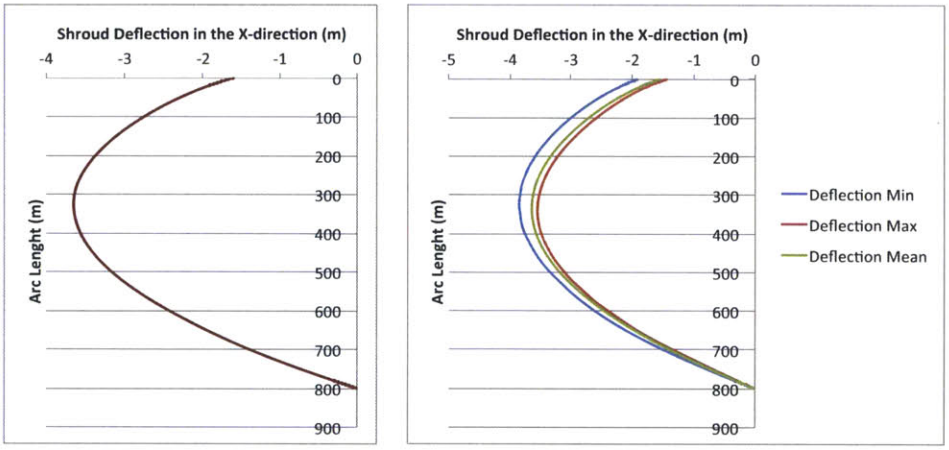

(a) (b)

Figure 6-4: Reference well - Shroud deflection with uniform current and pen (a) at t = 250s and (b) for the whole simulation.

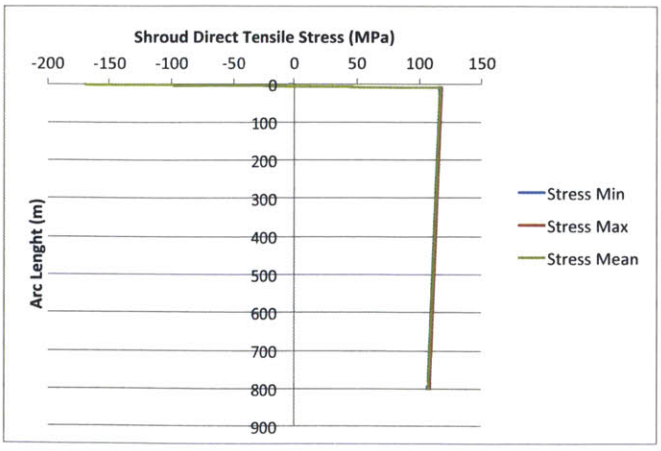

Figure 6-5: Reference well - Tensile stress (kPa) for uniform current with pen

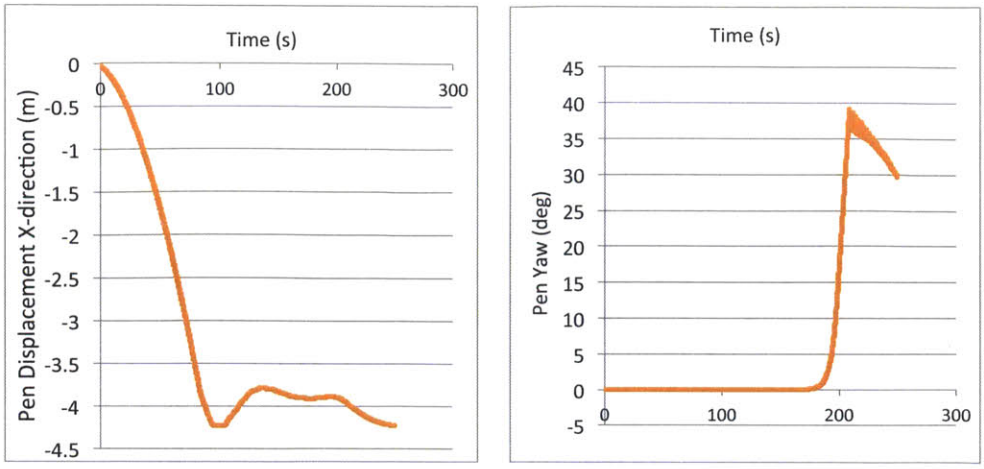

(a) (b)

Figure 6-6: Reference well - Displacement of the pen in x-direction over time for a uniform current and (b) pen rotation around its own axis (yaw) due to a uniform current.

Non-Uniform Current (with Pen)

In the section on the environmental data for the reference well, it is clear that the currents are generally significantly slower than the 0.2m/s uniform current, and they also vary over depth. The lower current speeds lead to a smaller deflection and a smaller contribution to the tensile stress in the material (see Table 6.7 and Figure 6-7). As could be predicted with the analytical model, this means that the tensile stress remains close to that caused by the buoyancy force alone. Furthermore, the catenary shape of the shroud deflection is lost due to the high currents that are focused at the top as seen in Figure 6-7(a). All together, the true conditions are less strenuous on the system than the 0.2m/s uniform current for which it was designed.

Table 6.7: Reference well - OrcaFlex results for non-uniform current (and pen)

Variable	OrcaFlex Results	
	Without Pen	With Pen
Maximum Deflection	0.29m	0.33m
Location of Shroud Top	0.17m	0.22m
Net Tension on the Shroud	2187kN	2188kN
Tensile Stress	111.4MPa	111.5MPa
Tension in the mooring lines		
Mooring Line 1	1545kN	1546kN
Mooring Line 2	1541kN	1541kN
Mooring Line 3	1541kN	1541kN

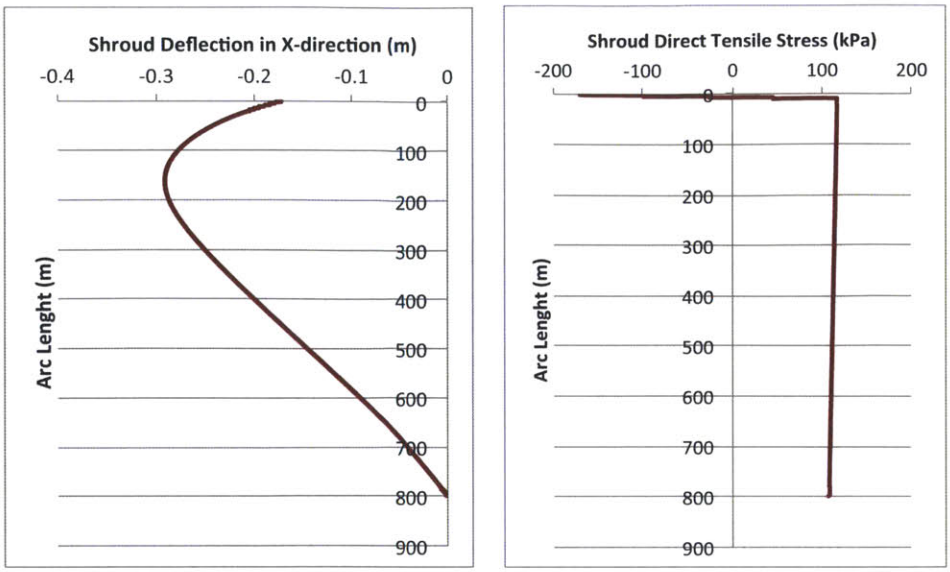

(a) (b)

Figure 6-7: Reference well - (a) Shroud displacement and (b) tensile stress on the shroud due to non-uniform current

Monochromatic Wave

Due to the orbital motion of the wave, the shroud is forced back and forth. The oscillatory motion has a maximum amplitude of approximately 0.5m (see Table 6.8). As Figure 6-8(a) shows, the deflection takes place along the entire shroud, but is slightly reduced towards the bottom. As can be seen from the movement of the top of the shroud (Figure 6-9), there is an equilibrium position around which the oscillations take place. The period of the moment is in line with the wave period. The amplitude of the movement is smaller than the wave height, and is assumed to depend on the stiffness of the system. The higher the stiffness, the smaller the deflection, such that the deflection is no longer identical to the wave height. Due to the oscillatory movement, the tensile stress on the material varies over time (Figure 6-8(b)). The maximum stress on the material is higher than that due to just the uniform current, but still far below the ultimate stress that it can take ($\sim$ 1300MPa).

Table 6.8: Reference well - OrcaFlex results for a monochromatic wave

Variable	OrcaFlex Results
Maximum Deflection (Amplitude)	0.5m
Location of Shroud Top	0.4m
Net Tension on the Shroud	1370kN - 2187kN - 2864kN
Tensile Stress	68MPa - 111MPa - 147MPa
Tension in the mooring lines	
Mooring Line 1	1468kN - 1545kN - 1623kN
Mooring Line 2	1472kN - 1541kN - 1609kN
Mooring Line 3	1472kN - 1541kN - 1609kN

Besides a high ultimate strength, the material must also have good fatigue resistance characteristics, due to the oscillatory motion. Fortunately, it seems that Kevlar (fibers) can handle cyclic forces for a time that exceeds the life expectancy of the system for the order of magnitude of the force that it is exposed to, especially as long as it remains under tension (*Burgoyne*, 2013).

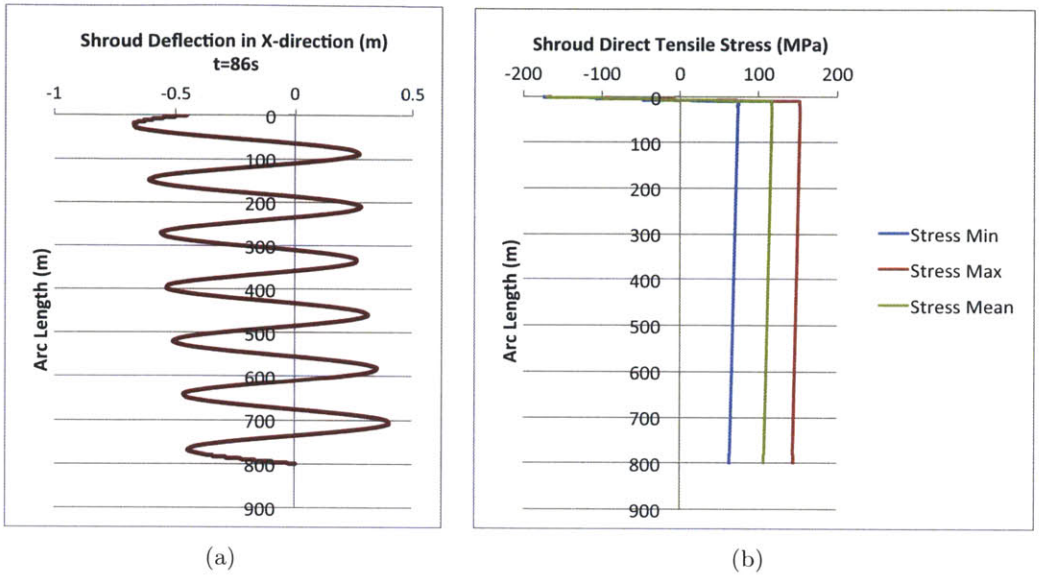

(a) (b)

Figure 6-8: Reference well - (a) Shroud displacement (m) at t = 86s and (b) tensile stress (kPa) on the shroud due to a monochromatic wave

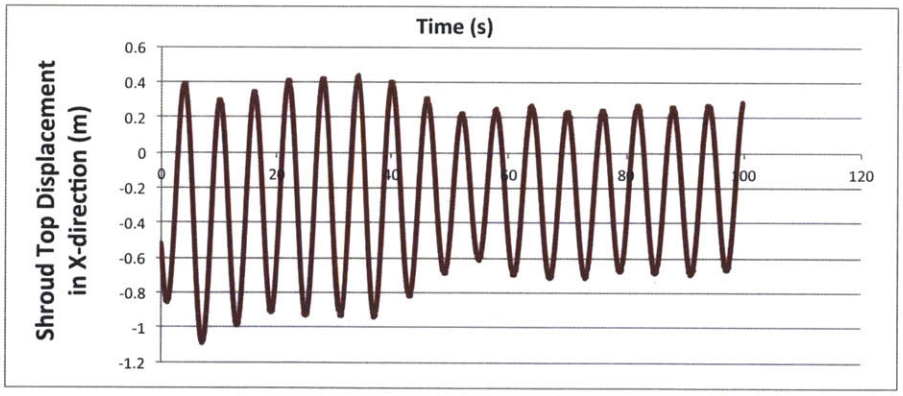

Figure 6-9: Reference well - Shroud top displacement in x-direction over time due to a monochromatic wave

Monochromatic Wave with Pen

The movement of the shroud is mostly similar to that without the pen (as was already inferred for the uniform current) as can be seen in Table 6.9 and Figures 6-10 and 6-11. From Figure 6-12 it can be seen that, due to the pen, there is a second order behavior in the oscillatory movement of the shroud, which means that there is no longer a clear equilibrium position

around which it oscillates. The oscillations still have the same period as the waves and the amplitude of the oscillations are hardly influenced by the presence of the pen.

Another interesting observation is the response of the pen itself to the wave motions. The design does well for the given monochromatic wave; it would be able to retain a significant layer of oil, without any 'spilling out'. However, it does pitch somewhat, which restricts how long the system would be able to collect oil without the need of a tanker pumping the oil from the pen. The other rotational movement of the pen is around its own axis (yaw); this rotation is kept under control by the links. The length of the links was chosen such that this rotation would have a maximum of 100 degrees (see Figure 6-13), without jeopardizing any other response of the pen to the waves. These calculations were done for static conditions.

Table 6.9: Reference well - OrcaFlex results for a monochromatic wave with the pen

Variable	OrcaFlex Results
Maximum Deflection	0.6m
Location of Shroud Top	0.1m
Net Tension on the Shroud	1336kN - 2194kN - 2860kN
Tensile Stress	67MPa - 113MPa - 148MPa
Tension in the mooring lines	
Mooring Line 1	1468kN - 1547kN - 1626kN
Mooring Line 2	1472kN - 1539kN - 1609kN
Mooring Line 3	1472kN - 1540kN - 1609kN

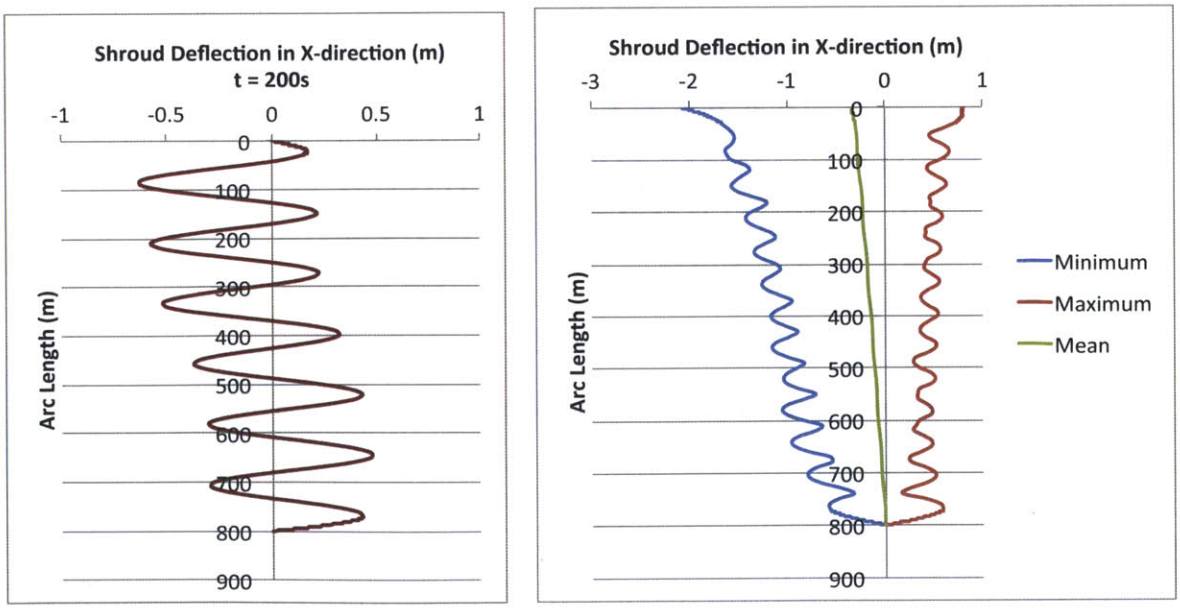

(a) (b)

Figure 6-10: Reference well - (a) Shroud displacement at t = 200s and (b) for the whole simulation due to a monochromatic wave with pen

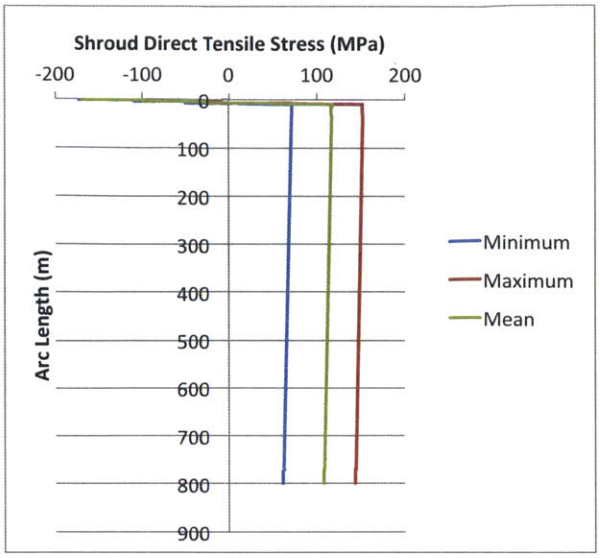

Figure 6-11: Reference well - Tensile stress (kPa) on shroud due to monochromatic wave with pen

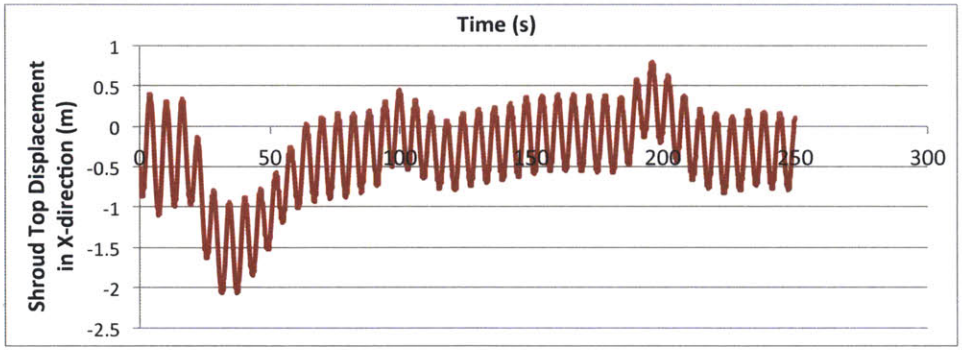

Figure 6-12: Reference well - Shroud top displacement in x-direction over time for a monochromatic wave with pen

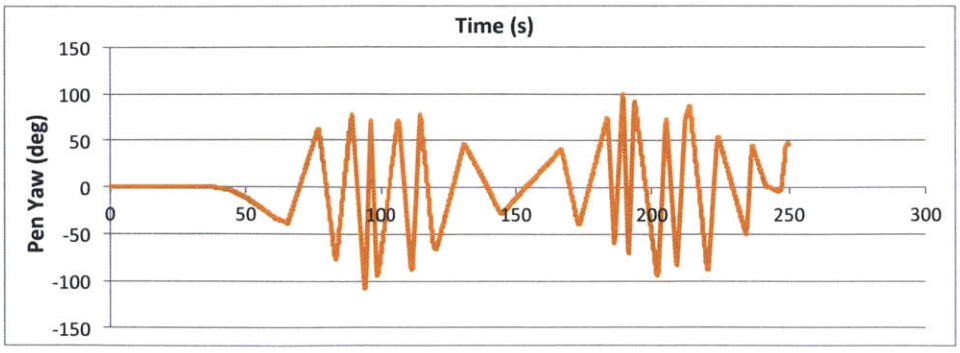

Figure 6-13: Reference well - Pen rotation around own axis (yaw) over time due to monochromatic wave

Monochromatic Wave and Uniform Current (with Pen)

The response of the shroud to the monochromatic wave and a uniform current looks as if the oscillatory motion of the wave response has been superimposed onto that of the uniform current. The equilibrium position of the oscillatory motion has become that due to the uniform current. Therefore, addition of the pen gives results that are similar to those for the monochromatic wave and pen alone. However, due to the uniform current, the oscillations are now offset to be around the catenary shape that the shroud takes on in response to a uniform current. The values of the displacement, tensile stress, etc. without the pen can be found in Table 6.10 and Figure 6-14 and Figure 6-15 and results for the simulations with the pen can be found in Figure 6-17, Figure 6-18 and Figure 6-19.

Table 6.10: Reference well - OrcaFlex results for a monochromatic wave and uniform current (with pen)

Variable	OrcaFlex Results	
	Without Pen	With Pen
Maximum Deflection	7.4m	7.5m
Location of Shroud Top	3.2m	3.9m
Net Tension on the Shroud	1462kN - 2190kN - 2802kN	1459kN - 2201kN - 2832kN
Tensile Stress	74MPa - 113MPa - 145MPa	74MPa - 113MPa - 147MPa
Tension in the mooring lines		
Mooring Line 1	1496kN - 1585kN - 1652kN	1496kN - 1593kN - 1667kN
Mooring Line 2	1459kN - 1519kN - 1594kN	1458kN - 1518kN - 1594kN
Mooring Line 3	1459kN - 1519kN - 1594kN	1435kN - 1514kN - 1594kN

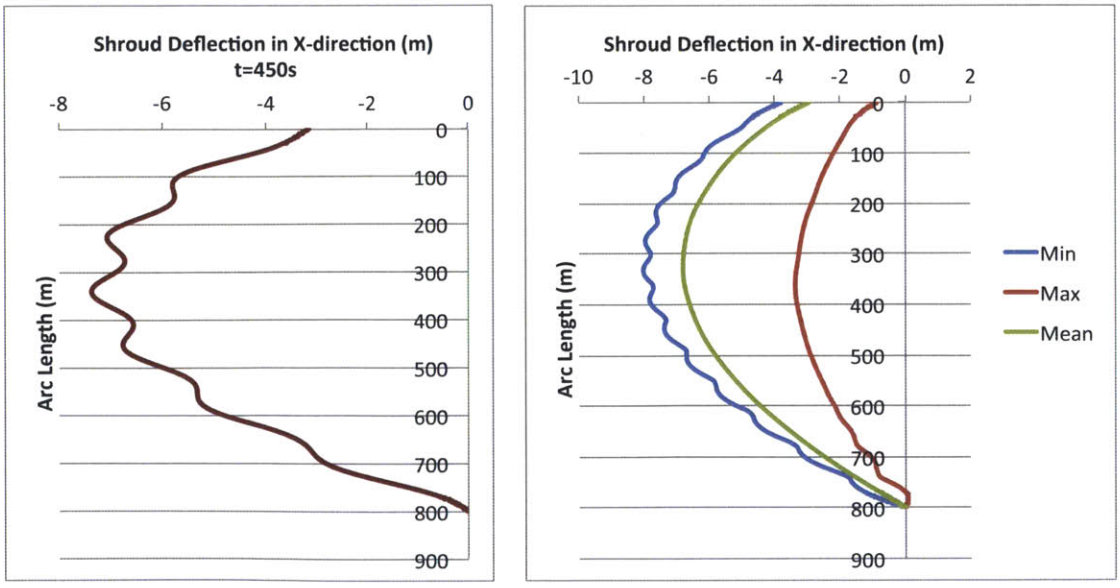

(a) (b)

Figure 6-14: Reference well - Shroud displacement due to a monochromatic wave and uniform current (a) for t = 450s and (b) for the whole simulation

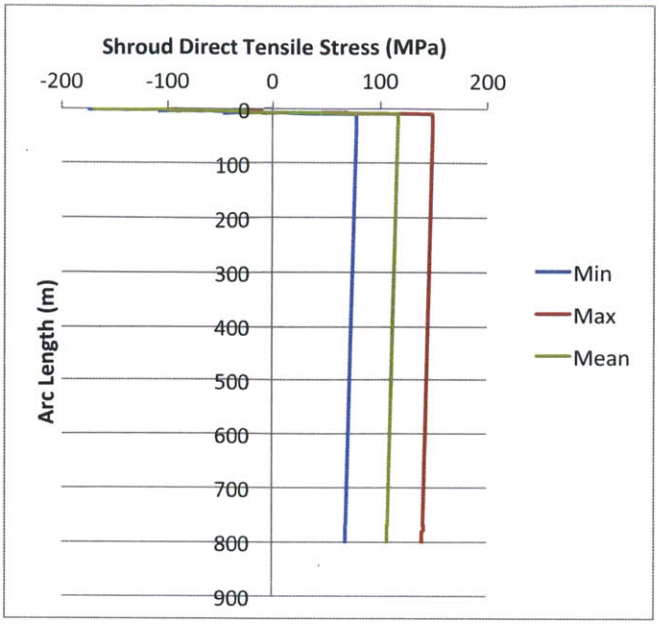

Figure 6-15: Reference well - Tensile stress (kPa) on shroud due to monochromatic wave and uniform current

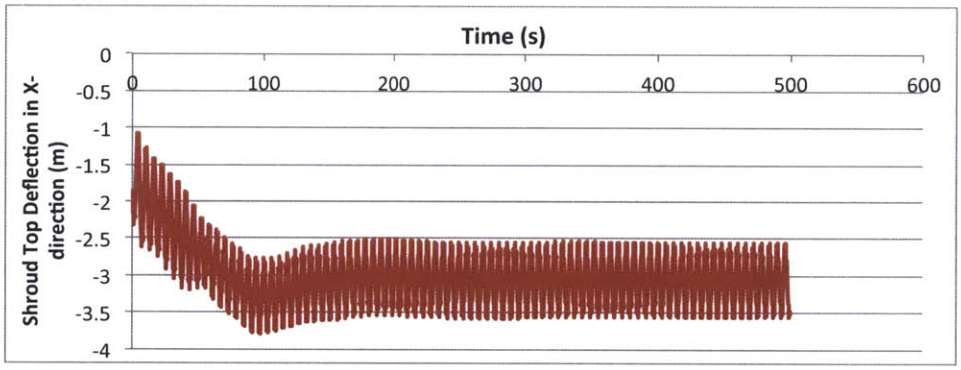

Figure 6-16: Reference well - Shroud top displacement over time due to a monochromatic wave and uniform current

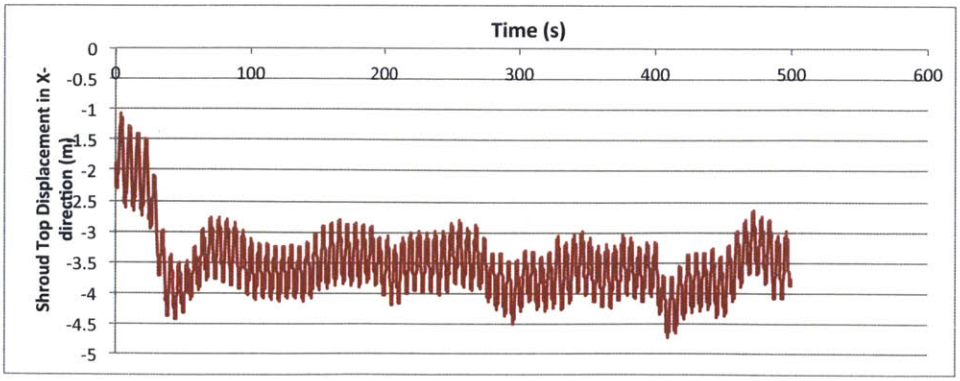

Figure 6-17: Reference well - Shroud top displacement over time due to a monochromatic wave and uniform current with pen

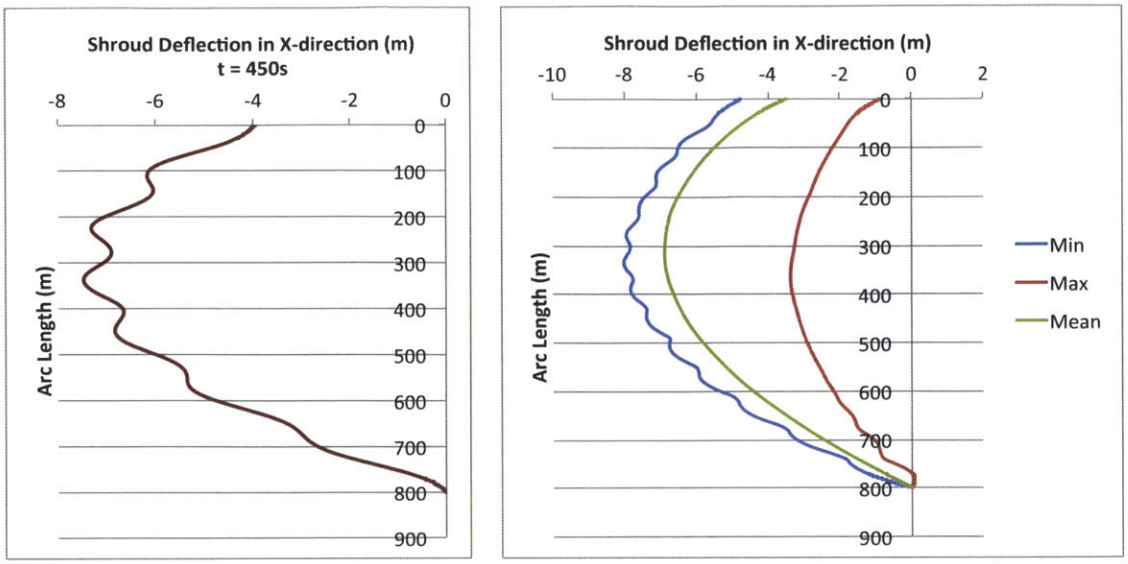

(a) (b)

Figure 6-18: Reference well - Shroud displacement for a monochromatic wave and uniform current with pen (a) at t = 450s and (b) for the whole simulation

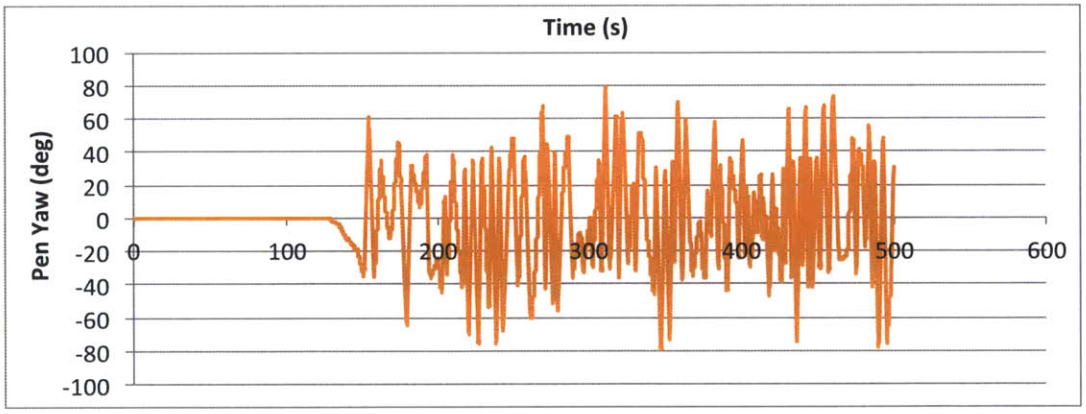

Figure 6-19: Reference well - Pen rotation around own axis (yaw) over time due to a monochromatic wave and uniform current

Wave Spectrum

In order to increase the level of realism in the simulations, we introduced different monochromatic waves representing different typical conditions measured at the reference well. Different methods (described below) were used to find the spectrum (including a directional spectrum) that best fits the data. In analyzing the behavior of the pen, a qualitative discussion is combined with an attempt to quantify the results. Firstly, the 3D views of the simulation give a good initial indication of the ability of the pen to follow the waves. Furthermore, a quantitative analysis can be done by comparing the rotation of the pen (pitch and roll, due to symmetry) to the maximum rotation at which part of the fence is entirely below the sea surface. This angle is 14 degrees for a pen with a diameter of 20m (as is the case for the

reference well system). For the monochromatic wave the pitch is the one to focus on, whereas for the spectral waves, we have to check that the roll and pitch rotations are smaller than 14 degrees.

- Range of Monochromatic Waves

This analysis points out that the system does better under some wave conditions than others. The combination of wave characteristics that were chosen are stated in Table 6.11; these are recommended wave periods for each wave height category as published in *Glenn* (1984) and based on wave measurements at the reference well.

Table 6.11: Combinations of wave characteristics measured at the reference well (*Glenn*, 1984)

Wave height range (m)	Average wave height (m)	Peak period (s)	Wave slope (degrees)
$0 - 0.9$	0.5	4	1.15
$1 - 1.9$	1.5	4.8	2.39
$2 - 2.9$	2.5	5.3	3.26
$3 - 3.9$	3.5	6	3.56

Using these wave combinations, it was found that the pen satisfies requirements for each case. The two smallest waves do not cause the pen to even come close to a 14 degree rotation, whereas the bigger two wave conditions occasionally produce rotations that cause the top of the fence to be submerged by a depth up to 2.3m below the surface (of the 2.5m fence), or a $\sim 13^{\circ}$ rotation. For the largest wave, the roll of the pen sporadically comes close to the maximum of 14 degrees for which the entire fence is under water. These large waves however will occur less than 1.5% of the time, so the reduced capabilities of the pen are not a concern. The disadvantage of this approach is that it does not tell us how the system (mostly the pen) would respond when forced by constantly changing wave conditions; this is why we have tried to work with the different spectral wave models as described below.

- Spectral Wave Models

Several methods were used in an attempt to simulate realistic the realistic sea state, with characteristics as documented by *Glenn* (1984) stated in Table 6.11. Since we do not have a measurement of the sea state at the reference well, we tried using different methods to define the energy spectrum based on the wave data that we have. OrcaFlex includes a number of models to develop a wave spectrum, of which we tried four. For one of them we did not have enough data for OrcaFlex to develop a full spectrum, and another does not output the spectrum that it produces, so we would rather not use that. The two remaining methods left in OrcaFlex are the JONSWAP and the ISSC wave spectrum models, where we put the focus on the JONSWAP and checked with the ISSC to see whether it would compute the same spectrum.

- JONSWAP

In OrcaFlex the JONSWAP spectrum is defined based on a significant wave height, peak

period, maximum frequency and wave origin. The remaining parameters (peak enhancement factor, the spectral width parameters and the spectral energy parameter) can either be set automatically by OrcaFlex or stated manually. When OrcaFlex is set to automatic, it calculates the peak enhancement factor, γ, according to *Isherwood* (1987). The spectral width parameters (σ_1 and σ_2) are fixed at standard values of 0.07 and 0.09 respectively. Lastly, the spectral energy parameter (α) is calculated to give a sea state with the specified Hs and Tp. Based on the values of these parameters, OrcaFlex calculates the spectral energy parameters based on the significant wave height and peak period. However, the program is not very specific as to the method used to calculate some of the parameters and it develops a value for α that is higher than is conventional. The equation to calculate the JONSWAP spectrum is:

$$S(f) = (\alpha g^2/16\pi^4) f^{-5} exp(-5/4[f/f_m]^{-4}) \gamma^b \tag{6.1}$$

where the range of frequencies and the number of components and seed (needed to start the random number generator that assigns the phases) can be input in the OrcaFlex wizard; the remaining parameters are pre-determined in the software. The random wave trains are represented by the number of component waves whose amplitudes and periods are selected by the program (based on an equal area approach), to give a sea state having the specified spectrum.

Table 6.12: OrcaFlex data needed for JONSWAP

Parameter	Value
α	0.0081
γ	3.3
σ_1	0.07
σ_2	0.09

Alternatively, it is an option to input the model parameters manually, since generally used values for the model parameters are known and between the equation that goes with the JONSWAP model, and the available wave data, several data points of the spectrum can be created. All the data used to define the spectrum is shown in Table 6.12 and Figure 6-20 shows the spectrum generated by OrcaFlex on the left and the JONSWAP spectrum defined by our data and a slightly different equation to compute the energy density, see the figure on the right.

Furthermore, based on data from *Glenn* (1984) on the wind directions, we could identify the governing wave directions to be SW to NE, with NW being the most common direction. This gives the directional spectrum to have a shape shown in Figure 6-21.

The results for the pen rotation around the x- and z-axis are shown in Figure 6-22 and 6-23 respectively. Here it can be inferred that the roll rotation does not reach the critical 14 degrees, but occasionally does exceed a rotation of 10 degrees, meaning that the effective fence height is reduced to 0.75m. With the oil density and flow rate that is expected for the reference well, that would result in oil containment in the pen up to almost 6 hours without the need to pump it out.

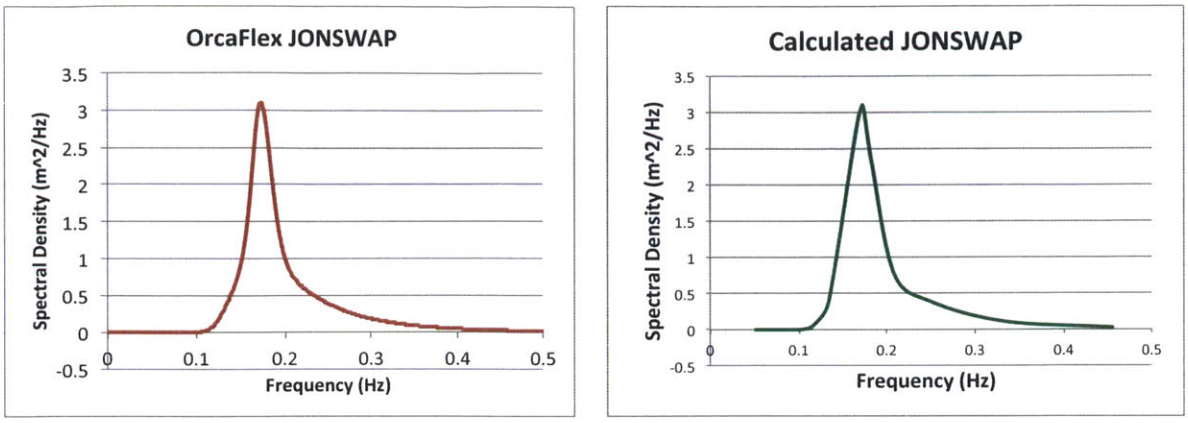

(a) (b)

Figure 6-20: JONSWAP spectra, (a) developed by OrcaFlex based on manually entered parameters and (b) results from calculations of spectrum for JONSWAP based on data given to us by ENI SpA (*Glenn*, 1984)

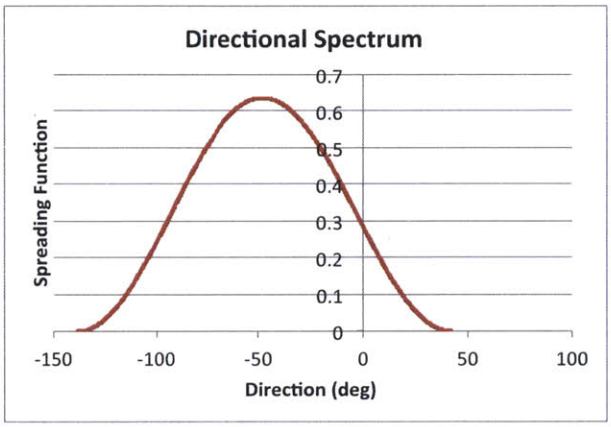

Figure 6-21: Directional spectrum based on data from ENI SpA

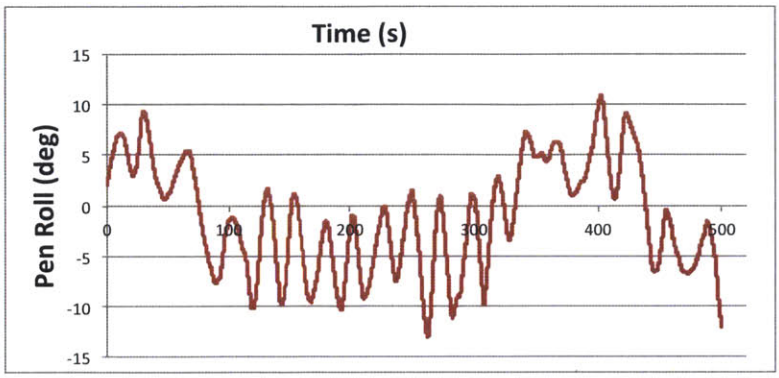

Figure 6-22: Reference well - OrcaFlex results for pen rotation (roll) due to the wave spectrum and a uniform current

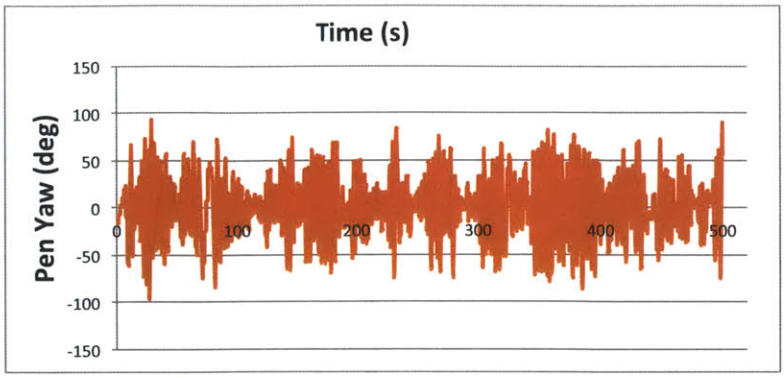

Figure 6-23: Reference well - OrcaFlex results for pen rotation (yaw) due to the wave spectrum and a uniform current

It is not entirely well understood why the pen appears to behave slightly less well when exposed to the spectrum as opposed to the worst monochromatic wave conditions. Since the wave spectrum also takes directionality of the waves into account, it initially looked like that could have been part of the reason why the behavior would change. To test this, simulations were run with the frequency spectrum without the directional spectrum (i.e. one wave direction), which did not show less severe rotation angles. Therefore, it seems like the directionality of the waves does not influence this outcome much. Therefore, currently the hypothesis is that the pen cannot adapt fast enough to the constantly changing wave conditions, thus occasionally experiencing high pitch and roll angles.

Results of the shroud response to the wave spectrum are shown in Figure 6-24. These results do not vary strongly from those with a monochromatic wave.

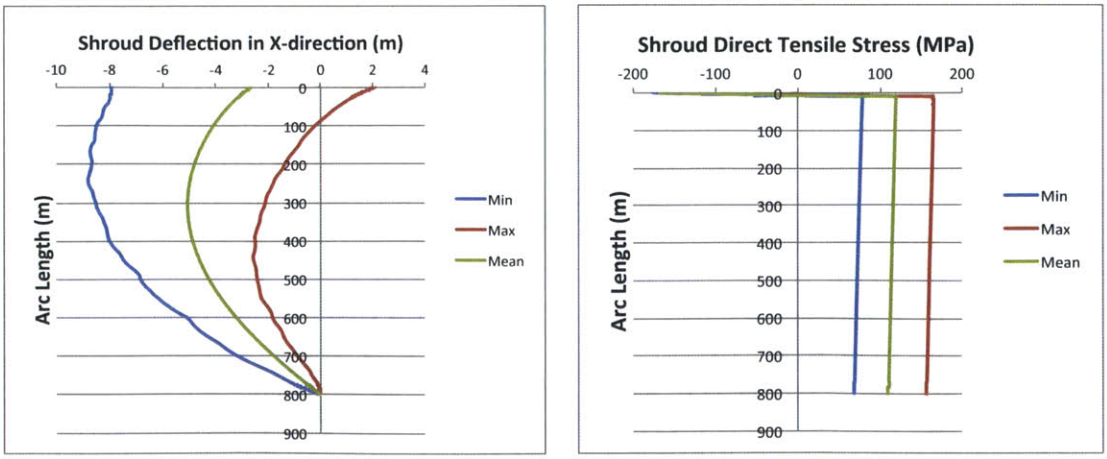

(a) (b)

Figure 6-24: Reference well - Shroud displacements (a) and tensile stress on the material (b) for a wave spectrum and uniform current with pen

6.4 Mooring Offset

An important check that has not yet been mentioned, is that of the sensitivity of the results to changes in the design parameters. The most important sensitivities are in the location of the mooring, since the manner in which the mooring blocks are deployed involves a margin of error of approximately $5 - 10$m. Therefore the following additional simulations were run:

Mooring Line 1		Mooring Line 2		Mooring Line 3	
x	y	x	y	x	y
+5	+10				
+10	+10				
+5	+5	+5	+5		
+5	+10	+5	+5	+5	+5

Results (not shown here) indicate that the overall behavior of the systems is the same, but the results are offset by several meters, as could be expected. The additional displacement is within an acceptable range and depends on how large the displacement is, as well as how many mooring lines are offset from the expected values.

The second run shows that even when the top of the shroud is pulled into the current further than the bottom mooring, the response of the rest of the shroud is still the same. This relates to the overall displacement and tensile stress. Therefore, the margin of error with which the mooring can be placed does not cause affect the final behavior of the system.

6.5 Vortex Induced Vibrations

Vortex induced vibrations occur when bodies are exposed to an external fluid flow. A submerged cylinder is a classical example of this phenomenon. When the boundary layer in the fluid separates from the body, vortices are formed. These vortices are shed off each side of the body at a frequency that is called the Strouhal frequency, which is defined as follows:

$$f_{St} = \frac{St\ U}{D} \tag{6.2}$$

where St is the Strouhal number, which is 0.21 for cylindrical structures, U is the velocity of the external flow and D is the diameter of the cylinder (shroud).

Every time a vortex is shed off the body a lift force is created on that side of the body, leading to a motion transverse to the flow. When a structure has a natural frequency that is within a factor of two or three of the Strouhal frequency, the transverse motions can become very large, because the structure starts to resonate to the Strouhal frequency.

The transverse vibrations are known to be a source of fatigue damage to offshore engineering structures, including oil risers. Since the shroud is also a slender cylinder exposed to an external current, it is necessary to check whether fatigue due to vortex induced vibrations

would be a source of failure. The majority of the analytical solutions, however, are for solid beams, or for flexible cylinders in low Reynolds number flow. Our containment system does not fit either of those models, which led us to look into numerical models. OrcaFlex has a package that includes the possibility of VIV analysis. This package links the OrcaFlex data to a second software that does the VIV analysis in the frequency domain. One of these softwares, VIVA, was developed by Professor Michael Triantafyllou, in the Mechanical Engineering Department here at MIT. It turns out, however, that VIVA no longer links to OrcaFlex nicely, leaving us to run the software as a separate tool.

6.5.1 Input for VIVA

The default configuration in VIVA is defined as a fully submerged, vertical, bare cylinder.

The user can input:

- The characteristics of the cylinder (length, mass per unit length, diameter, thickness, bending stiffness, damping ratio, tension applied at the top of the riser and boundary conditions).
- The position of the riser (if it is not vertical).
- Information about the fluid (flow): water density, kinematic viscosity, Reynolds number and strength and direction of the current with depth.

The VIV analysis will initially be done for the shroud subjected to only a non-uniform current, to check whether VIV would be a cause of concern at all. If so, then we could expand the analysis to include the current induced by the waves from the sea spectrum. The input parameters for VIVA that have not been mentioned before are described in Table 6.13.

On recommendation of Professor Triantafyllou we are making several simplifying assumptions:

- Since the deflection of the shroud due to a non-uniform current is less than 1% of the shroud length, it is not necessary to account for the deflected shape.
- Since VIVA has no good way to model the roughness of the shroud caused by the reduced cross-section between the ribs, we are therefore modeling the shroud as a simple, bare cylinder.
- VIVA models the fatigue life of the system, based on the fatigue characteristic of the material that are input. Since most materials have a log-log fatigue behavior (relationship between the number of cycles to failure and the peak load), the expected input in VIVA is therefore based on a log-log equation. Kevlar, however, like many other plastics, has a semi-log fatigue behavior (Figure 6-25) (*Burgoyne*, 2013), leaving it impossible to enter the correct behavior in VIVA. A conservative approximation has been made to describe the behavior; Table 6.13 shows the coefficients related to this equation: log(number of cycles) = log(A) - Blog(stress range in (N/m^2)).

Table 6.13: VIVA input data for the system for the reference well

Data Type		Design Value
Mass per unit length [kg/m]		7293.6
Added mass per unit length [kg/m]		7293.6
Net weight in water per unit length [N/m]		225.6
Tension at the top [N]		2,176,000
Damping ratio [%]		0.003 (as an estimate)
Fatigue analysis		
	A [-]	5.25 x 10^{165}
	B [-]	17.8
Non-uniform current [m/s]		see Figure 2-3
Boundary conditions		Both are pinned ends (input value is 0 in VIVA)

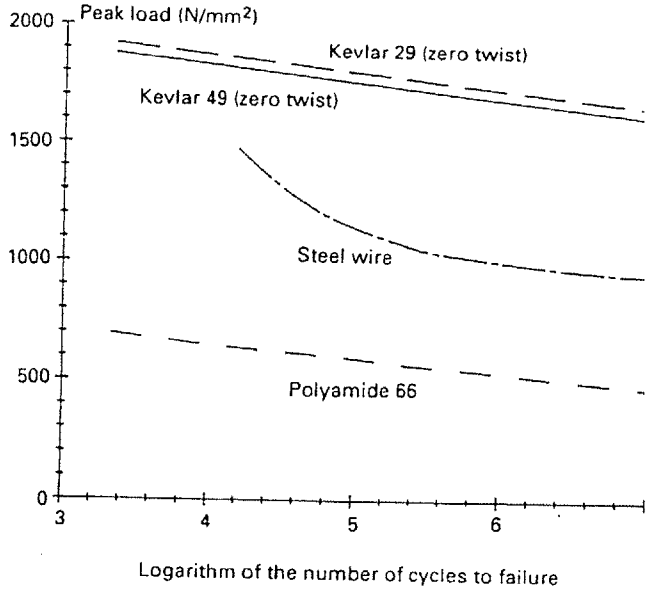

Figure 6-25: Kevlar fatigue behavior

6.5.2 Results from VIVA for Non-Uniform Current

VIVA calculates riser natural frequencies, mode shapes and fatigue life of the structure. The output for the shroud in a non-uniform current is shown in Table 6.14.

Given the results presented in Table 6.14 we can assume that VIV will neither lead to fatigue failure during the life time of the shroud (approximately six months) nor are the amplitudes a reason for concern, since they are only 2% of the shroud's length. The deflection of 2% is not much more than the steady state deflection due to the drag of the current. The reason that VIV is not a problem for the shroud system is a combination of the relatively high pre-tension we are applying with the air can and the high fatigue resistance of the Kevlar fabric.

Table 6.14: VIVA output data for the system for the reference well and a non-uniform current

Variable	Output
Dominant mode	1
Response frequency [Hz]	0.0075
Maximum amplitude [m]	1.96
Minimum fatigue life [yr]	1.6 x 10^{18} (failure will occur at the shroud top)

There are two sensitivities that need to be tested due to uncertainty of the input parameters: the damping coefficient and the fatigue characteristics. Firstly, for two extreme values of the damping ratio (0.001 and 0.07) we found that the fatigue life of the system is far above the design life of the shroud (by several orders of magnitude). Therefore, our estimate having some insecurity will barely affect the results. Secondly, to chose a more conservative approach to fatigue, we chose values for the coefficients A and B for a steel used for risers. In this calculation A = 1.05 x 10^{30} and B = 3, which results in a fatigue life of almost 11,000 years (failure will occur half way down the shroud length). From this we can conclude that even extremely conservative calculations result in a fatigue life that is orders of magnitude longer than the design life of six months.

After consulting with Professor Triantafyllou it was decided to run the analysis in which we add the current induced by the wave spectrum, since the increased shroud deflections imply that the increase of the current is not negligible. Since VIVA is a frequency domain software, we cannot account for the time-varying current and the oscillations of the shroud. Instead, we choose three (conservative) scenarios for which we will test the system. For all three scenarios we can use OrcaFlex to extract the values of the current that is a combination of the wave induced current and the non-uniform current. The three scenarios are necessary because the shroud oscillates, which also affects the magnitude of the tension that is on the system. The three scenarios are the following:

- A point in time at which the tension on the shroud is minimum
- A point in time at which the tension on the shroud is maximum
- A point in time at which the total, combined current has maximum values

The results for this analysis (using the fatigue behavior of a steel riser)indicate that the wave induced current has little affect on the occurrence of VIV and therefore the fatigue life of the structure; all three scenarios still show fatigue lives of approximately 11,000 years. That the wave induced current does not affect the VIV analysis much, is most likely due to the large pre-tension that is on the shroud.

Chapter 7

Installation

Section 4.8 already gave a brief introduction to the logistical process related to the deployment of the containment system. The sections in this chapter will elaborate on the details of getting the stored components transported to the location of the blowout and describe the required steps that need to be followed to deploy the system successfully.

7.1 Storing Onshore

As mentioned in Section 4.8 most of the components are already assembled onshore, therefore simplifying deployment. The components that are stored ready for use are:

- The 100m shroud sections, folded inside their protective steel frames. Each section already has the reinforcement rings assembled and in place in the sleeves in the shroud.
- The flexible (Kevlar) flared section is already stored with the reinforcement rib at the top, which connects to the first regular shroud section. Furthermore, small ballast blocks can already be attached to the bottom of the section, to make sure that the Kevlar fabric stays taut during descent, instead of opening up and increasing the resistance to descend. The ballast also helps make the shroud system less susceptible to cross-currents, therefore making it easier to lower it in the correct location.
- Since the pen is an assembly of parts, it will be kept onshore as a package with the different components (think along the lines of IKEA® furniture). The components of the package are
  - Pen skirt and fence can be made of a 10m wide Kevlar sheet, with the buoyancy rings attached to this. The buoyancy rings are still deflated. If the ballast ring will be a sand-filled ring, that can already be prepared onshore. The skirt and fence are built of one meter sections of Kevlar that are connected by the longitudinal reinforcement. This design means that this section can be folded/rolled up for storage and transportation.
  - The baffle with the four spokes (not yet attached)

  - Skimmer weir with four spokes (unattached) and the hose that will connect to the tanker
  - Mooring blocks (cubes and plates)
  - Mooring lines
  - Four links to connect the pen to the shroud

7.2 Transportation

The compartments of the shroud will be transported on the same multi-purpose vessel that will deploy the entire system. The requirements for the vessel are

- Crane with a lifting capacity of at least 60 tons
- At least a 5m diameter moonpool (needs to fit the shroud and the frame)
  - The dimensions of the moonpool influence the maximum size of the mooring plate, but more importantly, the flared section, as discussed before.
- Enough storage capacity
  - Shroud sections have a 3m diameter and the frames are 5m in diameter and 1.5m tall. They could be stacked on top of each other to save deck space.
  - Flared section; 5m high, so much taller than the other sections
  - Pen: it can be rolled up for transportation. Only baffle and the skimmer weir come separately, each with their spokes for later connection.
  - ROV's that guide the shroud down/connect it to the mooring lines
  - Ballast blocks and mooring lines
- Installation platform above the moonpool from where the sections can be connected, etc.

Most components are light enough that they can be lifted onto the vessel using a forklift. The heavier components might require a crane to lift them onto the vessel. This would mean that the shroud should be stored in a harbor that is big enough to have cranes with a lifting capacity of approximately 60 tons that are close to the docks.

7.3 Deployment

This section describes the consecutive steps that would be taken when deploying the shroud system.

7.3.1 Step 1: Mooring Blocks

There are two types of mooring configurations: one for the outer mooring lines that are connected to the top of the shroud and the other for the bottom mooring lines. The mooring blocks are exactly the same for both types of mooring; however the deployment varies slightly. The paragraph below will first describe the deployment for the outer mooring lines, followed by a paragraph discussing the changes for deployment of the bottom mooring lines.

Top Mooring

Positioning the mooring blocks is achieved by taking the following actions:

1. Use GPS positioning to find the correct location for the vessel
2. Connect the final mooring line to the mooring plate
3. Lower the mooring plate down the moonpool
4. Have a buoy attached to the top of the mooring line, so it is easy to relocate later, when it is needed to be connected to the top of the shroud
5. Lower the mooring cubes one by one. This can be done using a temporary deployment line and ROVs guiding the block to land on the plate. Then the ROV can disconnect the deployment line so that it can be pulled up to lower the next block.

This is done for each of the 3 mooring locations for the top mooring. Since the mooring points are several kilometers from the blowout point there is no risk to the vessel and its crew.

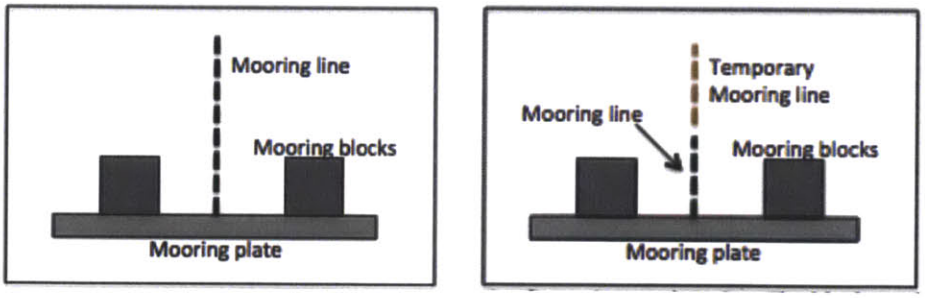

(a) (b)

Figure 7-1: Mooring design; (a) top mooring and (b) bottom mooring. The latter has a connection point between the permanent mooring line and a line that is just used to lower the permanent configuration during the deployment.

Bottom Mooring

As mentioned before, most of the activities presented in Section 7.3.1 are also relevant for the mooring at the bottom of the shroud. The dissimilarities originate from the fact that the three final bottom mooring lines are only 50m, since the lines only need to connect to the bottom of the flared section. Therefore activity 2 changes in that the short, permanent mooring line

is connected to a long temporary mooring line, which is then connected to the buoy at the surface. This needs to be done for all of the bottom mooring points.

Furthermore, ROV's will be needed to guide the blocks and plate to the right location on the seabed. This method allows the deployment vessel to stay at a safe distance from the blowout point. The top vessel is the one carrying the weight of the ballast block or plate, so that the ROV would simply push it to the correct location. The procedure is depicted in Figures 7-2, 7-3 and 7-4 and involves the the following steps.

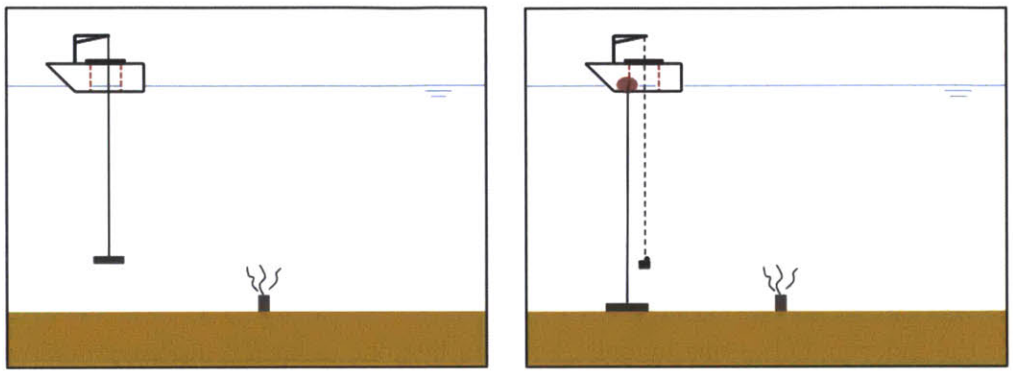

(a) (b)

Figure 7-2: Deployment step 1 - Lowering mooring plates and lines (a) and mooring blocks (b), where mooring lines are attached to buoys at the surface to easily connect them to the shroud top.

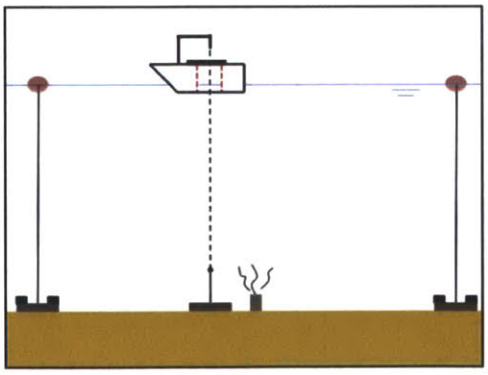

Figure 7-3: Step 1c - Deployment of bottom mooring

Step 1a: Lowering the first mooring plate through the moonpool, with the attached mooring line (Figure 7-2(a)). The mooring plate has the final mooring line, with a surface buoy at the top to be able to access it easily later on.

Step 1b: In Figure 7-2(b) the first mooring block is being lowered through the moonpool using a temporary cable.

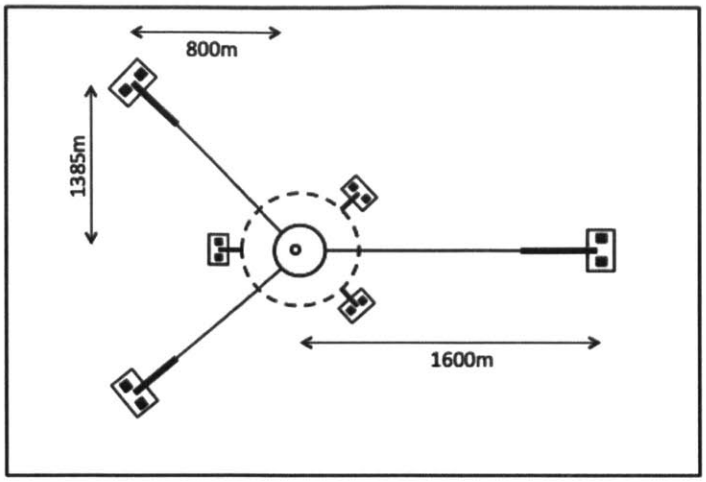

Figure 7-4: Final mooring configuration for the reference well system

Step 1a & Step 1b have to be done for all three far mooring points (see Figure 7-4).

Step 1c: Lowering the mooring plate through the moonpool for a bottom mooring point (Figure 7-3). Only the solid line will be an operational mooring line; the rest of it is temporary wire used for deployment purposes only.

7.3.2 Step 2: Lowering the Shroud

As soon as all the mooring is positioned, the deployment vessel can start lowering the shroud sections through the moonpool. During this entire step the vessel is positioned several tens of meters offset from the blowout point to ensure the safety of the vessel and the crew. At this point the system is not ready to start guiding hydrocarbons up to the surface, since there is no surface collecting device in place at this time.

Step 2a: Flared Section

Since the flared section is made of just Kevlar fabric (with some longitudinal reinforcement ribs) it can be deployed through the moonpool (see Figure 7-5). Onshore some ballast was already attached to the bottom of the flared section to facilitate the vertical descent (even in currents) and will be part of the final configuration. Therefore the deployment steps are the following:

- The flared section is partially lowered into the moonpool (while it is still folded)
- The flared section is attached to the platform above the moonpool
- The crane is connected to the first shroud section and it is lifted above the flared section
- The sections can be connected to each other, using shackles to attach to flanges on both reinforcement ribs (Figure 7-6).

- Lastly, a seal is created between a small Kevlar skirt dropping down from the shroud section and the top of the flared section, to keep water from entering the shroud at the connection.

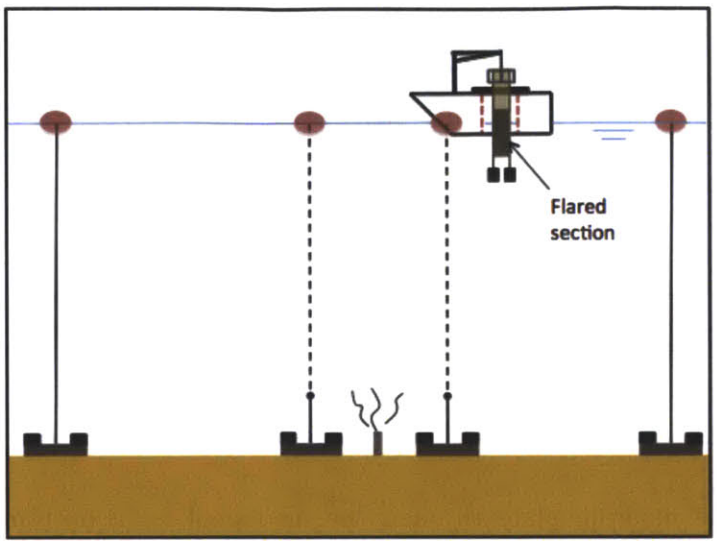

Figure 7-5: Lowering of flared section through the moon pool

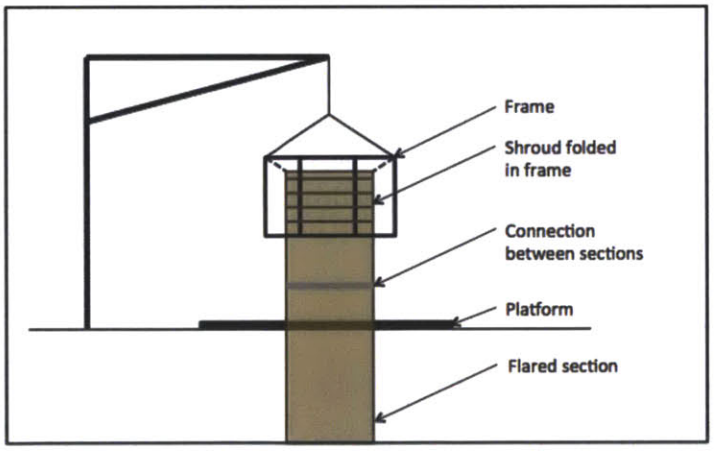

Figure 7-6: Attaching the first regular section to the flared section (from platform above the moon pool)

Step 2b: Middle Sections

Once the flared section and the first shroud section are connected, the shroud section can slowly be unfolded out of the frame through the moonpool, using the following steps.

- Completely unfold the shroud material
- The frame can be stabilized on the platform while the crane picks up the next shroud section.

- The frames on the shroud sections are left in place during operation, in order to reduce work/complexity. The drawback of the frames and the accordion effect is that an additional active mechanism needs to be added to make sure the section unfolds in a controlled fashion as supposed to a free drop due its own weight that could tear the Kevlar.

- After the crane hangs the upper section above the bottom section, the lowest reinforcement ring of the upper section can be linked with shackles to the lower section. As before, the remaining step is to then guarantee the seal between the two sections, using the Kevlar skirt from the upper section to create a sort of compression seal against the reinforcement ring of the lower section.

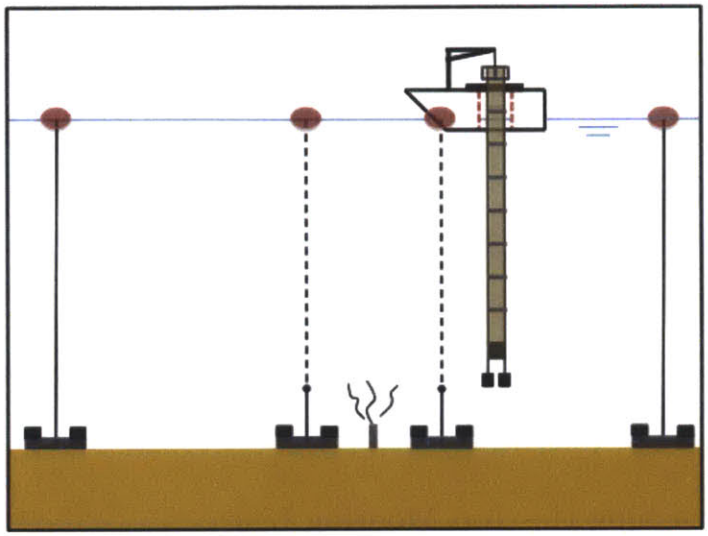

Figure 7-7: Lowering the shroud through the moon pool. The last section remains partially folded

Then the folded shroud section can be unfolded and the process repeats itself until all sections are connected (Figure 7-7). During its decent, the shroud is kept nearly vertical due to the ballast hanging from the bottom of the flared section. For extra control ROV's could be used to help keep the shroud offset from the blowout point.

Step 2c: Top Section

The steps for this section are the following

- The connection to the bottom section is the same as for the other shroud sections.

- The section is unfolded for three quarters of its final length (which might be shorter than 100 meters, which means that it stays partially folded in order to give the shroud the appropriate total length), since this isnt done until the shroud is hung in its final position above the wellhead.

- The frame of this section already has the air cans attached to it so the next step is to replace some of the water in the air cans with air to compensate for the shroud weight.

Only a relatively small part of the air volume is used to compensate for the shroud weight. More than half will be used to compensate for the weight of the mooring lines and approximately the remaining third leads to the pre-tension required to keep the shroud from deflecting too much as well as keeping the differential pressure from decreasing the cross-sectional area too much.

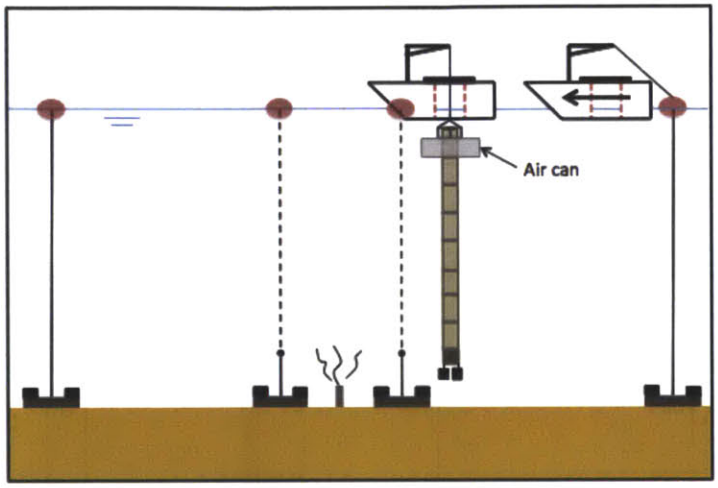

Figure 7-8: Indication of how to attach the mooring lines to the top section's frame

7.3.3 Step 3: Attaching the Top Mooring Lines

After all the shroud sections are in place the top mooring lines can be connected to the frame of the top section. The attachment of the mooring line adds significant weight to the shroud; therefore a series of actions need to be taken to avoid the system from sinking. Locating the mooring lines is simple due to the attachment of a buoy to the top end of the line during its initial positioning.

- Some buoyancy compartments should be added to the mooring lines, firstly to avoid the shroud from sinking when the mooring line is connected. Secondly, as the mooring line is guided to the top of the shroud by a second vessel (Figure 7-8), some of the chain is lifted off the seabed, adding weight that needs to be compensated (Figure 7-9). Initially the surface buoy (attached to the mooring line) will give the line enough added buoyancy to make sure the crane is only handling 60tons (the shroud ways $\sim$ 20tons, and each mooring line weighs 110tons in this configuration).

- Start replacing the water in the air can(s) (on the frame of the shroud top) by air in order to be able to compensate for the extra weight of connecting the first mooring line. At this point the top of the shroud is still connected to the crane on the deployment vessel, which can also take on some of the weight of the mooring line as is attached.

- Use ROV's or divers to connect the mooring lines to the frame of the top section of the shroud.
- Further replace the water in the buoyancy compartments with air until there is approximately enough to add the next mooring line.

The steps are repeated for each of the three mooring lines. Once all the mooring lines are attached the air can(s) have the designed air volume; however this does not yet mean that the system can be disconnected from the crane of the deployment vessel. Due to the waves and the current, the shroud would start to respond to the wave motion (see Chapter 6 for the OrcaFlex results predicting this), making it harder to connect the pen in the next and second to last phase. However, once all the mooring lines are connected, vessel 1 should detach from the shroud, then vessel 2 can reconnect, but with the shroud along side the vessel, instead of through the moon pool. This is needed to connect to pen to the shroud top.

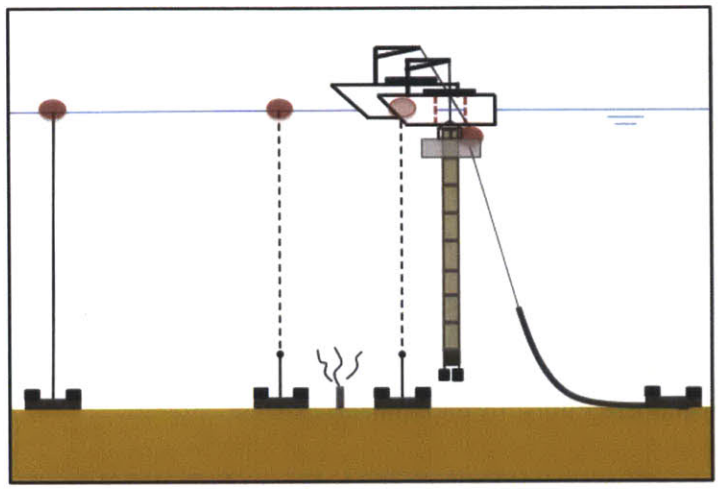

Figure 7-9: Attaching the mooring lines to the shroud top

7.3.4 Step 4: Deployment of the Pen

The pen is not yet fully assembled when it is brought onboard; therefore the first step is to assemble the pen.

- Unfold the pen and inflate the buoyancy rings and the circular reinforcement ring half way the skirt
- Attach the baffle and the skimmer weir (with the line to extract the oil)
- Connect the links to the skirt of the pen
- Use the crane to lift the pen overboard (Figure 7-10)
- ROV's or divers attach the shackles at the bottom of the links to the frame on the shrouds top section

- Connect the suction line from the weir to the tanker

At the end of this phase the system is almost entirely assembled, however it is still several tens of meters offset from the blowout point and the top section still needs to be completely unfolded.

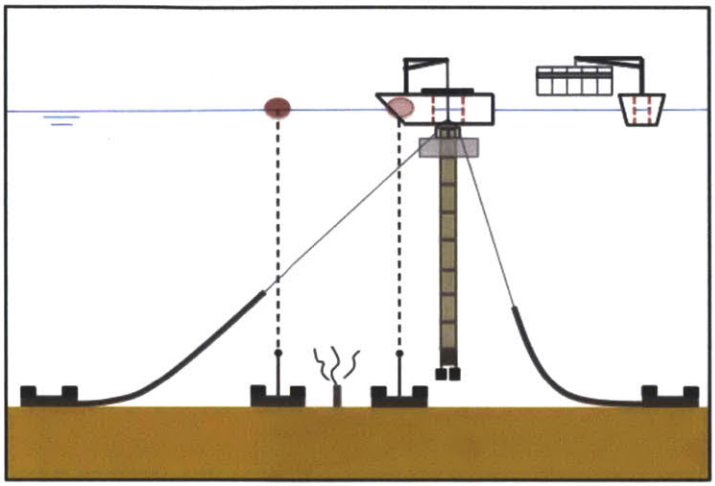

Figure 7-10: Lowering and connecting the pen to the shroud top

7.3.5 Step 5: Positioning of the System

Before a vessel tows the system to its final location, the system needs to be moved close enough for the bottom mooring lines to be connected.

- ROV's can connect the mooring lines to the bottom of the flared section after which the temporary mooring lines can be removed.
- Next, winches on the mooring lines will shorten the mooring lines, thereby guiding the shroud into its final position. During this process the mooring lines will open up the flared section.
- Lastly, the top section of the shroud can be completely unfolded. Doing this will make sure that the ballast hanging from the flared section comes to a rest on the seabed.

In doing this, the system will start to collect hydrocarbons that will rise to the surface. As soon as the oil layer in the pen is thick enough, the tanker can start extracting oil from the weir.

7.3.6 Final Steps

Once the pen is connected, the shroud the system is complete; next the whole system is towed into its final position above the wellhead (Figure 7-11).

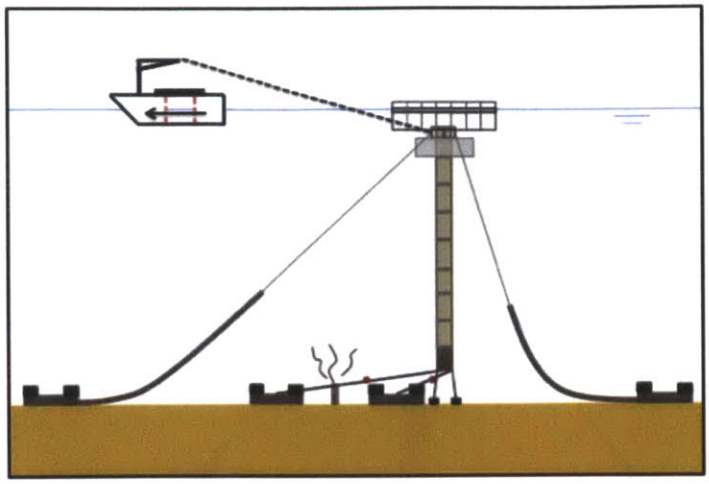

Figure 7-11: Positioning the shroud over the well head

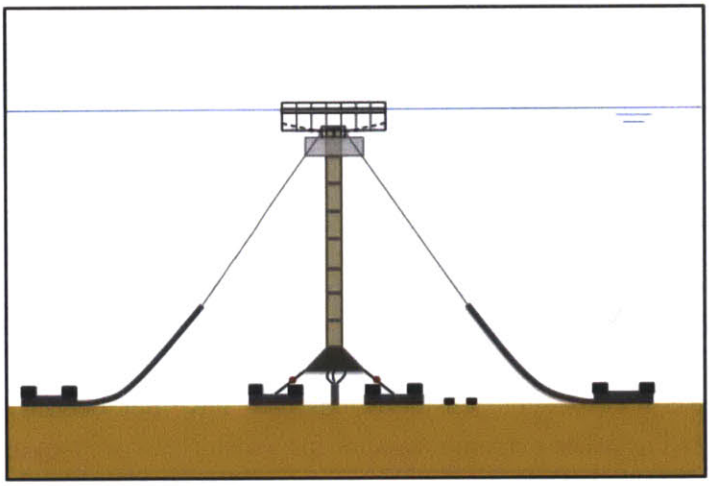

Figure 7-12: Unfold the top section of the shroud, therefore brining the bottom of the shroud closer to the well head and starting to collect hydrocarbons

With everything in place, we can proceed to unfold the top section completely, so that the shroud will start collecting the hydrocarbons (Figure 7-12). This method is chosen because it is an easier way to position the bottom of the shroud above the wellhead than trying to tow it through the plume (or jet) close to the wellhead.

7.3.7 Final Configuration

Figure 7-13 shows the shroud system in its final configuration. The shroud is designed to be operational for at least 6 months, so as long as weather conditions do not surpass the design conditions, that is the minimal lifespan that can be expected. During that entire time the shroud will be collecting high quality oil (and gas).

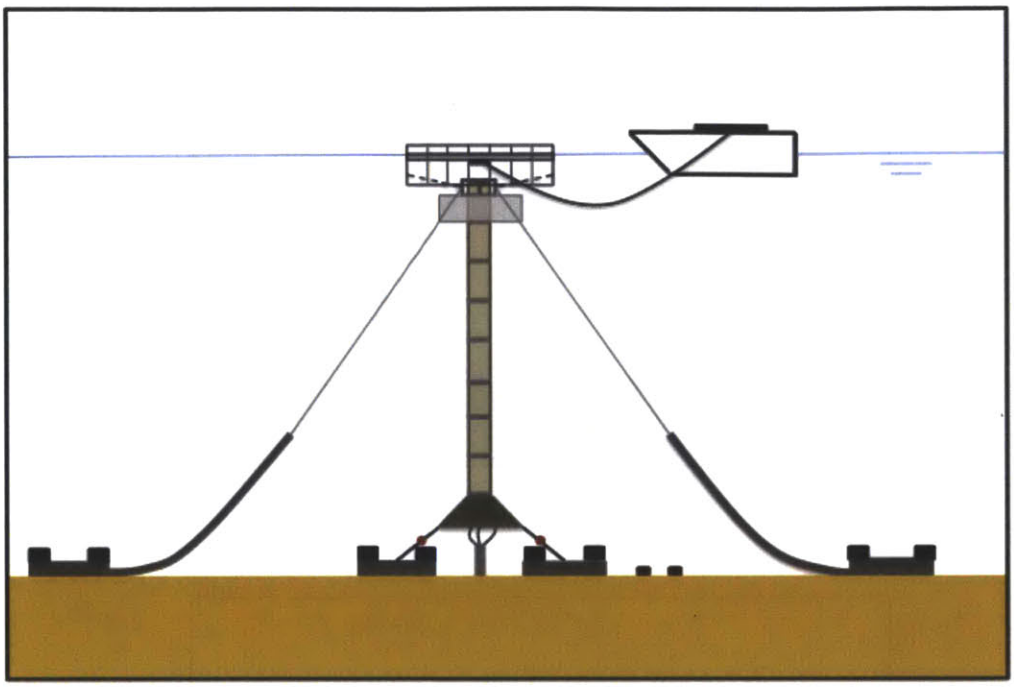

Figure 7-13: Final configuration

7.4 Further Considerations

The most important comment is that the deployment needs to be tested before the system can be signed off for use.

Furthermore, there are two other considerations that have not been discussed yet. The first concerns a hurricane or other extreme weather for which there are two options that would allow temporarily dismantling of the system:

1. Disconnecting the pen, but leaving the rest of the system in place. This might require making (parts) of the current design/system stronger so that it can withstand extreme weather. After the extreme weather the pen could simply be reconnected to the shroud.

2. Disconnect the air cans so that the whole system collapses onto the seabed. This would require a design of the air cans that makes it possible for them to be disconnected (and re-connected) easily. Furthermore long lines would need to be added from the shroud top to buoys at the surface to enable reinstallation of the system after the storm. Steps to make this work are the following:

    - Disconnect the pen
    - Disconnect one of the mooring lines at the bottom
    - Move the top of the system several tens of meters offset from the wellhead, to make sure that the bottom of the shroud does not end up on the wellhead
    - Connect a buoy on a long wire to the top of the shroud, if one is not already pre-attached

- Disconnect the air can, so the shroud will drop to the seabed, next to the wellhead

A disadvantage associated with the second option is that it would mean that ROV's would need to find a way to reattach the air cans while at full water depth since the system will be too heavy for the 60ton crane on the vessel. The only way to avoid this would be to disconnect the mooring lines as well and attach them to buoys (like during deployment), so that only the shroud itself sinks to the seabed. The shroud itself can be hoisted up by the 60ton crane, so that would mean that ROV's would only need to connect the lifting lines to the shroud top (frame). Once the shroud is in the right position again, the air cans and mooring lines could be added again.
Both options have advantages and disadvantages. The decision for either of the two depends mostly on what is most practical in the field, therefore requiring input from engineers managing the operational side of the deployment of offshore systems (like this).

Separately,we looked into the option to collect the gas as well, by changing the design of the pen. This type of design would, however, generate high gas concentrations locally inside this device. For practical and safety reasons, the pen is left open and the gas is not captured.

Chapter 8

Macondo Well

The previous chapters focused on finding a design for the system that would work for the reference well. However, as mentioned in Chapter 1, the concept is that one design of the system is able to operate under a large range of conditions. This work has focused on creating a design for the reference well, since this well is of interest to ENI S.p.A., the company sponsoring this research. Since the previous chapters defined the design values that satisfies all requirements for that well, the step is to apply the design for the reference well to the conditions of the Macondo well. In doing so, it becomes clear to what extent one design would be able to 'fit all', and which design components would need to be adapted to adjust for the more severe environmental conditions.

The following sections will first briefly summarize the conditions at the Macondo well, followed by the same analysis steps as were done for the reference well. This includes firstly, analyzing the flow, hydrates and gas concentrations, then discussing the structural performance of the design using (both analytical calculations and OrcaFlex simulations), and then including adjustments to the pen.

8.1 Environmental Conditions

Firstly, we would like to give a brief reminder of the conditions at the Macondo Well.

Table 8.1: Recap of environmental conditions for Macondo well

Parameter	Macondo Well
Water Depth	1500m
Typical Current	0.1 m/s
Bottom Temperature	4°C
Significant Wave Height	1.0 - 2.7m
Peak Wave Period	6 - 7.5s
Oil Flow Rate	0.10 m^3/s
Gas Flow Rate (at well)	0.09 Am^3/s

The temperature, density and current profiles for the Macondo well can be found in Chapter 2 in Figures 2-4 and 2-5 respectively. Since the shroud does not reach all the way to the

the sea surface, the design is tested on a 0.2m/s current. This value is considered a good depth- and (yearly) time-average velocity.

8.2 Flow Data

The flow conditions from the well were stated previously as well, but are repeated here to create an overview of the conditions at the Macondo well accompanied by oil/gas composition data (Table 8.2), based on *Camilli et al.* (2011).

Table 8.2: Hydrocarbon flow data

Parameter		Macondo Well
Oil		
	- Flow rate	0.10 m^3/s
	- Density	858 kg/m^3
Gas		
At the well head		
	- Flow rate	0.09 Am^3/s
	- Density	120 kg/m^3s
At the surface		
	- Flow rate	31 Sm^3/s
		(0.162 m^3/s at the bottom)
	- Density	0.73 kg/m^3s
Composition (mol %)		
	- Methane	82.5
	- Ethane	8.3
	- Propane	5.3
	- Others	3.9
	Total	100%

The data given in Table 8.2 will be used in the following sections to go through the same calculations as were done for the reference well in the previous chapters.

8.3 System Architecture

As mention in the introduction to the chapter, the goal is to find, if possible, one design that would fit wells across the spectra, taking the reference well design as a base line. In order to achieve this 'one size fits all' objective, we want to show in the following sections that leaving the design parameters the same (e.g. the diameter, material type and thickness, flared section and mooring line design), the system only occasionally requires small design adjustments, to adapt to other environments. Table 8.3 gives a brief overview of the design parameters as they are defined upfront and provides the design for the Macondo well that will be tested in the same fashion as was done for the reference well.

Table 8.3: Design data for Macondo well shroud system (parameters that are different from the reference well system are shown in italic).

Data Type	Design Value
Outer Diameter [m]	3
Inner Diameter [m]	2.996
Shroud Length [m]	1470
Mass per unit length (in air) [te/m]	0.023
Distance between reinforcement ribs [m]	10
Length Mooring lines [m]	3455
Air Can Volume [m^3]	840 (20m long)
Pen Diameter [m]	20

For clarity, components that remain the same are:

- Connection between the shroud sections
- Reinforcement Rib Design
- Flared (Bottom) Section
- Air Can Design (though bigger volume, therefore longer)
- Oil Collection System

The design of those components was discussed in Chapter 4. There are two important differences to note that are not clear form the table; the first is that the distance of the shroud bottom is lowered so that it is only 15m from the seabed as supposed to the 20m that were used for the reference well. This is needed because of the slightly more severe wave conditions, which would cause the top of the shroud to move with the wave orbital motion. If the shroud would be allowed to move with the waves in that manner, it would constrain the pen from following the waves, causing it to roll/pitch too much and therefore spill oil. We chose to avoid this shroud movement by lowering the shroud top out of the zone where the orbital motion is still strong enough to affect the system. The second change is made to the pen in order to make it more resilient to the more severe wave conditions, by increasing the effective buoyancy ring diameter, by adding a secondary ring. Another way to increase the pen's roll and pitch response is to lower its center of gravity. We can achieve this by connecting extra ballast to the bottom of the skirt. Furthermore, since the effectiveness of the adjusted design was proven with OrcaFlex as well, these changes will be further discussed there, in Section 8.9.

8.4 Flow Assurance

Using Equations 5.1 and 5.3 the parameters associated with flow in the shroud can be calculated for the Macondo Well, using the reference well design (diameter = 3m, f = 0.07, K = 0.8). As mentioned, the length of the shroud is 1470 meter, in order to leave the same 30m total margin at both ends of the shroud. For the given hydrocarbon flow rates and densities

at the wellhead and the data for the ambient water, the flow through the shroud is found to be 15.0m^3/s (Table 8.4). This flow rate is accompanied by a larger maximum pressure differential (at the bottom of the shroud) which is more than six times larger than the maximum differential pressure for the reference well. The large force will have a strong influence on the required rib distance as, described in Section 8.7.

Table 8.4: Depth-averaged flow parameters Macondo based on design variables

Design variables			
Length shroud	1470m		
Diameter	3m		
Input		Output	
Oil flow rate	0.10m^3/s	Flow rate	15.0m^3/s
Oil density	858kg/m^3	Velocity in shroud	2.1m/s
Gas flow rate	0.09m^3/s	Pressure difference	4159Pa
Gas density	120kg/m^3	φ	< 0.05

The large flow rate helps reduce the likelihood of hydrate formation and the risk of them plugging the system. The high flow rate and longer travel distance also reduce gas concentrations at the surface, though the high velocity in the shroud counteracts this effect. The following two sections will analyze what the final effect will be for both issues.

However, as mentioned in Section 5.2, the calculations behind the results presented above ignore the effects ambient water stratification and reduction of free gas due to dissolution. The first only causes a 2% reduction of the flow, while the latter could reduct the predicted flow rate by at least 20%. As mentioned for the reference well, this assumption leads to conservative results, which means we will keep using a flow rate of $15.0m^3/s$. The only check is whether a reduction of the flow rate could cause hydrates to form (Section 8.6).

8.5 Gas Concentrations

Just as for the reference well we can determine the bubble/droplet distribution for the Macondo well the bubble/droplet distribution by using the model described in Section 3.1.3.

Figure 3-3 shows the bubble/droplet distributions that are the results of the SINTEF model and Rosin-Rambler distribution. From this distribution the bubble diameters over depth can be computed according to Equations 3.11 through 3.14 in Section 3.3.

As can be seen in Figure 8-1, most of the bubbles will not dissolve as they rise to the surface. Especially for the ethane and propane, the process of dissolution is slowed down due to their liquid state through most of the water column. Combining the bubble diameters and the volume distribution (Figure 3-3 and Figure 8-1) we compute the gas concentrations over depth (Figure 8-2).

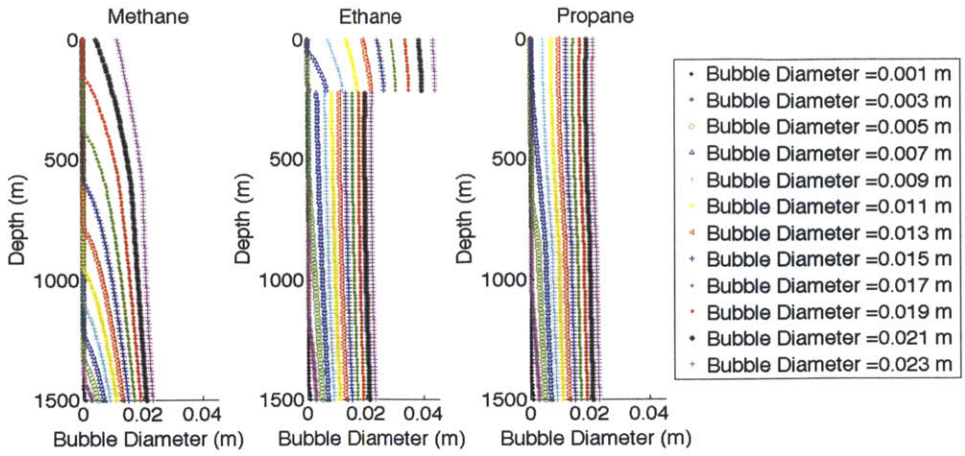

Figure 8-1: Macondo well predicted bubble diameter change over depth as rise through the shroud

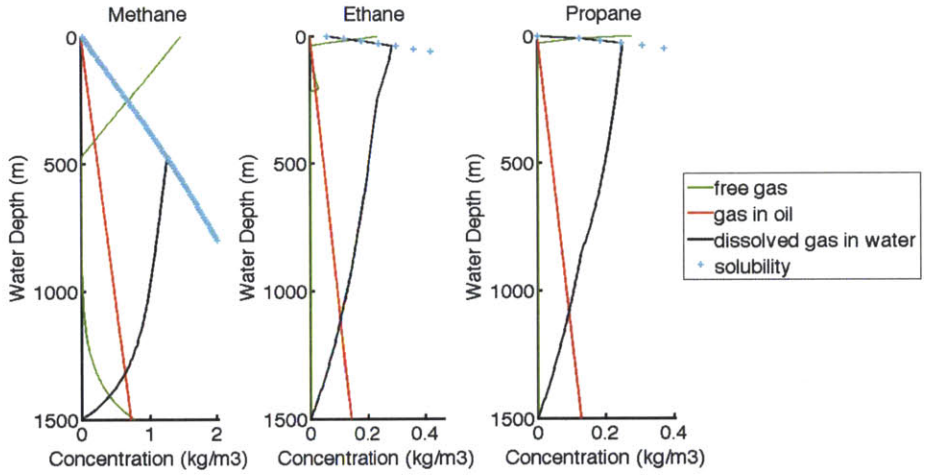

Figure 8-2: Macondo predicted concentration change over depth through the shroud

Since the gas flow rates are a factor of 30 higher than those for the reference well, but the flow through the shroud has only increased by a factor of three, the concentrations have increased by a factor of about 10 (Figure 8-2).

The concentrations at the surface can then be compared to the flammable limits, since it is required for the gasses to be below these thresholds. Table 8.5 points out that the methane gas concentration would be slightly above the 0.5% limit. However this could mean that a larger pen diameter than the assumed 20 meters of the reference well system might be necessary. Increasing the pen to a diameter of 35m is the minimal diameter to reduce the methane gas concentrations to below the 0.5% limit. The results presented are for a pen with a 20m diameter, to compare how the reference well design would do in the conditions of the Gulf of Mexico.

Table 8.5: Macondo surface gas concentrations above shroud as % of flammability thresholds

Gas	% of 0.5 lower limit	% of lower limit	% of upper limit
Methane	176	88	21
Ethane	15	7.5	2
Propane	12	6	1.5

8.6 Hydrate Prevention

Due to the much higher pressures and the lower temperatures at the Macondo wellhead, hydrates formation is more likely from a thermodynamics point of view. Figure 8-3 shows that for the conditions at the Macondo well the hydrates would be stable up to about 400m below the surface. However, as was seen for the reference well, the kinetics strongly influence whether or not solid hydrates can form. Besides, the solubility concentration has increased as well, due to the higher pressures and lower temperatures.

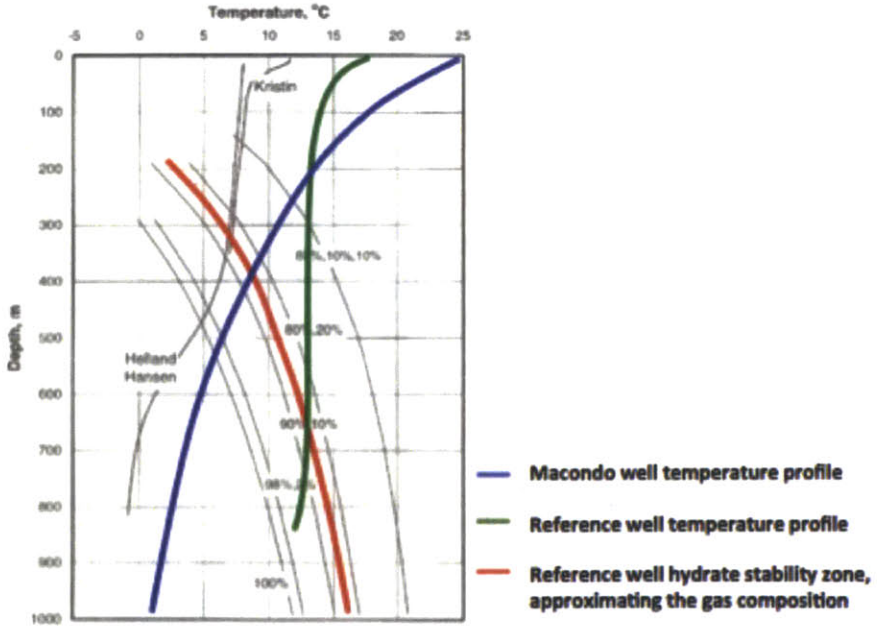

Figure 8-3: Thermodynamic conditions for hydrate formation for Macondo well (after *Johansen et al.* (1999)). As mentioned before, the line referred to as 'Helland Hansen' represents the temperature-pressure combination for the Deep Spill experiment.

Table 8.6 indicates the gas concentrations in the shroud (for the flow of $15.0 m^3/s$), the solubility concentration and the percent of saturation that is achieved in the shroud. Given the small values in the last column, it is very unlikely that solid hydrates would form; however hydrates could still form a shell around the bubbles.

Furthermore, the low percentages presented in Table 8.6 also justify our assumption to neglect the effect of ambient water stratification and gas dissolution to calculate the flow rate, even though this results in an overestimation of the flow. The percentages in Table 8.6 are so low that even a flow reduction by 50% would not cause hydrates to form, therefore we will keep using the 15.0m^3/s flow rate for the rest of the design process and verifications.

Table 8.6: Gas concentrations as a percentage of their saturation concentrations

	Concentration in shroud (kg/m^3)	Solubility concentration (kg/m^3)	% of Solubility in Shroud
Gas flow rate = 0.09 m^3/s			
Methane	1.625	3.488	46.59%
Ethane	0.329	9.209	3.57%
Propane	0.315	9.343	3.37%

The stoichiometric check evaluates what percentage of the flow would be occupied by hydrates, if all the gas would hypothetically form solid hydrate. Table 8.7 shows that this percentage would be very low, so it is highly unlikely that the hydrates would obstruct the flow through the shroud even if all the gas would form hydrate crystals. This means that a shroud with a diameter of 3m would satisfy this condition.

Table 8.7: Hydrate volume as percentage of the flow (stoichiometric check) for Macondo

Gas	Hydrate volume(m^3)	% of flow in Shroud
Methane	0.089	0.59
Ethane	0.0127	0.08
Propane	0.0168	0.11
Total	0.119	0.78

8.7 Structural Analysis

8.7.1 Global and Local Deflections

Because of the greater flow rates and shroud depth, we anticipate that the stresses and deflections for the Macondo well will be somewhat larger than those found for the reference well. As mentioned before, we account for this by reducing the rib spacing to 10m versus 20m. This modest change can be accommodated by designing the shroud sections with sleeves spaced every 10m, but filling only every other sleeve with a rib for the reference well system. Deflections and stresses for the Macondo well, based on a shroud diameter of 3m and a rib spacing of 10m, are presented in Table 8.8 using the same methodology as for the reference well.

Table 8.8: Deflections and stresses for Macondo well

Buoyancy (Tons)	Global deflection (Δ, m)	Local deflection (δ, m)	Remaining area %	Vertical displacement (m)	Total stress (MPa)
400	5.0	0.12	84.3	0.63	213
350	5.7	0.14	82.2	0.83	186
300	6.7	0.16	79.4	1.13	160
250	8.0	0.20	75.6	1.62	133
150	13.3	0.33	61.1	4.52	80
100	20.0	0.49	45.2	10.24	54

As with the reference well, the strictest requirement seems to be the constraint on cross-sectional area of the shroud. However, the reduced rib spacing makes it possible to use the shroud designed for the reference well at the Macondo well with less than a factor of two increase in buoyancy (from 210T to 350T), confirming our initial contention that the same basic design could be used for both sites. We also note that the required buoyancy could be reduced by either a further decrease in rib spacing or an increase in shroud diameter.

For example, with a diameter of 3m, the buoyancy could be reduced to 88T if the rib spacing were reduced to 5m, or if the rib spacing remained 10m, the buoyancy could be reduced to 240T by increasing the shroud diameter to 4m. However, the rib spacing and diameter are preferred to be kept at 20m and 3m respectively, due to practical reasons mostly related to industry preferences (are not used to working with large diameter systems) and that the shroud needs to fit through the moonpool. Medium support vessels we would need have dimensions of approximately $\sim 5m$ by $\sim$ 4m. Furthermore, creating 350T of buoyancy is realistic, as long as the design is kept simple, using one (or two) components (air cans in this case).

8.7.2 Reinforcement Rib Integrity

Regarding the design of the ribs, the internal pressure is higher for the Macondo well system than for the reference well system, but not by enough to prevent the same design from working. The high safety factor found for the reference well system suggests that the same ribs (I-cross section, surrounded by syntactic foam, and made up of three 120 sections, connected through flanges) would work at both sites. Conditions at Macondo only require the ribs to be spaced at half the distance of that for the reference well system.

8.8 Pen

The last aspect of the design is the pen. The design of the pen will be approximately the same as that discussed for the reference well, since the goal is to achieve one design to fit a large range of well sizes. The same checks need to be done to make sure the design performs well in the environmental conditions of the Gulf of Mexico as well.

- *Oil-Water separation*: the diameter of the pen needs to be big enough to have the water exit from under the pen with a velocity lower than the slip velocity of the smallest droplet. At the pen, the smallest droplet, has a diameter of approximately 1mm, with a corresponding critical slip velocity of approximately 3cm/s. The flow in the shroud of 15.0m^3/s would cause the exit velocity into the pen to be a factor of 1.6 larger than this slip velocity. Due to the baffle in the pen, the flow exiting the shroud will be further slowed down, therefore increasing the retention time and allowing the oil and water to separate. For a similar oil-water separation capability as for the reference well, the pen diameter would have to be 25m without a safety margin (that the reference well system does have). The 35m pen that would be necessary to dilute the gas concentrations below the thresholds, would give a safety factor of 2 with respect to the oil-water separation. As mentioned before, all further calculations and simulations are done for a 20m pen, in order to test the 'one design fits all' objective.

- *Storage Capacity*: For the oil flow rate of 8640m^3/day, the reference well pen design with a 20-meter diameter and 10-meter skirt/fence length, would be able to store oil for 2.5 hours, using less than one-third of the pen's capacity. Letting the pen fill up half way (therefore being able to guarantee the storage of the oil) the pen would hold 3.5 hours worth of oil. After 3.5 hours the pen is filled to approximately 40% of its capacity. In the case of the reference well it would not reach this percentage until after 24 hours. This calculation takes into consideration the fact that a larger oil depth would increase the risk of oil escaping the pen when it rolls due to wave motion.

- *Wave Response*: As mentioned before, the adjustment to the pen is to slightly increase the water plane area of the buoyancy rings as well as lower the center of gravity of the pen (by adding ballast onto the bottom of the skirt or change the relative proportion of the skirt to fence length) in order to increase the roll (and pitch) resistance. Of the checks mentioned in Section 5.6 for the pen for the reference well, increasing the water plane area only influences the response of the pen to the waves. The ability of the pen to ride the waves in heave remains approximately the same by this adjustment, since both the natural frequency of the pen in heave and the wave frequency have decreased. The roll/pitch natural frequency on the other hand are decreased far enough such that the pen does not rotate as much, therefore being able to maintain the oil inside it. The widening of the buoyancy ring diameter makes sure that the peak spectral density is approximately lowered by a factor of 3, thereby damping the response. At the same time lowering the center of gravity helps to reduce the roll and pitch natural frequency by about 20%. A reduction of the natural frequency means that it shifts further to the left, away from the peak frequency of the waves, which means that the pen becomes less responsive to the wave, which in this case is a good thing (other than the heave response, where we wanted the pen to ride the waves).

A pen with a diameter of 25m or larger might fit this size oil well better than the 20m diameter pen for the reference well. The bigger diameter would give the following benefits, counteracted by some (manageable) disadvantages:

- Satisfy the oil-water separation requirement
- Storage capacity goes up to 4.5 hours using only a third of the pen depth
- Larger pen diameter does not affect the heave response of the pen
- A larger diameter does affect the roll response in a negative manner, therefore increasing the risk of losing oil spilling over the fence. This however can be counteracted by increasing the skirt length, which would only minimally reduce the ability of the pen to follow the waves in heave.

Overall, increasing the diameter of the pen to at least 25m and increasing the skirt length to 15m would increase the capacity of the pen to satisfy all design requirements under a larger range of conditions. However, for this work we focussed on finding a design for the reference well and seeing how well that design (with two small minor adjustments) would perform in the Gulf of Mexico.

8.9 OrcaFlex Simulations

8.9.1 Input Data

The data used for the Macondo simulations is stated in Table 8.9 below, including the environmental data. Three scaling factors are used to find the design parameters for Macondo:

- The design parameters related to the mooring are all scaled by the water depth minus 10m (which is the height above the seabed at which the top of the shroud is designed to be).
- The shroud length is designed based on the water depth minus 30m (15m above the shroud, 15m between the seabed and the bottom of the shroud).
- The pen and the links need to be scaled up by the same factor, which depends on the oil flow rates and the preferred retaining capacity of the pen as well as the wave conditions (wave height over wave length).

Several important differences from the reference well design are:

- Air can volume
- Distance of shroud bottom from the seabed
- Changes to pen design

Table 8.9: OrcaFlex input data for Macondo

Data Type	Design Values	
Shroud Length	1470m	
Mooring Line Locations	X	Y
Mooring Line 1	2940m	$0m$
Mooring Line 2	-1470m	2546.5m
Mooring Line 3	-1470m	-2546.5m
Mooring Lines		
Total Length	3455m	
Wire	1645m	
Chain	1801m	
Air Can Volume	840m^3 Split over 4 clumps of 130m^3. Attachment points of clamps: 1.5m, 6.5m, 11.5m and 16.5m from the top of the shroud. This air can volume results in a pre-tension of the shroud associated with a 173MPa tensile stress.	
Pen		
Diameter	20m	
Skirt Length	7.5m	
Fence height	2.5m	
Links		
Length [m]	12m	
Stiffness	500kN/m	
Offset from Shroud Top	2.5m	
Environmental Conditions		
Uniform Current	0.2m/s	
Non-Uniform Current	average of two lines in Figure 8-4	
Monochromatic Wave Data ($NOAA$)		
- Significant Wave Height	2.45m	
- Peak Wave Period	7s	

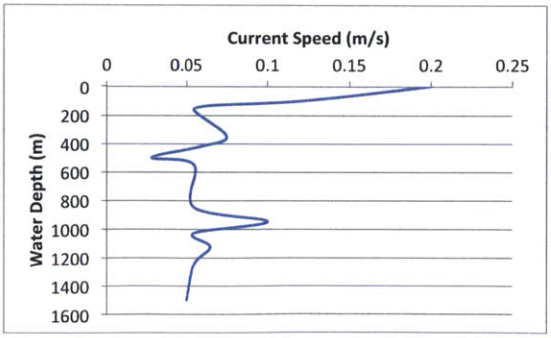

Figure 8-4: Realistic current profile at location of the Macondo well

The volume of the air can is determined by the air volume required to compensate for the weight of the mooring lines as well as the needed tension force to keep the internal cross section from reducing below 80% of the design area. The first volume is determined using the catenary equations to find the shape of the mooring lines. The calculated shape gives an approximation of how much of each mooring line will rest on the seabed, from which it can be inferred how much weight needs to be compensated by the air can. The remaining required air volume is found using the catenary equation (Equation 5.7) to find the needed tension associated with a given pressure differential, rib distance and a maximal cross sectional area reduction to keep the cross-sectional area at least 80% of its designed value along the entire shroud (Section 5.5.1).

Furthermore, there are two important differences to note that are not clear form the table; the first is that the height of the shroud bottom above the seafloor is reduced to only 15m, as supposed to the 20m that was used for the reference well. The reason for this is that from the simulations in OrcaFlex it became clear that the more severe wave conditions were causing the top of the shroud to be affected largely by the wave motions, therefore interfering with the ability of the pen to follow the waves. In addition, the shroud top following the wave motion was leading it to be pushed down far enough that the system no longer was under tension at all times. The variations from tension to compression could lead to damage on the system when it snaps back into being under tension. A 'one size fits all' design could include lowering the reference well shroud by 5m as well, since this should not cause any negative behavior, however, this was not verified in this work.

Lowering the shroud bottom is only one of two ways to solve this; another would be to shorten the shroud length by several meters. The second change is made to the pen in order to make it more resilient to the more severe wave conditions. As mentioned before in Chapter 6 there is a critical rotation (in roll and pitch) that we can allow the pen to undergo without spilling the oil over the top. It turned out that the wave conditions of the Gulf of Mexico requires more resistance in roll, which we achieve by adding an extra, small, buoyancy ring to the pen to increase the total ring diameter to 1.5m instead of 1m. Additionally, lowering the center of gravity of the pen also helps increase roll resistance, which we achieve by adding some (extra) ballast to the bottom of the skirt.

8.9.2 OrcaFlex Simulation Results

Since there already is an understanding of the model from the results and analysis done for the reference well, the discussion of the results for Macondo is more compressed and will focus more on unexpected behaviors based on the knowledge from the case of the reference well.

Uniform Current (with Pen)

Once the mooring lines are attached to the shroud, the $840m^3$ of air results in approximately 350ton of pre-tension. As mentioned before this air can volume originates from upscaling the reference well design based on the increase in the water depth. The results of the shroud being

forced with a 0.2m/s current are presented in Table 8.10 and Figure 8-5. Comparing the results from the Macondo simulations, it is found that, here too, the results fit well with the analytical results and a remaining cross sectional area of 80% of the designed value can be guaranteed for most of the shroud length. Furthermore, here too, addition of the pen causes the top of the shroud to shift by approximately a meter downstream, but the equilibrium position it finds is only 0.45m downstream of the original position (Figure 8-6(a)). This results in the stress only changing marginally (Figure 8-6(b)). As for the behavior of the pen itself, already in this simulation it starts to rotate around its own axis, however, the (absolute) magnitude of the rotations are negligible. In general, the links are designed such that the rotation does not go beyond a 100-degree angle to keep them from rotating around each other too much.

Table 8.10: Macondo well - OrcaFlex results due to a uniform current (with pen)

Variable	OrcaFlex Results	
	Without Pen	With Pen
Maximum Deflection	8.15m	8.22m
Location of Shroud Top	3.30m	3.75m
Tensile Stress	173MPa	173MPa
Tension in the mooring lines		
Mooring Line 1	2395kN	2396kN
Mooring Line 2	2339kN	2338kN
Mooring Line 3	2339kN	2338kN

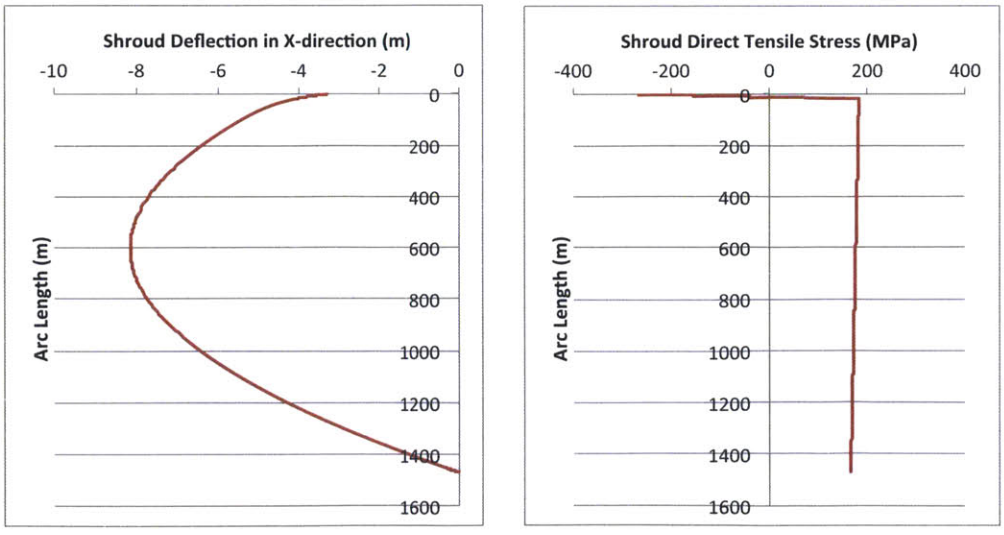

(a) (b)

Figure 8-5: Macondo well - (a) Deflection (m) and (b) tensile stress (MPa) profiles due to a uniform current (without pen)

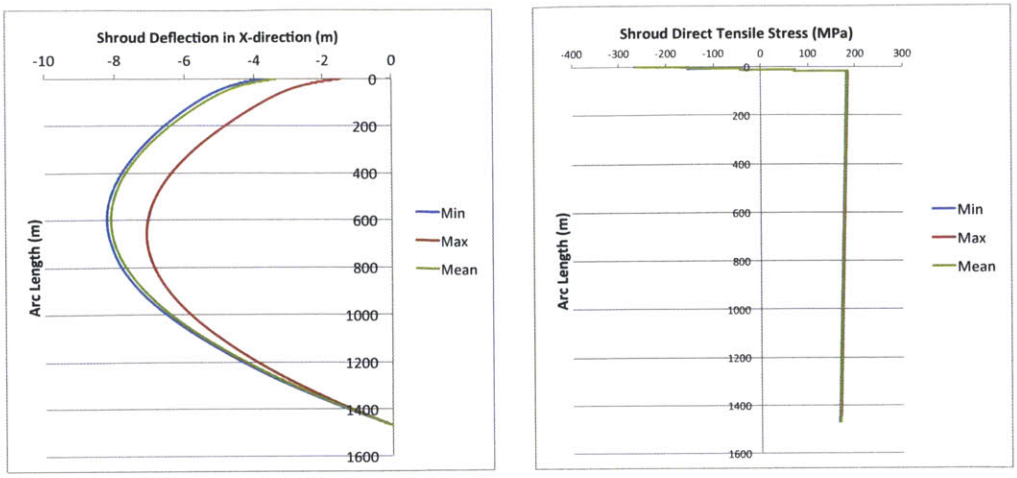

(a) (b)

Figure 8-6: Macondo well - (a) Deflection (m) and (b) tensile stress (MPa) profiles due to a uniform current with pen

Non-Uniform Current (with Pen)

It is very evident from Figure 8-7(a) that the realistic conditions of a non-uniform current are a lot less stringent on the system than the uniform current of 0.2m/s. The maximum deflection is only approximately one meter. What is further interesting to notice is that, like in the analytical results, the strength of the current does not significantly influence the tensile stress on the material. The tensile stress on the material is governed by the strength of the buoyancy force; therefore this result does not vary much between the simulations with the uniform current and the non-uniform current (compare Figures 8-5(b) and 8-7(b) without the pen or compare Figures 8-6(b) and 8-8(b) with the pen).

Addition of the pen causes the system to be moved downstream by about 0.15m, which is in line with the results thus far, and again the tensile stress remains approximately the same.

Table 8.11: Macondo - OrcaFlex results due to a non-uniform current (with pen)

Variable	OrcaFlex Results	
	Without Pen	With Pen
Maximum Deflection	0.93m	1.03m
Location of Shroud Top	0.51m	0.65m
Tensile Stress	173MPa	173MPa
Tension in the mooring lines		
Mooring Line 1	2364kN	2365kN
Mooring Line 2	2355kN	2355kN
Mooring Line 3	2355kN	2354kN

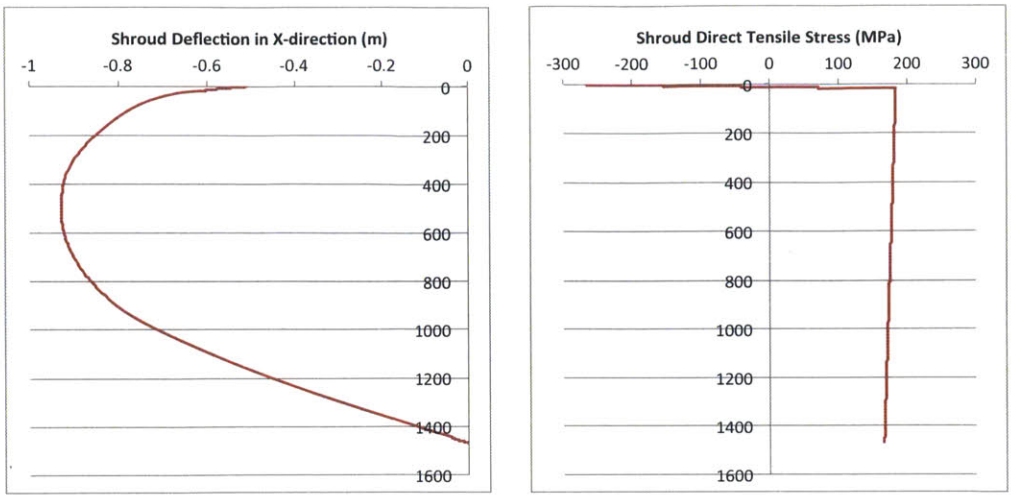

(a) (b)

Figure 8-7: Macondo well - (a) Deflection (m) and (b) tensile stress (MPa) profiles due to a non-uniform current (without pen)

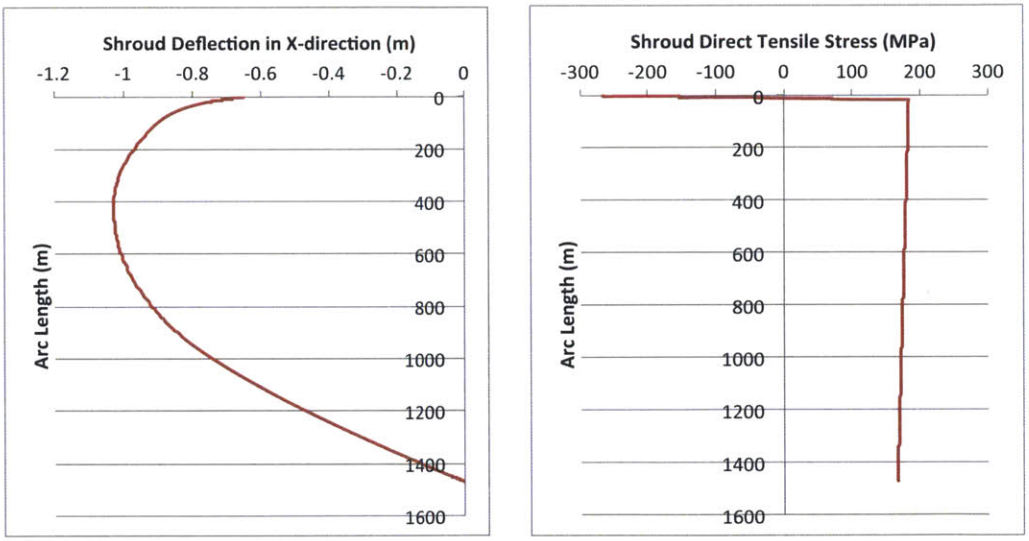

(a) (b)

Figure 8-8: Macondo well - (a) Deflection (m) and (b) tensile stress (MPa) profiles due to a non-uniform current with pen

Monochromatic Wave

Like for the reference well simulations, the shroud is found to be oscillating along its entire length, the entire shroud moves back and forth a bit. The oscillatory movement of the top of the shroud is presented in Figure 8-11, where just as in the case of the reference well, the shroud oscillates around equilibrium, which is slightly downstream from its original position (Figure 8-9). In the discussion of the results for the reference well the theory was presented

that the amplitude of the oscillatory motion is not the same as the wave amplitude due to restriction of the movement based on the buoyancy force as well as that due to the mooring lines. The results here are in agreement with this theory, since this time the amplitude of the shroud movement is about that of the waves, so it seems that the Macondo well design might be slightly less constrained than the shroud for the reference well. Lastly, it is important to notice that, due to the oscillatory motion, the tension stress on the material varies quite significantly (Figure 8-10). We have designed the shroud with high restrictions on the lateral displacement in response to a current, which results in the requirement of a high buoyancy force. The additional benefit from this high buoyancy force is that there the tensile stress is high enough that the shroud will always be under tension.

Table 8.12: Macondo well - OrcaFlex results to a monochromatic wave

Variable	OrcaFlex Results Without Pen
Maximum Deflection	0.69m
Location of Shroud Top	0.28m
Tensile Stress	$89 - 173 - 261$MPa
Tension in the mooring lines	
Mooring Line 1	$2292 - 2361 - 2433$kN
Mooring Line 2	$2271 - 2355 - 2437$kN
Mooring Line 3	$2271 - 2355 - 2437$kN

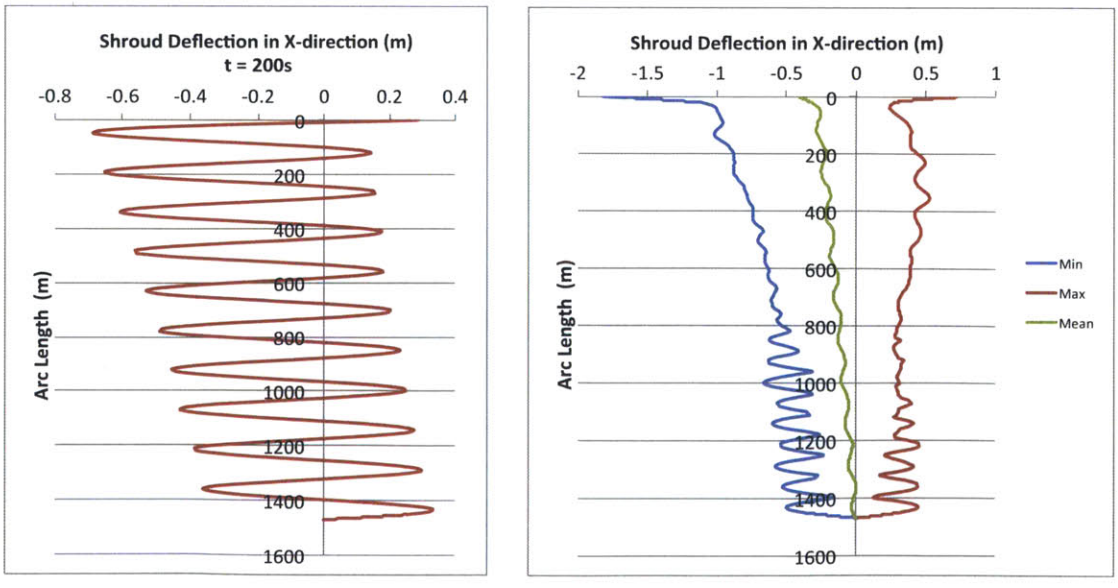

(a) (b)

Figure 8-9: Macondo well - (a) Deflection (m) at t= 200s and (b) deflections (m) for the entire simulation due to a monochromatic wave

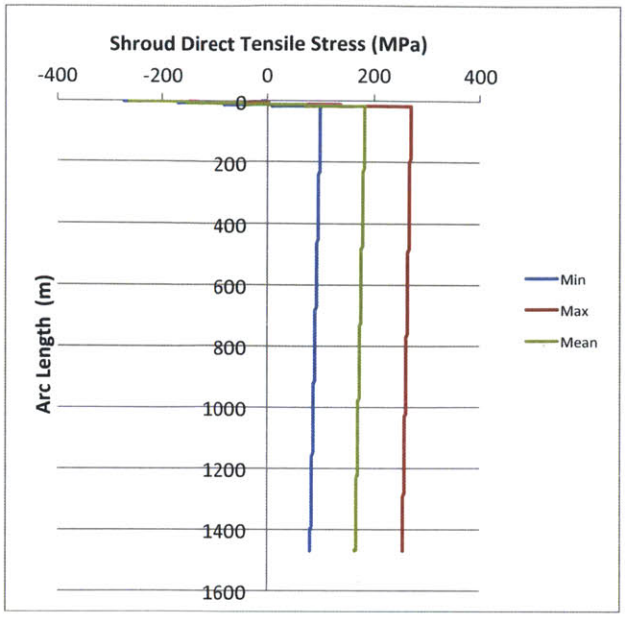

Figure 8-10: Macondo well - Tensile stress profile due to a monochromatic wave

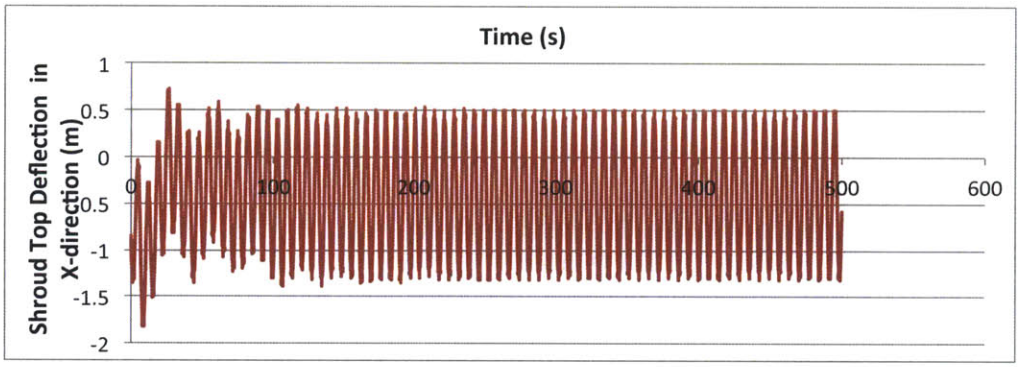

Figure 8-11: Macondo well - Displacement of the shroud top over time due to a monochromatic wave.

Monochromatic Wave with Pen

As seen for the reference well, the results show that the addition of the pen does not affect most of the behavior of the system very much (Figures 8-12 and 8-13). In the beginning, the model needs some time to find the stable position for the system. It is interesting to note that the shroud top does oscillate around an equilibrium position; somewhere between 1-1.5m downstream from the starting position, however it is not a clean oscillatory motion (Figure 8-14). Comparising with the other modeling steps, it appears that there is some interaction from the pen onto the shroud. The secondary oscillation is caused by the pen pulling on the shroud top, followed by the mooring lines constraining the lateral movement of the shroud. Furthermore, the rotational behavior of the pen is still within the required values (Figure 8-15).

Table 8.13: Macondo well - OrcaFlex results due to a monochromatic wave

Variable	OrcaFlex Results Without Pen
Maximum Deflection	1.28m
Location of Shroud Top	0.8m
Tensile Stress	$111 - 179 - 240$MPa
Tension in the mooring lines	
Mooring Line 1	$2299 - 2370 - 2453$kN
Mooring Line 2	$2261 - 2353 - 2431$kN
Mooring Line 3	$2279 - 2352 - 2418$kN

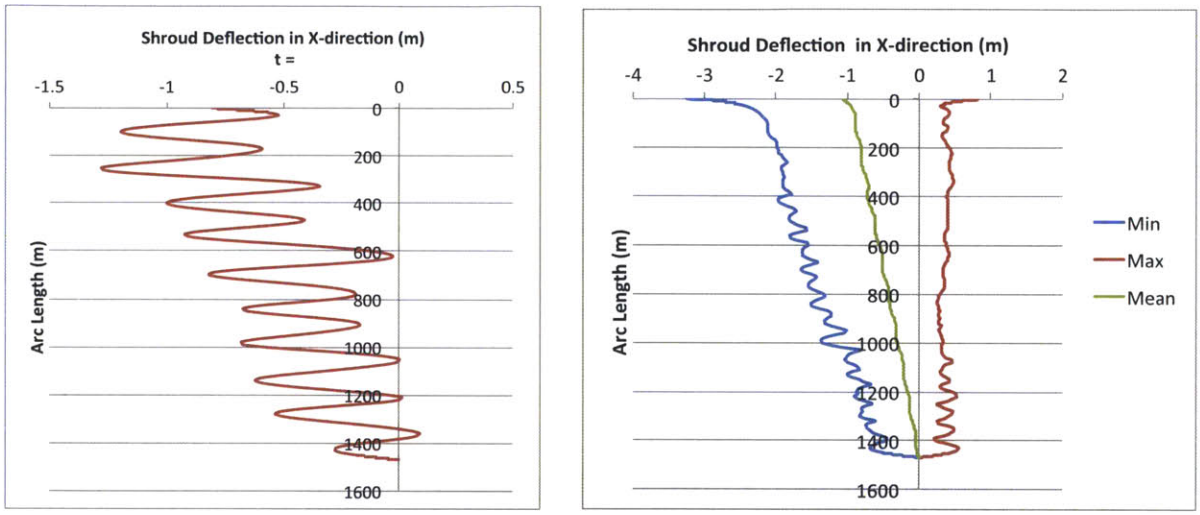

(a) (b)

Figure 8-12: Macondo well - (a) Deflection (m) at t= 250s and (b) deflections (m) for the entire simulation due to a monochromatic wave with pen

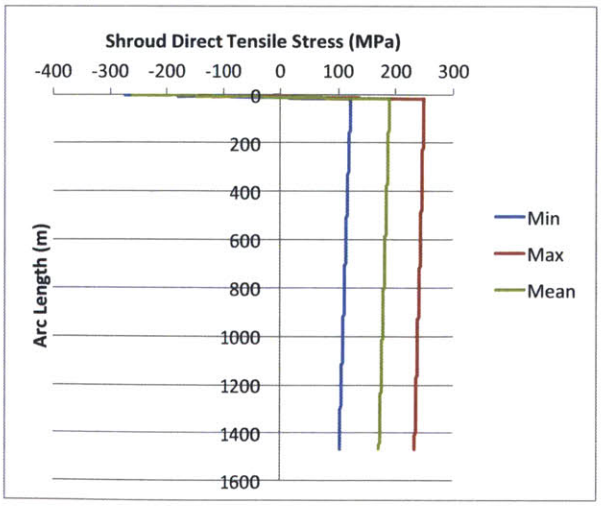

Figure 8-13: Macondo well - Tensile stress (MPa) profile due to a monochromatic wave with pen

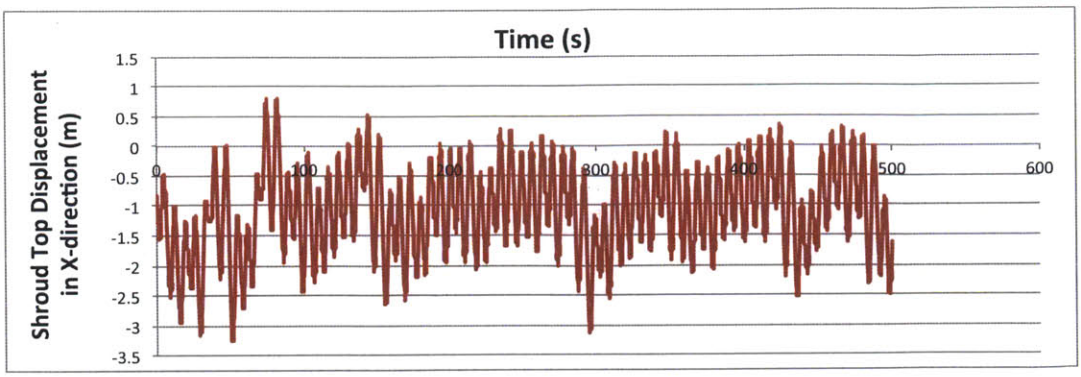

Figure 8-14: Macondo well - Displacement (m) of the shroud top with pen over time due to a monochromatic wave.

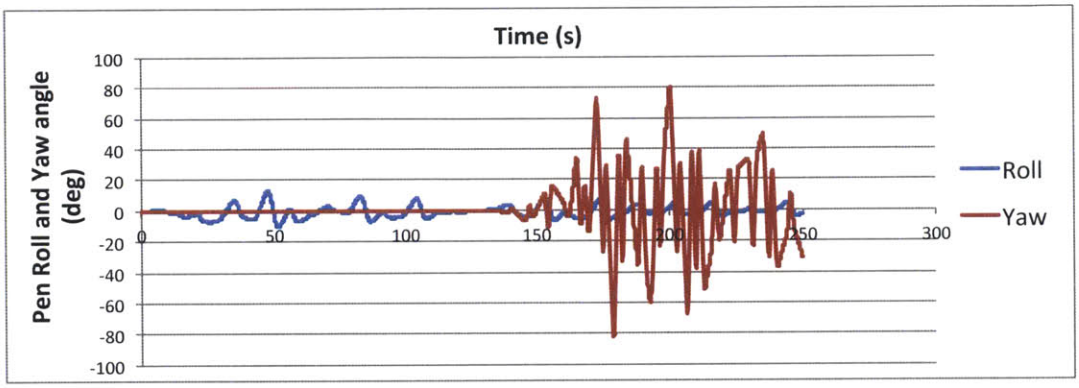

Figure 8-15: Macondo well - Roll and yaw response of the pen due to a monochromatic wave

Monochromatic Wave and Uniform Current (with Pen)

The results for the monochromatic wave and the uniform current are similar to what was found for the design for the reference well. The deformed shape looks like an interesting superposition of the two responses, which together result in a deformation that is larger than either separately (Figure 8-16). The tensile stress is similar to that of the monochromatic wave, also in the variation during the oscillation (Figure 8-17). Again, the oscillations have an amplitude that is slightly smaller than that of the wave and take place around an equilibrium (Figure 8-18).

The addition of the pen, like in the other cases, does not change much of the behavior (Figures 8-19, 8-20, 8-21 and 8-22). The main difference is that the system does not seem to find a final equilibrium position on the global scale; however the variations are within a 1m range.

Table 8.14: Macondo well - OrcaFlex results for a monochromatic waves and uniform current (with pen)

Variable	OrcaFlex Results	
	Without Pen	With Pen
Maximum Deflection	13.0m	14m
Location of Shroud Top	5.0m	6.7m
Tensile Stress	$90-174-260$MPa	$108-180-245$MPa
Tension in the mooring lines		
Mooring Line 1	$2341-2420-2471$kN	$2334-2434-2514$kN
Mooring Line 2	$2250-2324-2414$kN	$2259-2319-2406$kN
Mooring Line 3	$2250-2324-2414$kN	$2259-2319-2406$kN

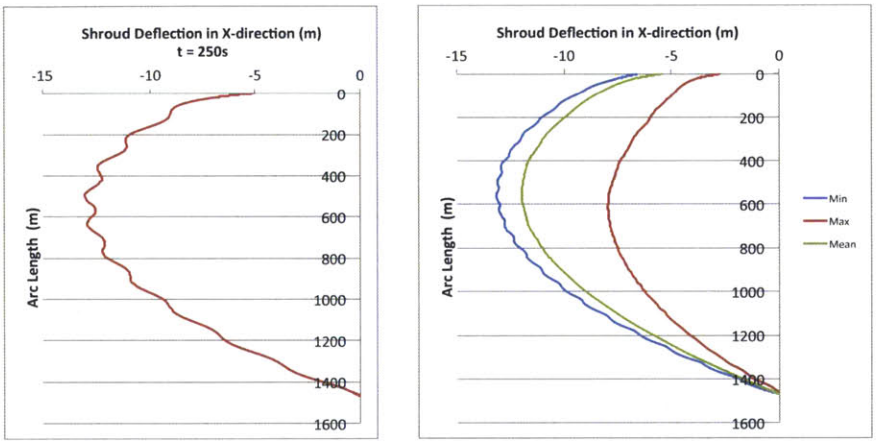

(a) (b)

Figure 8-16: Macondo well - (a) Deflection (m) at t= 250s and (b) deflections (m) for the entire simulation due to a monochromatic wave and uniform current

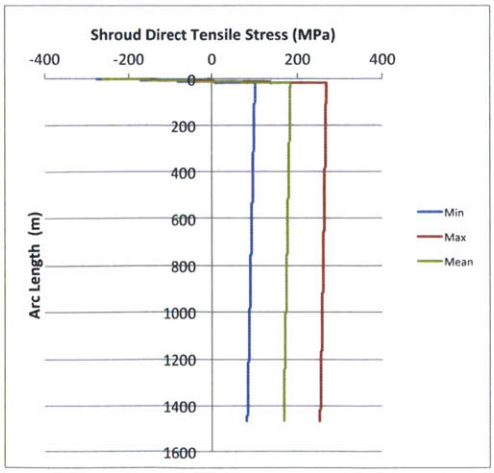

Figure 8-17: Macondo well - Tensile stress (MPa) profile due to a monochromatic wave and uniform current

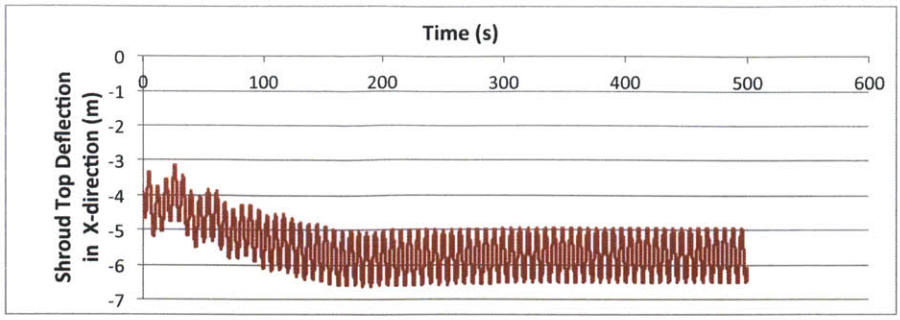

Figure 8-18: Macondo well - Displacement (m) of the shroud top with pen over time due to a monochromatic wave and uniform current.

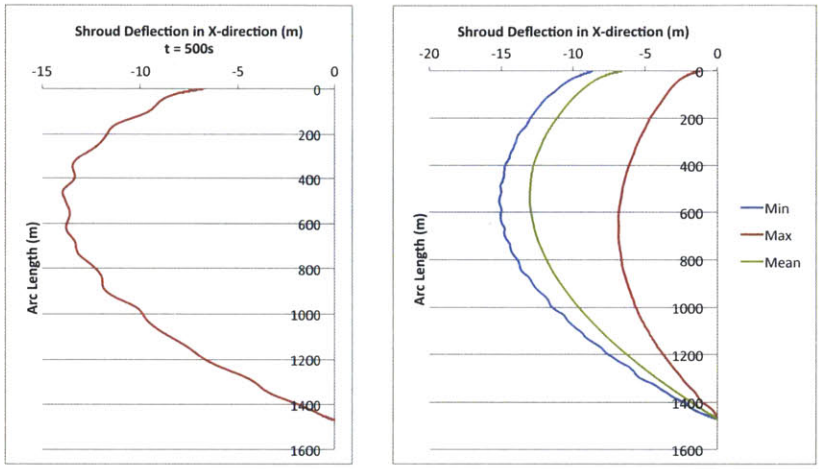

(a) (b)

Figure 8-19: Macondo well - (a) Deflection (m) at t= 250s and (b) deflections (m) for the entire simulation due to a monochromatic wave and uniform current with pen

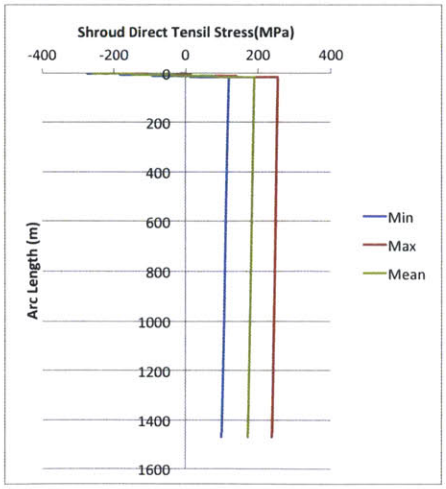

Figure 8-20: Macondo well - Tensile stress (MPa) profile for the system with pen subjected to a monochromatic wave and uniform current

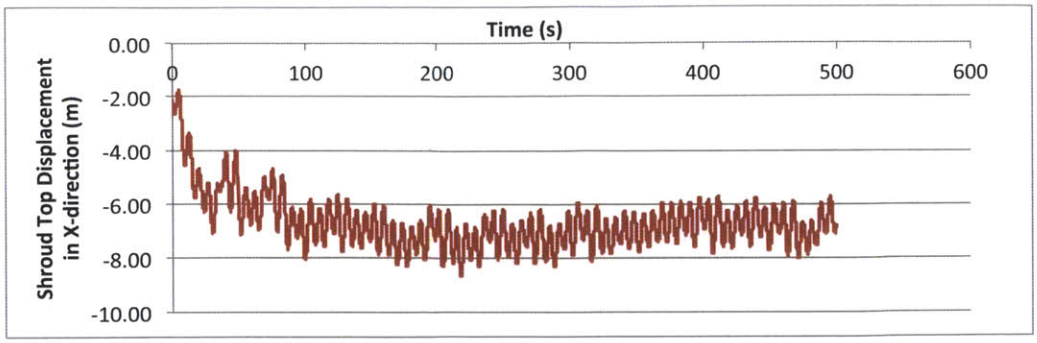

Figure 8-21: Macondo well - Displacement (m) of the shroud top with pen due to a monochromatic wave and uniform current.

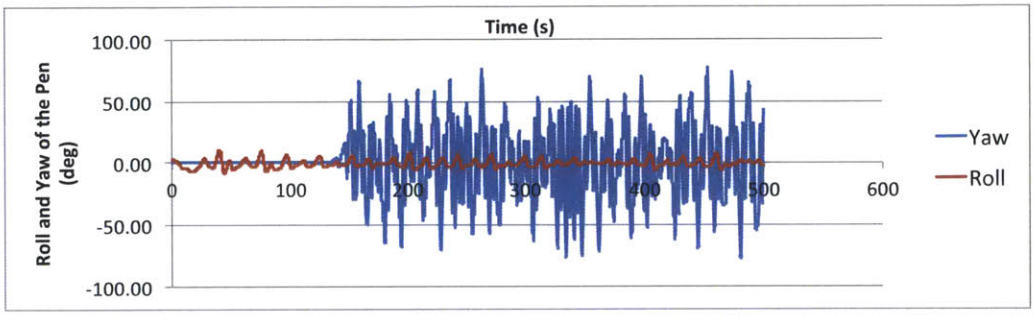

Figure 8-22: Macondo well - Roll and yaw response of the pen over time due to a monochromatic wave and uniform current.

Wave Spectrum

Like for the reference well, we have attempted to create a wave spectrum that represents realistic wave conditions. In this case we have done so based on wave data from the Thunderhorse BP platform, which is made public through the NOAA Buoy Data Center *NOAA*. This fixed drilling platform is chosen due to its location close to the Macondo Well and only marginally larger water depth (1850m). The JONSWAP model (Equation 6.1) is used again to create the spectrum. The data from the BP drilling platform represents data from May and June of 2010, which is also the time of the Macondo Well oil spill. The spectrum that we find is shown in Figure 8-23. Figure 8-24 shows the directional spectrum that belongs to the Thunderhorse well site.

The results for the OrcaFlex simulations for the wave spectrum and uniform current are given below in Table 8.15 and Figures 8-25 through 8-27. As can be seen, all results point out that the system would do well even under the more stringent conditions of the Gulf of Mexico. Similarly to the results found for the reference well, we find here that the pen rotations are the critical component. The roll and pitch rotations go up to maximum acceptable values once or twice during the simulations, which would restrict the thickness of the oil layer in the pen to approximately 3m. (Due to density differences with the water, about 1/4 of the thickness will be above the water level).

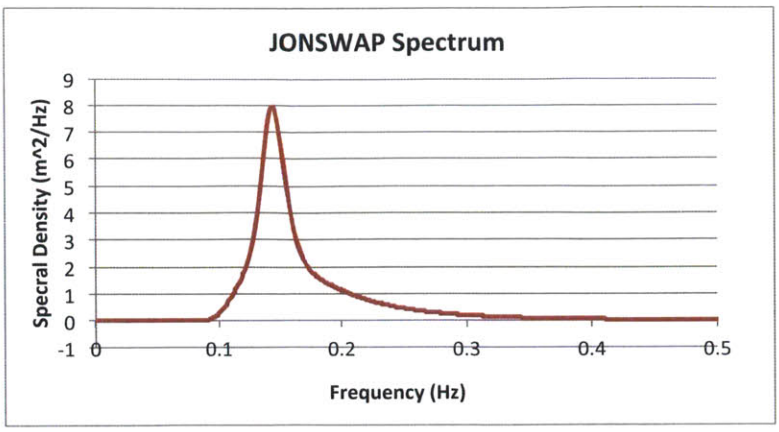

Figure 8-23: JONSWAP wave spectrum that represents the wave conditions measured at the BP Thunderhorse platform, located close to the Macondo well

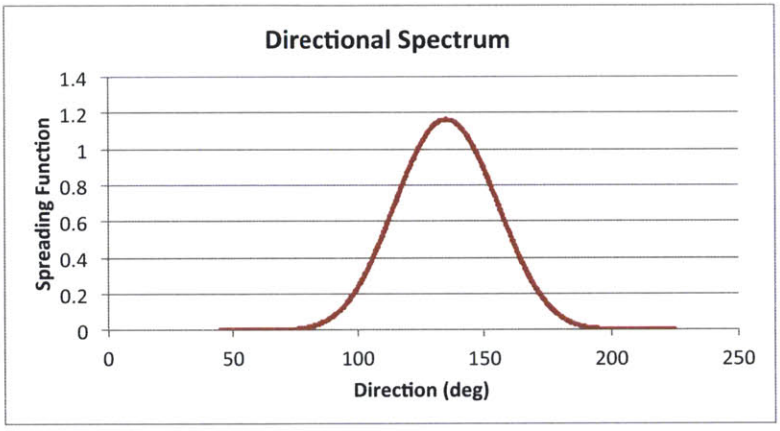

Figure 8-24: Directional wave spectrum that was measured at the BP Thunderhorse platform

Table 8.15: Macondo well - OrcaFlex results for a wave spectrum and uniform current with pen

Variable	OrcaFlex Results
Maximum Deflection	14.4m
Location of Shroud Top	4.8m
Tensile Stress	115 – 182 – 252MPa
Tension in the mooring lines	
Mooring Line 1	2315 – 2414 – 2533kN
Mooring Line 2	2190 – 2329 – 2424kN
Mooring Line 3	2197 – 2331 – 2440kN

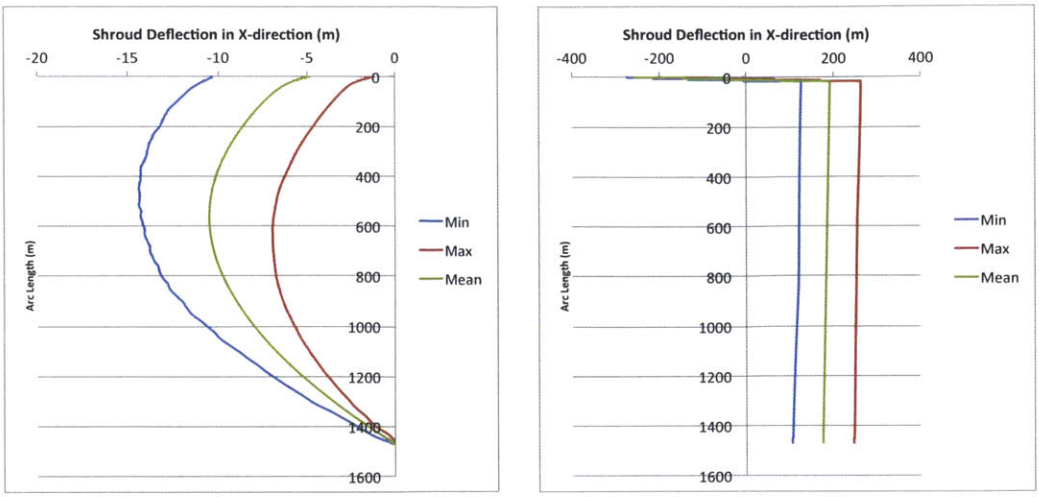

(a) (b)

Figure 8-25: Macondo well - (a) Deflections (m) during the entire simulation and (b) tensile stress (MPa) on the shroud material due to previously defined wave spectrum and uniform current with pen

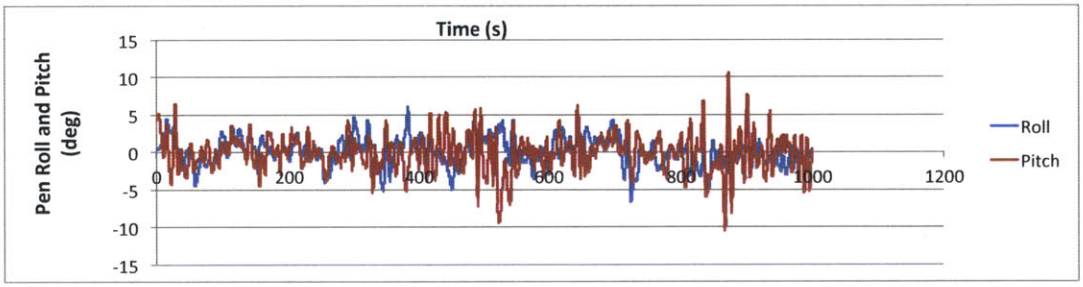

Figure 8-26: Macondo well - Roll and pitch response of the pen over time due to a wave spectrum and uniform current.

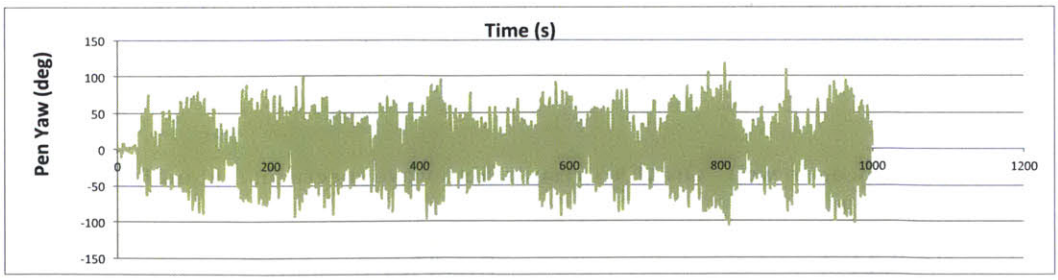

Figure 8-27: Macondon well - Yaw response of the pen over time due to a wave spectrum and uniform current.

Overall the design for the reference well (with minor adjustments) appears to still satisfy all requirements even under the more severe environmental conditions that are present at the Macondo well. The next paragraph will go into a sensitivity analysis that was done for a number of parameters; it gives insight into how their values influence the response of the system.

8.10 Sensitivity Analysis (with OrcaFlex)

Since the goal is to find one design that works for a wide range of wells, we use the exact same pen design and an extrapolated shroud design for the initial simulations for the Macondo well. This design works well for the modeling steps with just a (non-)uniform current. However, there are two ways in which the system's response to the waves does not satisfy requirements: firstly, the shroud is no longer under tension at all times and secondly, the pen rotates beyond a maximum value, which causes the fence of the pen to become partially submerged. In trying to resolve these concerns without significantly altering the design, we observed a number of sensitivities, discussed below, that were not anticipated.

- *Water depth of shroud top*: If the shroud top is located too close to the water level it gets displaced quite significantly by the orbital wave motion. This behavior has two consequences; firstly, the shroud is pushed downward far enough that the air can can no longer keep the shroud under tension at all times. The transition from compression to tension could cause the material to tear due to a sudden pull on the material. For this reason the shroud should remain under tension at all times. Secondly, the big displacements of the shroud top causes it to pull down on the pen. The pen can therefore no longer respond freely to the wave motion. The enforced restriction occasionally causes the pen to end up being partially submerged.

  Since the orbital motion of the waves decays exponentially with the water depth ($\sim e^{kz}$ where z runs from 0 to -H (water depth)) it is enough to lower the position of the shroud top by just 5-10m to reduce the two phenomena identified above. There are two ways to lower the shroud top. The first is to reduce the height of the shroud bottom from the sea bed. Using the winches on the bottom mooring lines to bring the flared section closer to the well head is one example of how to achieve this. The other option would be to not unfold the top section of the shroud to its full length of 100m. The unfolding mechanism is designed to make it possible to lower only a number of sections between ribs; meaning that 10m sections can be lowered if that is necessary. Due to the simplicity of the first method (just lowering the shroud), we give preference to that solution.

- *Pen response to waves*: The more severe wave conditions in the Gulf of Mexico make it harder for the reference well pen design to contain the oil. The worsened behavior is especially apparent in the roll/pitch response. Looking into the effect of each of the design components we find that the best way to reduce the roll and pitch response is to either increase the net diameter of the buoyancy rings or to lower the center of gravity of the pen. The first approach has a straight forward solution: larger buoyancy rings or adding a smaller ring around the existing one. The disadvantage of this solution is that it (slightly) reduces the ability of the pen to ride the waves in heave. The second approach, to lower the center of gravity in order to stabilize the pen, can be achieved in several ways: either by adding ballast to the bottom of the skirt or by simply increasing the length of the skirt. Both options have the advantage that they can be done modularly, keeping one (base) design that can match all requirements.

Furthermore, Section 8.8 describes how the 20m diameter would be too small if we want all the droplets to separate from the water plume. Increasing the diameter to 25m was suggested as a way to eliminate this problem. It turns out, however, that increasing the diameter reduces the restoring capacity of the pen in roll and pitch. Since the roll and pitch response were already a slight concern, increasing the diameter would leave us no choice but to increase the skirt length and lower the center of gravity of the pen to make sure that the roll and pitch rotations stay within the required thresholds. The disadvantage of this solution is that we would have to step away from the 'one design fits all' objective.

Understanding how variations in these parameters affect the response of the pen to waves allows us to adjust the basic design to better fit the existing environmental conditions. The shroud design does perform well as a 'one size fits all'.

8.11 Vortex Induced Vibrations

Similarly as for the design for the reference well, we can use VIVA to run the vortex induced vibration analysis. Most of the input is the same, since most values are given per meter length. The only differences are the tension at the top of the shroud, which in this case is as high as $3x10^6$N and the values for the non-uniform current, which can be found in Figure 2-5. In order to find conservative results for the fatigue life, we use the fatigue characteristics for steel (A = 1.05 x 10^{30} and B = 3).

8.11.1 Results

For the case of the Macondo well, VIVA finds the the output shown in Table 8.16.

Table 8.16: VIVA output data for Macondo and a non-uniform current

Variable	Output
Dominant mode	1
Response frequency [Hz]	0.0052
Maximum amplitude [m]	3.04
Minimum fatigue life [yr]	147,000 (failure will occur half way down the length of the shroud)

From the results in Table 8.16 it can be concluded that VIV is also not a concern for the Macondo well, firstly because the amplitudes of the oscillation are less than 1% of the shroud length and secondly, because even for very conservative fatigue behavior of the material, the shroud has a fatigue life that is much longer than the six months of operation for which we are designing the system. Similarly as for the reference well, we find that the currents induced by the waves defined by the sea spectrum do not change the non-uniform currents enough to have any noteworthy affect on the VIV response of the shroud.

We therefore conclude that VIV is not a concern for the integrity of the shroud and therefore does not need to be designed for.

Chapter 9

Conclusion & Future Work

In this chapter we would like to reflect on the process that we used to design the shroud system and briefly state the conclusions that we found through this research. As the final part of this work we look ahead to try to identify the analyses that need to be done in the future to validate the design (assumptions) that were made, as well as to test the system.

9.1 Conclusions

This work has shown that this new type of flexible containment system for deep ocean oil spills can be designed to contain the vast majority of the hydrocarbons exiting the wellhead, and do so for wells with very different flow and environmental conditions under the objective of 'one design fits all'.

Based on the buoyancy flux created by the hydrocarbons we found that using a three meter diameter for the shroud induces a flow that is large enough to dilute the gas bubbles to a level far below saturation. As long as the concentration is below saturation, solid hydrate crystals will not form; at the most crystal shells will form on the gas bubbles. Meanwhile, the velocity through the shroud is low enough to support dissolution of the gas into the water column, making sure the surface gas concentrations are below legal thresholds related to workers' safety.

Catenary equations were used to model the response of the shroud to a simple, yet conservative 0.2m/s uniform current as a function of the applied pre-tension on the system. The analysis pointed out that attaching a 520m^3 air can attached to the shroud top can create enough pre-tension to compensate for the weight from the mooring lines and keep the deflections of the shroud within 2.5% of its length. The associated tensile stress on the Kevlar remains below 15% of its strength. Reinforcement ribs every 20m and the pre-tension ensure that the cross-sectional area of the shroud does not drop below 80% of its design value, despite a relatively high pressure differential over the material. The small reduction of the cross-section eliminates the possibility of flow separation and associated dead zones that might give hydrates a chance to agglomerate. It also minimizes the effective roughness, reducing friction and thus minimizing loss of flow. The reinforcement ribs (circular I-beams with syntactic foam) are designed to withstand the buckling force caused by that same pressure differential.

The top of the shroud connects to the containment pen through four links. The links are long, flexible nylon wires, in order to allow both the shroud and pen to move independently (but constrained enough to make sure that the hydrocarbons are transferred from the shroud into the pen successfully). The pen is designed to ride the waves in heave, yet be somewhat restricted in roll, pitch and yaw, to keep the oil from flowing over the fence. Lastly, the size of the pen diameter in combination with the baffle ensure water-oil separation so that the skimmer weir collects oil with a low water content. Storage of the oil on the tanker requires a low water content for safety reasons, and gives the opportunity to still refine and sell the oil.

Simulations with the finite element software OrcaFlex produced results that were within several percent of the analytical results; giving us the confidence to run more complex environmental conditions. As predicted, the realistic non-uniform current puts even less strain on the system than the previously mentioned uniform current. Also, as expected, addition of the pen only slightly increases the shroud deflection (due to the relatively small drag on the pen). Next, simulations for a characteristic, monochromatic wave pointed out that the orbital motion of the waves will cause the system to oscillate around an equilibrium position. Besides the back and forth oscillation of the shroud as a whole, the waves also force a wave to travel along the length of the shroud. The oscillatory motion causes the tensile stress on the Kevlar to vary within a 100MPa range, yet the shroud always remains under tension.

A monochromatic wave and uniform current together lead to a superposition of the results for each of the behaviors individually. Addition of the pen still does not affect the behavior significantly. The roll-, pitch- and yaw-response of the pen itself to the monochromatic wave stay within the required range and the simulations also confirm that the pen can ride the waves in heave. Use of a wave spectrum to simulate more realistic conditions pointed out that the response of the shroud does not change much; the pen has an increased response in roll and pitch, though still within the acceptable range of rotations.

The simulations in OrcaFlex pointed out two important sensitivities that were not anticipated. Firstly, if the shroud top comes too close to the surface it gets affected strongly by the orbital motion of the waves, causing a constraining effect on the pen motion, which leads to loss of oil. Lowering the shroud resolves this problem. Secondly, the response of the shroud is sensitive to the design of the mooring lines in combination with the volume of the air can. Due to the large weight of the chain section of the mooring lines, the behavior of the shroud is affected strongly by how much of the chain rests on the seabed. The buoyancy provided by the air can influence this, making the combination a complex system to design.

The last analysis deals with the occurrence of vortex induced vibrations, since the shroud is a cylindrical structure exposed to a current. With the use of the software tool VIVA it was found that the high pre-tension on the shroud ensures that VIV is not a concern. Failure of the system from fatigue due to VIV would not occur until far beyond the lifetime of the system.

The analyses described above were repeated for a scaled up version of the design for the

reference well that could be used at the Macondo well. The system would have more modules, longer mooring lines and a bigger air can. The results point out that the design still satisfies the design requirements, but is pushed closer to the limits of acceptability. The only needed adjustment to the shroud is to lower the top, so that it stays out of the strong orbital motion of the waves. The pen, however, can only barely satisfy design requirements: the rotational responses approach the maximum acceptable values (to prevent oil loss) more frequently, especially for the simulations that model the system's response to a wave spectrum. Increasing the pen diameter to 25m and the skirt length to 15m would improve the response significantly. Furthermore, a larger pen would also be needed to properly separate the water from the oil as it exits the shroud.

Over all, this work has shown that 'one design can fit all'; large wells would only require minor adjustments in order to maintain a safety margin between its operational response and the design requirements. The two most important ones to the shroud system are the increase volume of the air can and halving the distance between the reinforcement ribs (the sleeves were already in place, the design for the reference well only fills every other sleeve with a rib). As for the pen, the 20m diameter used for the design for the reference well, might be too small to dilute the gas concentrations at the surface below the allowable thresholds. Furthermore, this pen diameter does not allow all oil droplets enough time to separate from the water exiting the shroud. Both these issues can be resolved by increasing the pen diameter to at least 25m. As for its response to waves; the 20m diameter pen for the reference well responds well in heave, but occasionally rotates too far in roll and pitch, causing oil to leak out from the pen. By adding an additional buoyancy ring to increase the water plane area, and lowering its center of gravity by adding some ballast to the bottom of the skirt we can reduce the pen's response to waves in roll and pitch. These adjustments, therefore make it possible for the pen to contain the oil at all times.
We analyzed the system for modest conditions and then extrapolated the design to more extreme conditions. We realize that we could have done it backwards and used the Macondo well conditions as a starting point, which probably would have given us a slightly over designed system for the reference well. Still, a different conclusion could have been that it was better to aim for 3 or 4 basic designs (each to cover a smaller range of conditions); we would thereby reduce the chance that a system would be pushed to its operating limit.

Based on the chosen design we developed a deployment plan that can make sure that the system can be operational within a couple of days. The sections and most of the mooring configuration are already assembled onshore and are stored in a warehouse from which a large number of wells are easily accessible. The pen itself is assembled and can be is stored in a folded up fashion; only the skimmer weir and baffle are still detached. If a blowout occurs, a multi-purpose vessel (with a moonpool) will transport everything to the well. The installation of the system will almost entirely take place offset from the well, for safety of the crew, and parts will mostly be lowered through the moonpool. The shroud sections are attached to each other as the system is lowered; at the end the air can and pen are attached to the top section. The final steps entail attaching the mooring lines and placing the system over the wellhead.

We have shown that the deployment of the system is possible, but requires attention for practical details.

In the event of bad weather, e.g. a hurricane, there are two ways in which we could protect the system. One way would be to just take of the pen, but leave the rest of the system in place, since it is below the surface. Another way would be to take of the pen, air can, and mooring lines and have the shroud rest on the seafloor (with a buoy attached to it, in order to relocate it again after the storm. The mooring lines would also have buoys attached to them, like during the deployment, also in order to find them and attach them to the shroud again after the storm. In order to make a decision for either of the solutions practical input is needed from people working on the deployment (similar) offshore systems, and therefore no preference is stated at thus far.

9.2 Validation

The analysis and computational simulations resulted in the design of a system that would likely work for future deep sea oil spills. Before that can be guaranteed, however, pars of the system should be tested in the laboratory. One set of experiments would verify the response of the pen-uppershroud system to a spectrum of waves. Related to this, another set of experiments would explore the dynamics of oil sloshing in the pen, and hence its tendency to leak when excited by strong waves. (Recall that the analysis conducted so far was only static based on the degree of predicted pen rotation in roll and pitch.) A third experimental activity would explore the ability of the pen to separate the rising oil and water allowing a better estimate of capture efficiency. Because the shroud system is several hundreds of times taller than it is wide, a full system can not easily be tested in a scale model. The focus would need to be on the pen and the upper shroud.

Finally, validation of the deployment plan is crucial. Some of the aspects of the plan can still be analyzed and revised on paper. However, once the plan is completed with help of experienced crews, actually executing it will point out further complications that might have been overlooked before. Performing this deployment exercise is especially important because it could bring to light that certain components require redesigning. A good opportunity to do so would be during a deep ocean spill experiment, similar to the Deep Spill experiment off the coast of Norway. A field experiment provides a great chance to test both the deployment as well as the capabilities of the structure in real life conditions.

Appendix A

Benchmarking

The benchmarking analysis is done for two reasons:

1. To identify the other existing solutions for deep ocean oil spills that are protected by patents in order to see which components of the shroud design could be patented.

2. Learn from the existing designs and possibly find applications or uses of details to the shroud design.

The patents used in the analysis are all types of containment system, ranging from dome-like structures to open, flexible system. In the evaluation four categories were identified. For each category the benefits and drawbacks are identified, followed by a detailed analysis for a number of patents of which the design has useful components for our system.

A.1 Categories

The four categories defined for this benchmarking analysis are the following:

1. Hard Seal Systems

   (a) Examples: Capping Stacks, hydraulic seal, etc.

   (b) Characteristics
   - Metal-to-Metal connection (closed)
   - Attached to BOP
   - These systems have a mechanical device that can shut off the flow

2. Soft Seal Systems

   (a) Examples: Cofferdam-like systems, etc

   (b) Characteristics
   - Are not attached to the wellhead
   - Edges are resting on the seabed (soft seal)
   - Can be either rigid of soft materials

3. No Seal Systems

   (a) Examples: rigid versions of the shroud design

   (b) Characteristics
   - Edges are NOT resting on seabed
   - Made of rigid material (e.g. steel)
   - The system is not attached to the wellhead

4. No Seal, Flexible/Modular Systems

   (a) Examples: Designs similar to our shroud

   (b) Characteristics
   - Edges are not resting on seabed
   - The system is not attached to the wellhead
   - The systems have a recovery system
   - Material is soft and flexible

Sections A.3 through A.6 will further describe the designs in each category and identify the strengths and weaknesses of each of the group, both in general as compared to the shroud system.

A.2 Overview/Summary

A number of characteristics have been identified that are either preferred to be included or excluded from a deep ocean oil containment system. Table A-1 states an overview of these characteristics and compares how each of the categories as well as the shroud design do on each of the characteristics. Characteristics 1-9 would be advantages to a design, while characteristics 10-12 are not desirable.

Combining the description of the categories and the results from Table A-1 it is clear that categories III and IV are the most similar, IV even more so than the third category. These two categories are therefore the most important ones, from which the most significant lessons can be learnt.

From the table it also becomes clear that the shroud design has the highest number of desirable characteristics, this could potentially make the design patentable. This document will be used to show that inducing a chimney effect to guide the hydrocarbons to the surface is an original concept. The suction of large volumes of ambient seawater into the shroud help guarantee low gas concentrations (beneficiary to safety considerations) as well as eliminating the potential threat of hydrate formation. Two characteristics that are extremely valuable to a containment system and are not offered by other available design concepts.

Characteristic	Category I (Hard seal)	Category II (Soft seal)	Category III (No seal)	Category IV (No seal flexible)	Our Shroud Design
1. According to drilling standard	++	+	NA	NA	NA
2. Dilution of gas concentrations	NA	+	++	++	++
3. No need for accurate positioning	NA	NA	++	++	++
4. Low weight of the system	NA	NA	+	++	++
5. Lack of active components	NA	++	++	++	++
6. Serve distributed source	NA	+	++	++	++
7. Ability to disconnect top facility	++	NA	NA	NA	+
8. Works for different leaking sources (e.g. including sunken oil tanker leaks)	NA	+	++	++	++
9. Fits all water depths	++	++	Some	++	++
10. Oil-Water Separation	- -	Some	Some	Some	++
11. Requirement of clean interface	- -	NA	NA	NA	NA
12. Interaction with the ocean water	NA	Not really	- -	- -	- -

Figure A-1: Overview of categories for benchmarking
NA = Not Applicable

A.3 Category I - Hard Seal Systems

A.3.1 General Discussion

A good example of the type of system that falls into this category is the capping stack (Figure A-2). It is a large metal structure that is placed on the BOP in case of failure. Temporary lines can tap the hydrocarbons from the capping stack and guide it to the surface. Systems in this category generally use industry standards or well understood mechanisms, so are highly preferred by the industry.

Figure A-2: Capping stack developed by Marine Well Containment Company

Advantages of systems that fall into this category are the following:

- No interaction with the ocean. Since it is a metal-to-metal seal, this has a number of consequences
  - Potentially no loss of hydrocarbons
  - Same quality oil is salvaged as would have been extracted from the riser
  - Lower risk of hydrate formation;

    1. Due to low water content due to no entrainment of water
    2. The high temperature of the hydrocarbons exiting the well is maintained, keeping conditions well out of hydrate formation region

- The systems are built according to drilling standards, meaning that they will fit any regular drilling rig with dynamic positing

- As soon as the capping stack is in place, the well can be closed and the vessel can be disconnected

- Therefore, the system may work without any top-side equipment during the time needed to drill the relief well

Besides the advantages, there are a number of drawbacks to this type of design:

- The system needs accurate positioning. However, if it can be lowered from the drilling rig, it is easy to accomplish this

- The system is very heavy, so the drilling rig or vessel with cranes needs to have a large lifting capacity

- The interface of the old (broken) riser needs to be suitable to fit the mechanical seal. In the case of Macondo a part of the riser needed to be sawed off and adjusted in order to get access to the undamaged flange

- In the event that the well or casing integrity is of concern, this type of system is not applicable, since addition of the capping stack could cause the pressure to go up rapidly, increasing the risk of the wellhead bursting and the blowout ending up worse than it was before attempting to mediate it

A.3.2 Example of Patented Systems

Patent# WO2012012648

This is a system has a subsea containment assembly connected to a blowout preventer. A riser assembly comprising a vertical pipe (103) and a flexible riser (102) is connected to the containment assembly (112). The permanent connection to the BOP prevents fluids from escaping.

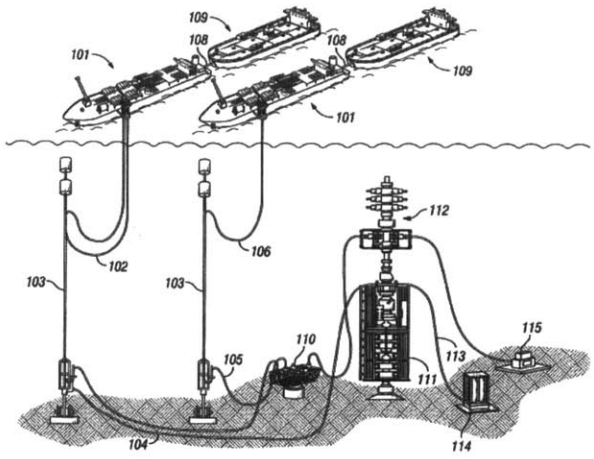

Figure A-3: Patented capping stack system

A.4 Category II - Soft Seal Systems

A.4.1 General Discussion

The systems in this category are all designs similar to the cofferdam. Most of them are steel structures that rest on the seabed, where they are passively moored down, which makes the designs all look like one another. Remarkable is that only a few of them take the hydrate risk into consideration (since there is some interaction with sea water) and have therefore added compartments to remediate this issue.

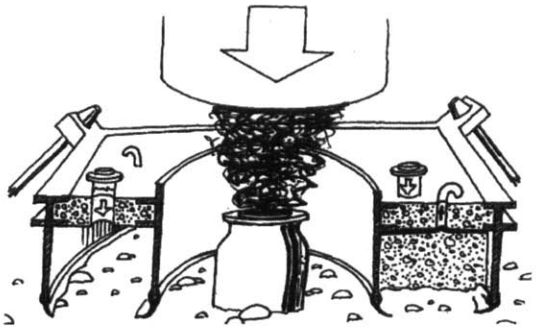

Figure A-4: Example of a patented soft seal system

Advantages of this type of system:

- A system like the cofferdam will not need to be deployed with the help of ROV's, but this is not true for all of them
- Would be able to capture hydrocarbons from a more distributed source

Drawbacks

- Hydrates could be a problem during the start-up when there is a lot of interaction with the cold water in the closed compartment. During operation there is still contact with

the cold water as well. Therefore making this a less attractive option than the Hard Seal Systems.

- High weight

It is clear that this category does not have many advantages; however, the simplicity of the system is a great advantage.

A.4.2 Examples of Patented Systems

Hard Covers

1. Patent# 8025103

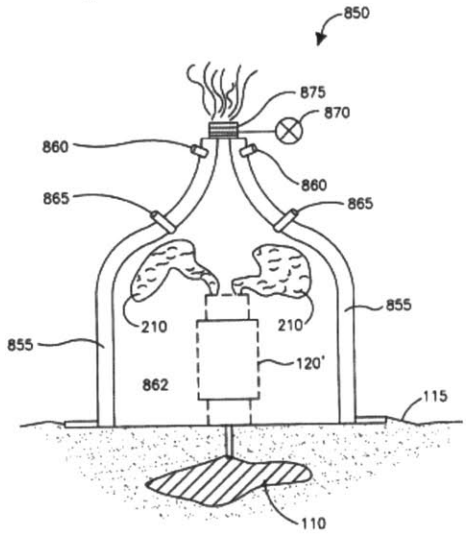

This apparatus entombs the defective BOP stack; it is positioned on the ocean floor. The system includes a hollow wall and a large diameter high pressure valve mounted on an upper opening of the containment assembly. The large diameter pressure valve is maintained open. The hollow wall of the assembly is filled with reinforcement material via a set of valves and the inner cavity could be filled with reinforcement material as well.

Learning point: Interesting way of adding reinforcement material later on into a void.

2. Patent# US2012027517

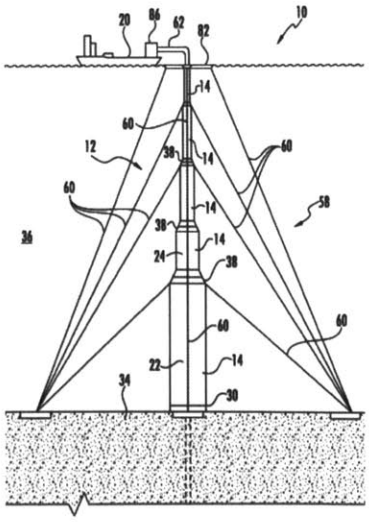

The containment system is formed from a generally extendible, conically shaped containment structure including a plurality of decreasingly sized housing sections extending from an inlet to a smeller sized outlet. The housing sections may be formed from flexible materials. The outlet directs the hydrocarbons to a vessel.

Learning Point: Interesting way to reduce the diameter without giving hydrates a location to form/conglomerate.

3. Patent# US2012024533

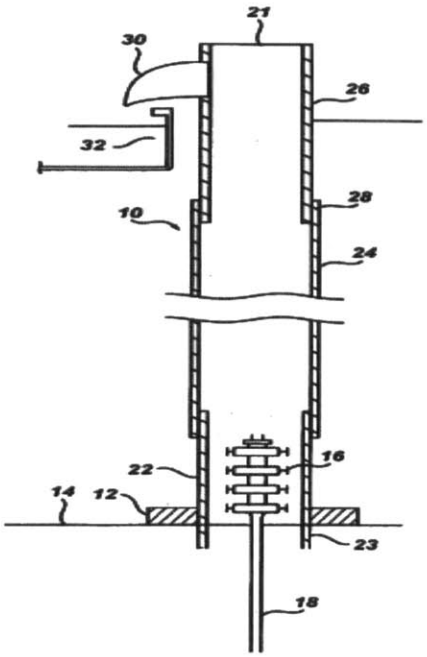

The ring shaped base is positioned on the sea bottom and is formed from a non-corrosive metal. The tubular member extending from the seabed is then sealed to a middle portion, which is formed from a non-corrosive non-metal.

Learning Point: Interesting passive collection device at the surface.

Soft Covers

1. Patent# JP2012021357

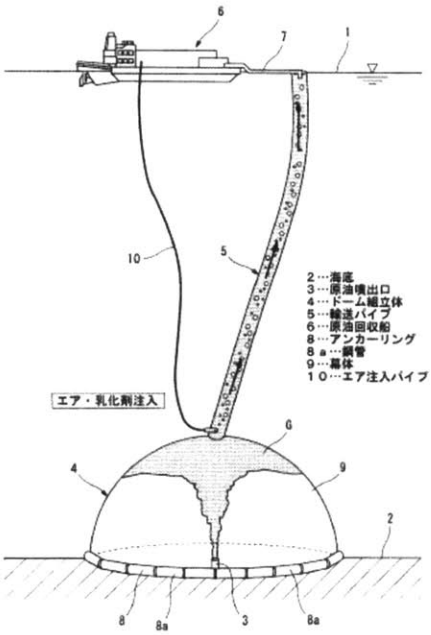

Transport pipe is connected to the curtain, which is sunk to the sea bed, so that the frame surrounds the crude oil jet nozzle. The dome assembly is fixed to the sea bed by setting the frame (8) as an anchor. The crude oil is collected in the curtain, which gets a dome shape by the buoyancy of the crude oil.

Learning Points:
- Simplicity (no ribs, simple foundation)
- Does not require mooring lines

2. Patent# WO2012007389

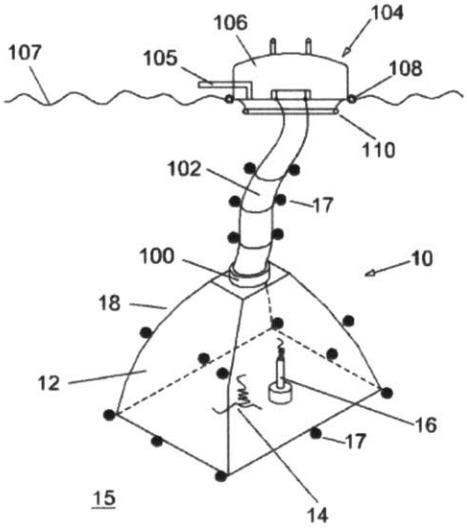

From the description of the patent and the figure, there are some characteristics that are comparable to those of the shroud design
- Reinforcement rings
- Buoyancy elements
- Containment system at the surface

Learning Point: Hydrocarbons are always collected into the flexible pipe

3. Patent# 2011274495

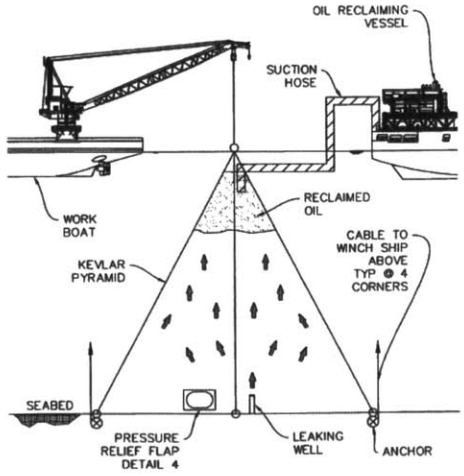

A containment vessel deploys the pyramid and allows the oil to be suctioned off or float naturally and unrestricted in the top of the pyramid. The oil can then be reclaimed by pumping the oil from the reservoir provided by the pyramid and flotation collar into an oil reclamation tanker. An oil compatible sheeting such as Kevlar, reinforced plastic or rubber coated sheeting is used to construct an outer skin of the containment device. Anchors hold the base of the pyramid to the ocean floor. The sheeting is fabricated to the required dimensions dictated by a spill site. The pyramid is able to cover more than one leak point. It will be possible to lift the base of the pyramid off the seabed to leave enough space for ROV's to pass under the pyramid.

Learning Points:
- Other way to use a Kevlar membrane
- Letting the oil/gas sit at the surface to separate from the water before extracting it

A.5 Category III - No Seal Systems

A.5.1 General Discussion

This category contains the systems that do not rest on the sea bed, therefore having no seal at the bottom. Furthermore, they all combine at least the following characteristics

- Modular
- Collection of a distributed source
- Large diameter

The biggest difference between the devices comes from the choice of collection device at the surface.
The advantages of this type of system are

- The characteristics stated above are strong advantages
- Large diameter gives rise to - Dilution of the gas, which also helps to avoid hydrate formation - Less strong requirements on positioning than a closed system/simple open system
- These systems can handle a wide range of leaking sources (possibly horizontal pipelines like during the Macondo spill where one of the spills originated form riser horizontally on the sea bed)
- Since the systems are not contacted with the wellhead, they will not increase the pressure within the well.

On the other hand the drawbacks are

- These systems are big structures (dome with pipelines vs. long, flexible shroud with big diameter)
- Slightly higher complexity (more components than e.g. dome)

The designs discussed in this section are very similar to the shroud design, except that they are mostly rigid structures, which means that some of the fundamentals and strengths of our design are not included in these systems.

A.5.2 Examples of Patented Designs

1. Patent# DE102010023551

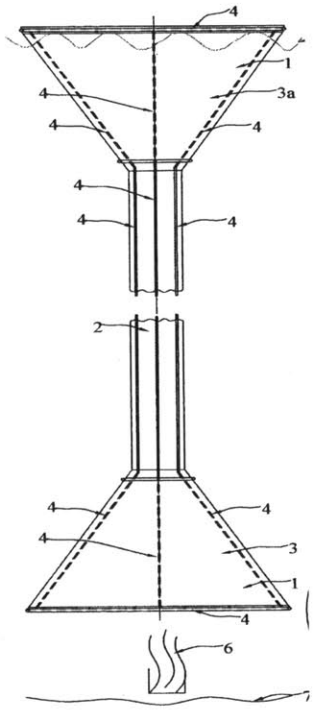

This design is a flexible tube made of a strong canvas (or similar material). It is a double walled construction that is deployed inflated and unfolded. Once on the seabed the structure can be inflated to obtain its final configuration. Furthermore, the flow of hydrocarbons through the system will help maintain its shape.

Learning Points:
- Interesting way to accordion the entire structure while in storage and then use the long wires to unfold it
- Can learn from the spokes system in this structure for the pen/flared section

2. Patent# 2011315233

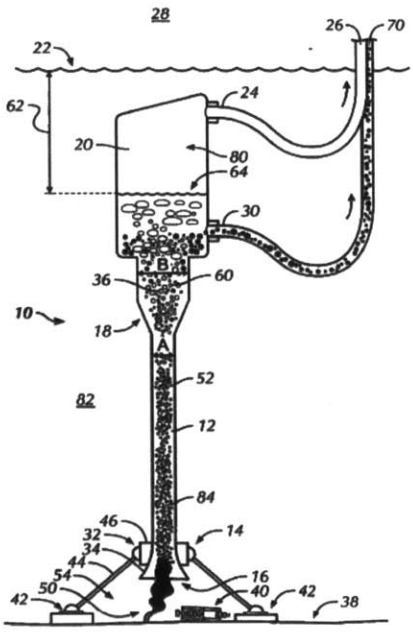

The system has a conduit whose upper end is located near to the water surface while the lower end is positioned over a leaking man-made structure. A containment tank is located in the upper portion of the interior of the conduit, which includes a first tube to pump the liquid in the tank to a vessel. This creates a differential pressure is created between the pressure within the interior of the conduit and the pressure outside of the conduit to induce an upward flow of fluids within inside the conduit. A second tube is used to release the gas from the tank.

Learning Points:
- Containment tank at the top, where oil and gas can separate naturally, without the problem of the wave dynamics
- Creating an upward flow due to pumping the liquid out of the top

3. Patent# 2011318107

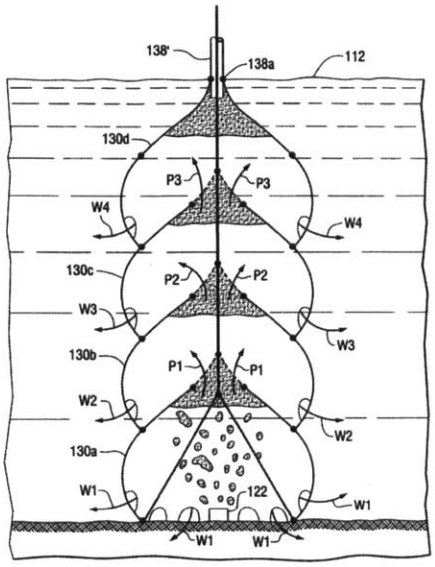

A series of interconnected canopies, which allow leaked fluid to be captured and displace seawater and the canopies guide the leaked fluid upward to the surface. The canopies are in series with exit arrangements for leaked fluid from a lower canopy to the next upper canopy. The canopies are made of an impervious material. The uppermost canopy is provided with a final leakage fluid exit arrangement for transfer to an above sea level location.

Learning point:
Connection between the sections

A.6 Category IV - No Seal, Flexible/Modular Systems

A.6.1 General Discussion

As mentioned earlier, this is the section that has systems that are most similar to our shroud design, since they have the following characteristics

- Flexible material
- Modular
- Collection of a distributed source
- Large diameter

As in Category III the dissimilarities between the systems in this group are based on the collection device at the surface, however here the type of reinforcement is also varies interestingly between the different designs. However, all together they have the following advantages and drawbacks.

Advantages

- The most important ones are stated above
- Large diameter gives rise to - Dilution of the gas, which also helps to avoid hydrate formation - Less strong requirements on positioning than a closed system/simple open system

- Less weight due to the flexible material, this makes deployment easier

Drawbacks

- Lateral reinforcement is required
- The need to avoid large number of mooring lines

A.6.2 Examples of Patented Designs

1. Patent# 2012070231

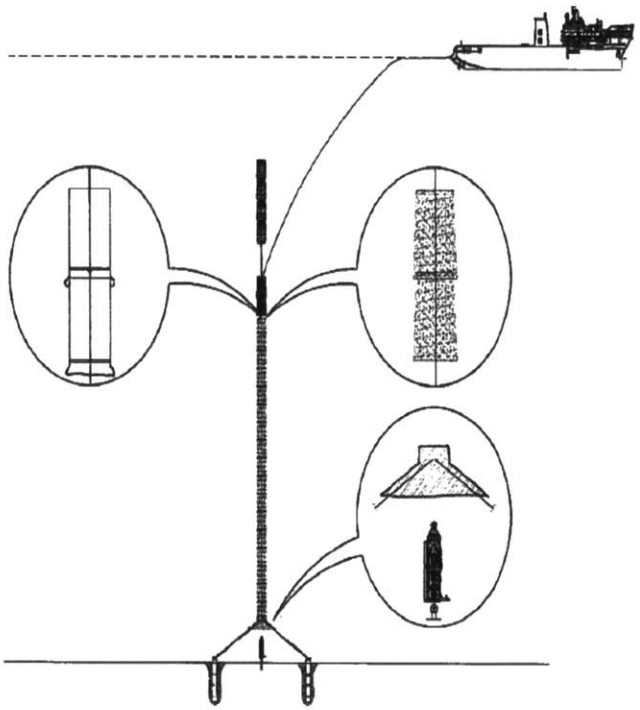

The design is built up of a funnel structure positioned over the well-head, a plurality of interconnected skirts serially joined above the funnel and lastly a collection dome above the skirts which is connected to the rest of the structure by a hose. The skirts could be supported by one or more central internal longitudinal supports, such as a drill pipe or solid rods. There may be multiple supports and/ore multiple skirts per support. The skirts are preferably sealed to the dome, the funnel and each other. The system is held in place using cables secured to two or more anchor points (suction piles). The system may be moved aside by manipulating the cables, thereby providing access to the leak.

Learning Points:
- Sections are sealed together
- The ability to manipulate the cables at the bottom
- Can inject a liquid or gas into the flow to reduce the density in the system, that way assisting and/or facilitating the hydrocarbon collection through the system
- Collection dome at the top, with a hose connecting it to the sections
- Suction piles as mooring

2. Patent# WO2011161179

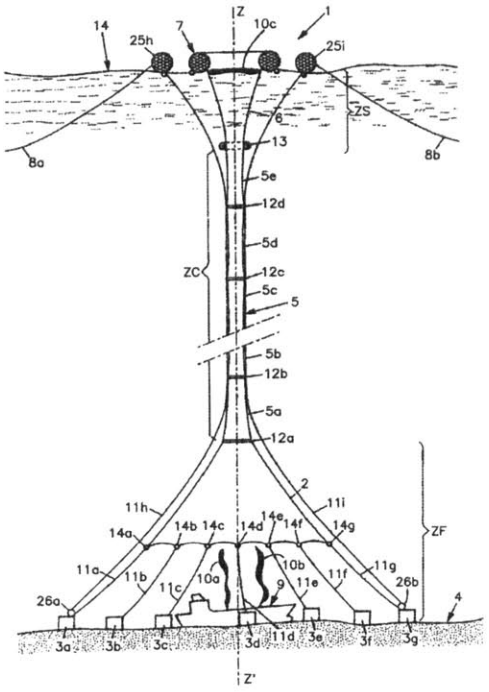

The apparatus has a set of flexible modular elements connecting a flexible base and a surface structure. A set of connecting rings connects the surface structure, the base and the modular elements to each other. A set of anchoring units is provided for anchoring with the base. A set of vertical lines extends among the surface structure, the modular elements, the base and the anchoring units for anchoring the base. A set of reinforcing elements extends between the connecting rings located on the ends of the modular elements.

Learning Points:

- Big flexible base, minimizing formation of crystals and a more simple design for the flared section at the bottom

- The components of the apparatus could be manufactured simultaneously by multiple suppliers, which would reduce manufacturing time

3. Patent# US2011293372

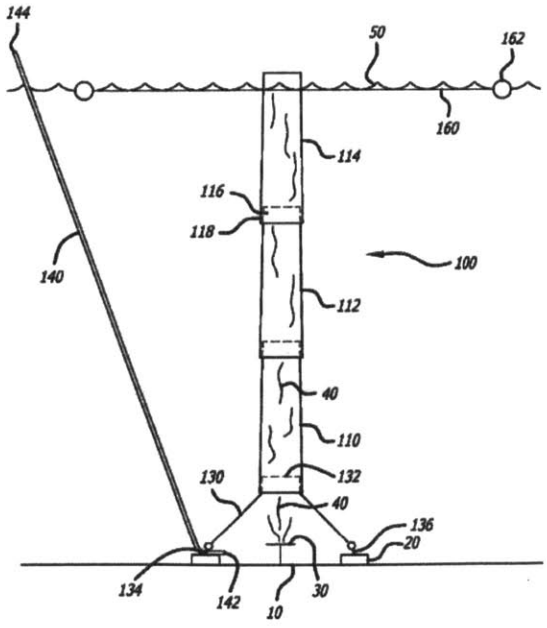

This system is a large diameter duct formed of flexible material; the bottom section is position adjacent to a well and extending upward toward the top section of the duct. A buoyant member is attached near the top of the duct, where there is also a floating catch basin reservoir.

Learning Points:

- The flared section is just a cover over the mooring lines
- Nice way to create a connection between the sections (very similar to what we have in mind)

A.7 Overview of Learning points

Over the previous sections learning points have been identified from the analyzed patents. However, these learning points are not all equally applicable to the shroud system. In order to point out which are the ones could be directly useful to improve our design, the learning points are ranked in the table below. The learning points that are rated with zero relevance are points that are interesting, but that discuss design components that are not in line with the design fundamentals of our shroud system.

Table A.1: Overview of learning points

Learning Point	Relevance	Patent#
Adding mooring weight once block is in place by pumping cement into the void	0	8025103
Telescoping diameter over depth	0	US2012027517
Foundation designed as ballast ring on the floor	+	JP2012021357
Buoyancy buoys attached to outer surface of the flexible tube at location of reinforcement ribs	++	
Natural separation of oil, gas and water in containment device slightly below the surface where little affected by wave. After which can be extracted separately.	0	2011274495
Can also be done in containment tank	0	2011315233
Flared section with spokes	+	DE102010023551
Manipulate length of mooring lines at the bottom	+	2012070231
Suction piles as mooring	-	"
Sealing together of the sections	+	"
Big flared section, held open by small 'mooring' lines	++	WO2011161179
Flared section is just a cover over the mooring lines	++	US2011293372

The most relevant learning points are related to the design of the flared section, the mooring lines, the buoyancy section and the reinforcement rings. The patents that describe the relevant learning points were read through in more detail, looking for useful design components.

A.8 Other Existing Patents

During the search through patents related to deep ocean blowout containment system there were other interesting designs that are worth mentioning, but are definitely not relevant for our design. A handful of these designs are shown below, to given an impression of what other systems are out there.

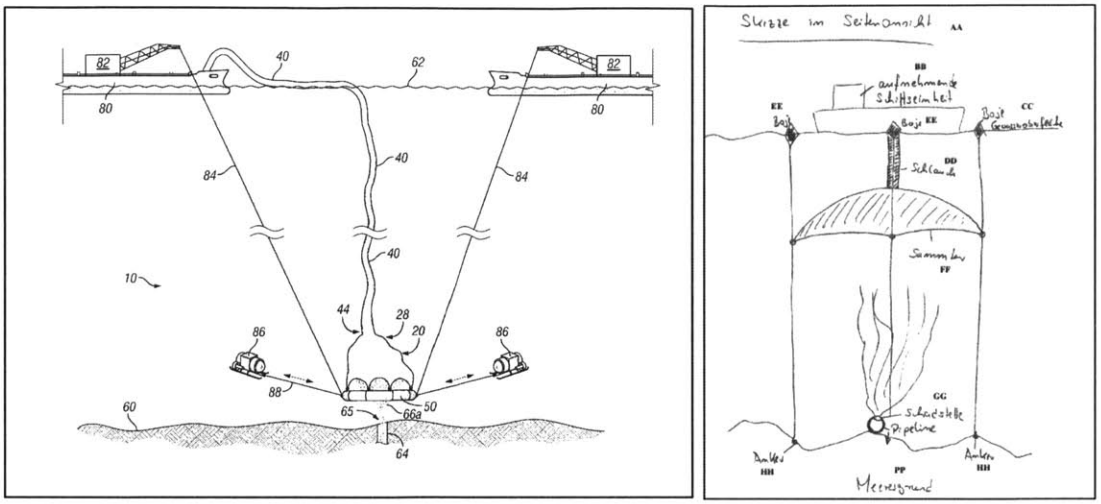

(a) (b)

Figure A-5: Patents (a) WO2011143276 and (b) WO2012022277

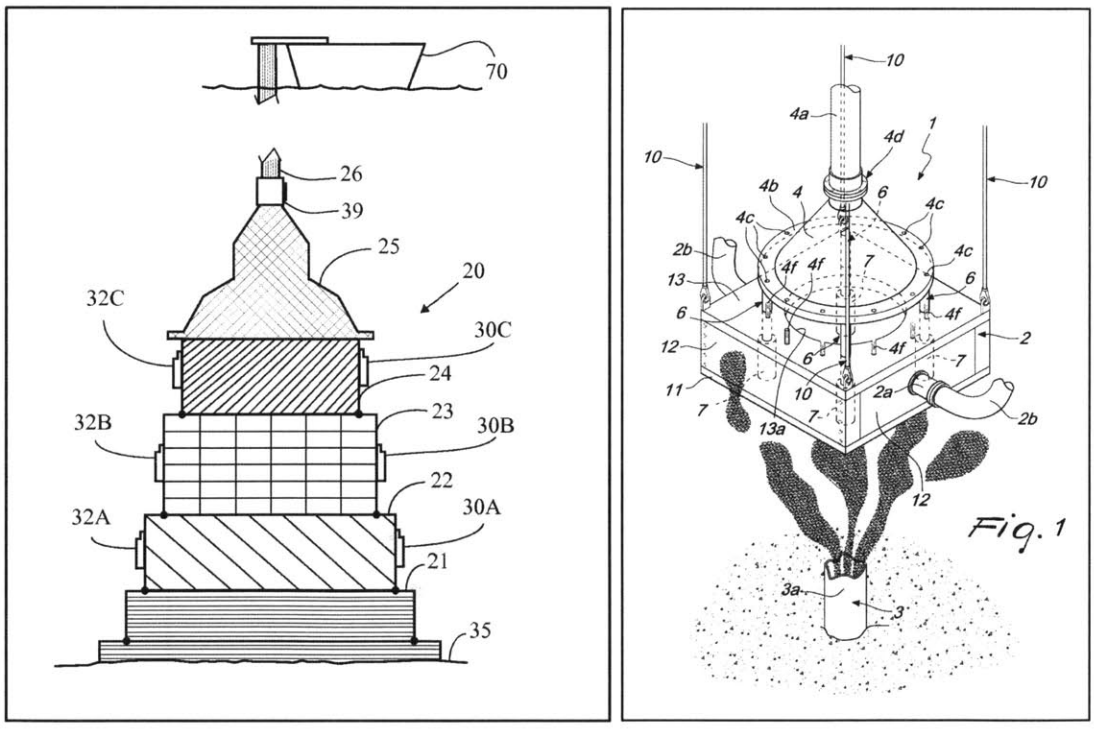

(a) (b)

Figure A-6: Patent (a) unknown and (b) WO2012007357

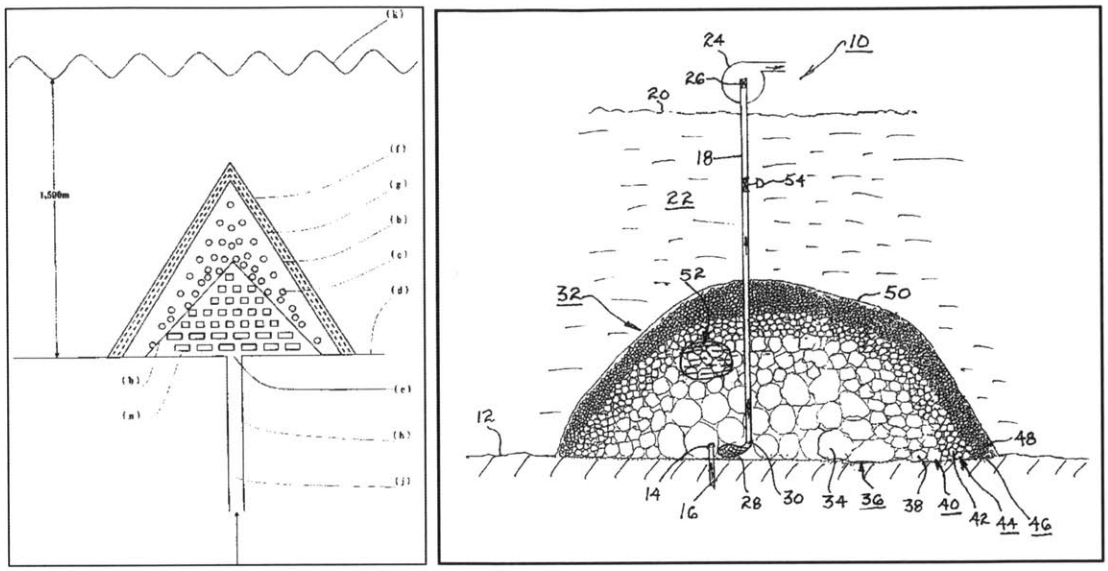

(a) (b)

Figure A-7: Patents (a) JP2012007316 and (b) US2011297386

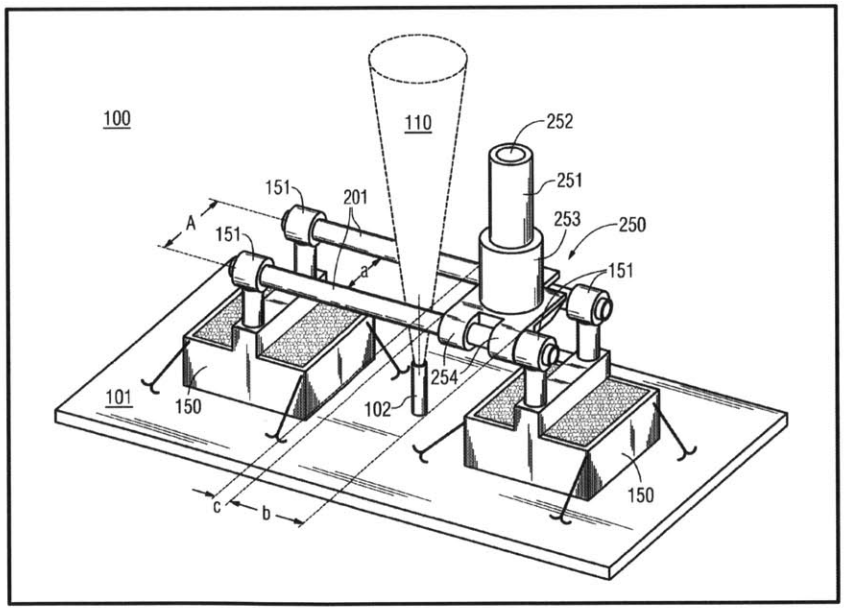

Figure A-8: Patent US2012006568

Bibliography

Bailey, A. G., W. Balanchandran, and T. J. Williams, The rosin-rammler size distribution for liquid droplet ensembles, *Journal of Aerosol Science*, *14*(1), 39–46, 1983.

Brandrik, P., O. Johansen, F. Leirvik, U. Farooq, and P. Sidaling, Droplet breaking in subsurface oil releases - part 1: Experimental study of droplet breakup and effectivenss of dispersant injection, *Marine Pollution Bulletin (in Press)*, 2013.

Burgoyne, C. J., *Construction Materials Reference Book*, chap. Aramid Fibres for Civil Engineering Applications, Routledge, 2013.

Camilli, R., et al., Acoustic measurement of the deepwater horizon macondo well flow rate, *PNAS*, 2011.

Chow, A. C., and E. E. Adams, Particle laden flows through an inverted chimney with applications to ocean carbon sequestration, *Environmental Fluid Mechanics*, 2010.

Deng, D., D. P. Pendergast, J. MacFarlane, R. Bagatin, F. Stellacci, and P. M. Gschwend, Hydrophobic meshes for oil spill recovery devices, *American Chemical Society*, *5*(3), 774–781, 2013.

Exploration, E., and P. Division, Cube-aquila feasibility study, *Tech. rep.*, ENI SpA, 2011.

Federal Interagency Solutions Group, O. B. C. S., and E. Team, Oil budget calculator deepwater horizon, *Tech. rep.*, 2010.

Glenn, A., Meteorological - oceanographic conditions affecting planning and design of petroleum facilties offshore of brindisi, italy, 827 meter chart depth, *Tech. rep.*, Technomare Venice, 1984.

Hirai, S., K. Okazaki, N. Araki, H. Yazawa, H. Ito, and K. Hijikata, Transport phenomenoa of liquid co2 in pressurized water flow with clathrate-hydrate at the interface, *Energy Conversion and Management*, *37*(6-8), 1073–1078, 1996.

Isherwood, R. M., A revised parameterisation of the jonswap spectrum, *Applied Ocean Research*, *9*(1), 47–50, 1987.

Johansen, O., Deep spill jip - experimental discharges of gas an oil at helland hansen - final technical report, *Tech. rep.*, SINTEF Applied Chemistry, 2001.

Johansen, O., Physical/chemical fate of gas from deep water blowouts, *Tech. rep.*, SINTEF Applied Chemistry, 2004.

Johansen, O., P. S. Daling, H. Jensen, A. G. Melbye, and H. Rye, Feasibility of a field experiment to study the behavior of a deepwater blowout, *Tech. rep.*, SINTEF Applied Chemistry, 1999.

Johansen, O., P. Brandrik, and U. Farooq, Droplet breaking in sub-surface oil releases - part 2: Productions of droplet size distributions with and without inject of chemical dispersants, *Marine Pollution Bulletin (in Press)*, 2013.

McCain, W. D., *The properties of petroleum fluids*, PennWell Books, 1990.

NOAA, Noaa buoys center, `http://www.ndbc.noaa.gov/`.

NOAA, Noaa buoy center - current data, `http://www.ndbc.noaa.gov/station_page.php?station=42921`, 2012.

Poulain, P. M., M. Gacic, and A. Vetrano, Current measurements in the strait of otranto reveal unforeseen aspects of its hydrodynamics, *EOS - American Geophysical Union*, *77*(36), 345–352, 1996.

Rehder, G., I. Leifer, P. G. Brewer, G. Friederich, and E. T. Peltzer, Controls on methane bubble dissolution inside and outside the hydrate stability field from open ocean field experiments and numerical modeling, *Marine Chemistry*, *114*(1-2), 19–30, 2009.

report, T., Doc.n: 11-277 rev-0, *Tech. rep.*, TEA Sistemi S.p.A., 2011.

Riebesell, U., et al., A mobile sea-going mesocosm system - new opportunities for ocean change research, *Biogeosciences (under review)*, 2013.

Sacks, W., and V. Meyn, Pressure and temperature dependence of the surface tension in the system natural gas/water. principles of investigation and the first precise experimental data for pure methane/water at 25c up to 46.8mpa, *Colloids and Surfaces. A; Physicochemical and Engineering Aspects*, *94*, 291–301, 1995.

Sloan, E. D., and C. A. Koh, *Clathrate Hydrates of Natural Gases*, CRC Press, 2008.

Socolofsky, S., E. E. Adams, and R. C. Isherwood, Formation dynamics of subsurface hydrocarbon intrusions following the deepwater horizon blowout, *Geophysical research letters*, *38*, 2011.

Sturges, W., E. Chassignet, and T. Ezer, Strong mid-depth currents and a deep cyclonic gyre in the gulf of mexico, *Tech. rep.*, US Department of Interior - Minerals Management Service - Gulf of Mexico OCS Region, 2004.

Timoshenko, S., *Theory of elasticity*, McGraw-Hill, 1970.

Trieste, O., Temperature and density data for the southern adriatic, `http://doga.ogs.trieste.it/medar/climatologies/DJ3/dj3.html`.

Zheng, L., and P. D. Yapa, Buoyant velocity of spherical and nonshperical bubbles/droplets, *journal of Hydraulic Engineering, ASCE, 126*(11), 852–855, 2000.